

**STUDY OF THE CHARACTERISTICS
OF SCALP ELECTROENCEPHALOGRAPHY SENSING**

KHOA WEI LONG, GEOFFREY
(B.ENG., NATIONAL UNIVERSITY OF SINGAPORE)

**A THESIS SUBMITTED FOR
THE DEGREE OF DOCTOR OF PHILOSOPHY
DEPARTMENT OF MECHANICAL ENGINEERING
NATIONAL UNIVERSITY OF SINGAPORE**

2013

DECLARATION

I hereby declare that the thesis is my original work and it has been written by me in its entirety. I have duly acknowledged all the sources of information which have been used in the thesis. This thesis has also not been submitted for any degree in any university previously.



Khoa Weilong Geoffrey

23 April 2013

ACKNOWLEDGEMENTS

First of all, I would like to express my deepest gratitude to my supervisor, Professor Li Xiaoping, Director of the Neuroengineering Laboratories, for his gracious guidance, a global view of research, strong encouragement and detailed recommendations throughout the course of this research. His kind patience, encouragement and support always gave me great motivation and confidence in conquering the difficulties encountered in the study.

I would also like to offer special thanks to the following collaborators of the Neuro-engineering Initiative for all their valuable inputs to this study:-

1. Professor Einar Wilder Smith (Director, Clinical Neurophysiology NUH)
2. Professor Gopalakrishnakone (Chair, Venom and Toxin Research NUHS)
3. Professor Lian Yong (NUS Provost's Chair, IEEE Fellow)
4. Professor Lim Shih Hui (Senior Consultant, SGH)

I am also thankful to my colleagues, Associate Professor Zhou Jun, Dr. Fan Jie, Dr. Masha, Dr. Ng Wu Chun, Dr. Ning Ning, Dr. Rohit Tyagi, Dr. Shao Shiyun, Dr. Shen Kaiquan, Dr. Wu Xiang, Dr. Zhao Zhenjie, Miss Ye Yan and Miss Wang Yue for their kind help, support, and encouragement in my work.

Last but not least, I am deeply grateful to my parents Mr Khoa Hee Tiang and Mdm Tan Chiew Kian for their constant understanding and support all this while. As such, I would like to dedicate this thesis to my parents for their self-less love and unconditional support throughout the study.

TABLE OF CONTENTS

DECLARATION.....	i
ACKNOWLEDGEMENTS	ii
TABLE OF CONTENTS.....	iii
SUMMARY	vi
LIST OF PATENT AND PUBLICATIONS FROM THIS WORK	vii
LIST OF FIGURES	viii
LIST OF TABLES	xii
LIST OF SYMBOLS	xiii
Chapter 1 Introduction	1
1.1 Motivation.....	4
1.2 Objective	7
1.3 Organization of the Thesis	8
Chapter 2 Literature Review	10
2.1 EEG Basics	10
2.1.1 Physiological Background of EEG.....	10
2.1.2 Properties of EEG	11
2.1.3 Measurement of EEG.....	12
2.1.4 Distribution of EEG electrodes	16
2.2 Factors Affecting Electrode-Skin Contact Impedance	19
2.2.1 Effect of Electrode Material on EEG Signal Quality	21
2.2.2 Effect of Electrolyte on EEG Signal Quality	22
2.2.3 Effect of Impedance on EEG Signal Quality	26
2.3 Electrical Impedance of the Human Head	27
2.3.1 Electrical Impedance of the Skull.....	27
2.3.2 Electrical Impedance of the Skin.....	29
2.4 Advantages and Limitations of EEG.....	31
Chapter 3 in-vitro study of the human skull resistivity	33
3.1 Regions of Interest for Skull Impedance Measurement	36

3.2 Experiment Setup	37
3.2.1 Saline Solution.....	37
3.2.2 Setting up of the Skull Sample	39
3.3 Results and Discussions	43
Chapter 4 Head Profile Measurement and Categorization	49
4.1 Protocol Design	49
4.2 Material and Methods	51
4.2.1 Segment Length and Arc Length Calculation	51
4.2.2 Database for Human Head Shape Data Collection	52
Microsoft SQL	53
MySQL	53
PostgresSQL.....	53
Oracle.....	54
4.2.3 User Input Graphical User Interface (GUI).....	55
Data Communication.....	56
Data Presentation.....	56
4.2.4 3D model planning.....	58
4.2.5 Optical Measurement System - Polaris® Spectra®	59
4.2.6 Subjects	62
4.2.7 Procedures	62
4.3 Result and Discussion.....	62
Chapter 5 Study to achieve uniform scalp impedance	65
5.1 Design Considerations	67
5.2 Materials and Methods	68
5.2.1 Subjects	68
5.2.2 Experiment Procedures	68
5.2.3 Novel Self-Clamping Headset Design	75
5.3 Results and Discussion	76
5.3.1 Impedance-indentation on the hand.....	76
5.3.2 Impedance Variation along T7-C3-CZ-C4-T8.....	82
5.3.3 Impedance Variation along FPZ-FZ-FCZ-CZ-PZ-OZ	83

5.3.4 Load Variation for Constant Impedance	84
5.3.5 Optimized Loading Index for Constant Impedance.....	88
5.4 Impedance checks.....	90
Chapter 6 Gated capillary action biopotential sensor for a portable biopotential recording system.....	91
6.1 Types of EEG measuring electrodes	92
6.2 Design Consideration	95
6.3 Material and Methods.....	101
6.3.1 Novel Electrode Design	101
6.3.2 Novel EEG Headset Design	104
6.3.3 Fabrication process of a electrode	107
6.3.4 Experiment Protocol for the Testing of the Novel Electrode Design	108
Portable EEG Acquisition System	109
Electrode-amplifier Interface	111
6.4 Results and Discussion	112
6.4.1 Basic EEG Wave Detection Capability	112
6.4.2 Signal Quality of the Gated Capillary Action Electrode	113
Chapter 7 Conclusions.....	115
References	117
Appendix A - Derivation of Mathematical Representations.....	128
Appendix B - Spline Line Calculation.....	131

SUMMARY

With the discovery of EEG in the 1920s, various measurement techniques have been widely discussed, explored and developed. It has also gave rise to a vast number of EEG-based applications such as mental fatigue measurement and intervention systems and the rapid triage systems. However, the basic technology of using electrodes with electrolytes has not evolved too much and that restricted the use of EEG in various industries. Not only is it troublesome to set up and users always have to wash their hair after usage, EEG measurement itself is prone to noise.

The objective of this thesis is to provide a fundamental and comprehensive understanding of scalp electroencephalography measurement. The factors includes the study of the human skull's profile and its resistivity, and the effects of skin compression on electrode-skin impedance which was used for the development of a novel method to achieve uniform impedances across the scalp. With that, a gated capillary action bio-potential sensor for a portable bio-potential recording system was patented, designed, developed and validated.

LIST OF PATENT AND PUBLICATIONS FROM THIS WORK

PATENTS

Li Xiaoping, **Khoa Wei Long Geoffrey** and Ng Wu Chun, “Dry EEG Sensing and Neural Stimulation”, US Provisional Patent No. 61/383,611 (2010)

Li Xiaoping, **Khoa Wei Long Geoffrey** and Ng Wu Chun, “EEG Electrodes with Gated Electrolyte Storage Chamber and an Adjustable Headset Assembly”, US Patent No. WO/2012/036639 (2012)

JOURNALS

J. Fan, Z.H. Lee, W.C. Ng, **W.L. Khoa**, et. al. , “Effect of pulse magnetic field stimulation on calcium channel current” Journal of Magnetism and Magnetic Materials Vol. 324, Issue 21, 3491–3494, 2012

W.L. Khoa, X.P. Li, "The effect of compression on the impedance at skin-electrode interface: an in-vivo measurement study" Journal of Biomechanics (Submitted for journal publication)

W.L. Khoa, X.P. Li, “A novel method to achieve uniform scalp Impedance for dry bio-potential measurement.” Journal of Neuroscience and Neuroengineering (Submitted for journal publication)

CONFERENCE PAPERS

W.C. Ng, **W.L. Khoa**, Y. Ye, X.P. Li, “In-vivo Measurement of the Effect of Compression on the Human Skin Impedance.” International Forum on Systems and Mechatronics, 40, 2010

W.L. Khoa, X.P. Li, “Achieving Uniform Scalp Impedance for Dry EEG Measurement.” International Conference on Engineering and Applied Sciences, 40, 2013

LIST OF FIGURES

Figure 1: Typical EEG Waves	11
Figure 2: The UI 10/5 system (Valer, Daisuke and Ippeita 2007)	13
Figure 3: Standard EEG system with EEG caps	16
Figure 4: Effect on EEG by electrodes located within 120 deg	16
Figure 5: Effect on EEG by electrodes located within 60 deg	16
Figure 6: Effect on EEG by electrodes located within 20 deg	17
Figure 7: Effect on EEG by electrodes are located within 40 deg	17
Figure 8: Effect on EEG by electrodes are located within 180 deg	18
Figure 9: Cross-sectional view of the human skin	19
Figure 10: Long-term DC-stability of Ag/AgCl electrodes in continuous recordings	21
Figure 11: Equivalent circuit model of the electrode-electrolyte-skin interface.....	23
Figure 12: Equivalent circuit model for the conventional wet electrode.....	24
Figure 13: Equivalent circuit model for the cup electrode	24
Figure 14: Equivalent circuit model for the spike electrode.....	25
Figure 15: A cross-sectional view of the human skin	29
Figure 16: Spatial and temporal resolution of various neuro-diagnostic methods.....	31
Figure 17: fMRI results on a dead salmon.....	32
Figure 18: Layers of Different Bone Tissue of the Human Skull	34
Figure 19: Magnetic Resonance Image of Realistic Head Model.....	35
Figure 20: Schematic Representation of BEM model.....	35
Figure 21: Locations for which readings were taken	36
Figure 22: Skull Model Constructed from MRI scans	36
Figure 23: Schematic of the In-Vitro Experiment Setup	37
Figure 24: Characteristic of Frequency Respond of the Saline Solution.....	38
Figure 25: Schematic Drawing of Electric Circuit	39
Figure 26: CAD drawing of the Holder	41
Figure 27: Experiment setup	42
Figure 28: Skull Resistivity vs Thickness at 20 Hz.....	44

Figure 29: Skull Resistivity vs Thickness at 50 Hz.....	45
Figure 30: Skull Resistivity vs Thickness at 100 Hz.....	46
Figure 31: Close-up views of locations for which readings were taken.....	47
Figure 16: Flowchart to calculate segment length and arc length.....	51
Figure 34: Overall database model.....	52
Figure 20: Overall database model.....	54
Figure 21: User interface design	55
Figure 22: Data presentation graphical format.....	56
Figure 22: Customable database fields	57
Figure 22: Filter/search option	57
Figure 22: Data analysis option.....	57
Figure 40: Spectra Pyramid Volume	59
Figure 41: Reference pointers ranges	61
Figure 42: Equivalent circuit of the skin	65
Figure 43: Setup for impedance and indentation measurement	68
Figure 44: Indentation positions (a) Outer (extensor) forearm, (b) Inner (volar) forearm.....	71
Figure 45: Experiment Setup	73
Figure 46: Procedure for using the spring based impedance-load tester	74
Figure 47: Reconfigurable self-clamping module (Left) and Tensioning mechanism (Right) of the headset	75
Figure 48: (a) Load-indentation and (b) Impedance-indentation curves on the volar forearm.....	76
Figure 49: Two consecutive cycles of the impedance-indentation curve of on the volar forearm.....	77
Figure 50: Changes in normalized skin impedance ('o') and load ('□') in relation to indentation depth	78
Figure 51: (a) Comparison of impedance change with indentation depth on volar forearm and extensor forearm. (b) Comparison of load-displacement curve between these two sites.....	79

Figure 52: Enhancement method by coupling compression and gel penetration. (a) Variation of skin impedance with time for conventional wet electrode method on inner forearm of the same subject (b) Variation of impedance with indentation depth on inner forearm with electrolyte gel	80
Figure 53: Skin resistance variation with indentation on the inner forearm.....	81
Figure 54: Skin capacitance variation with indentation on the inner forearm.....	81
Figure 55: Graph of impedance with respect to position at 50 grams	82
Figure 56: Graph of impedance with respect to position at 100 grams	82
Figure 57: Graph of impedance with respect to position at 150 grams	83
Figure 58: Graph of impedance with respect to position at 50 grams	83
Figure 59: Graph of impedance with respect to position at 100 grams	84
Figure 60: Graph of impedance with respect to position at 150 grams	84
Figure 61: Sample best fit linear regression line	85
Figure 62: Sample best fit exponential regression line.....	86
Figure 63: Load variation to minimize impedance mismatch. A and B shows values determined by linear and exponential curve fitting respectively. C and D show resultant impedances for linear and exponential curve fitting method.....	87
Figure 64: Graph showing optimized loading on at different locations	88
Figure 65: Impedance variation on the scalp by Linear Curve Fitting	89
Figure 66: Impedance variation on the scalp by Exponential Curve Fitting	89
Figure 67: Impedance Test on the Novel Dry Electrode with the EEG Headset	90
Figure 68: Skin model with typical impedance values at 10Hz (Taheri et al. 1994) ..	93
Figure 69: Feasibility study of HD-EEG measurement system.....	97
Figure 70: A cross-sectional view of the novel electrode.....	101
Figure 71: Effective skin model with typical impedance values at 10Hz	103
Figure 72: Effective skin model with typical impedance values at 10Hz	103
Figure 73: Design of the Reconfigurable self-clamping assembly	104
Figure 74: MRI compatible configuration of the self-clamping assembly	105
Figure 75: Full Reconfigurable self-clamping assembly.....	105
Figure 76: Tensioning Mechanism of the EEG Headset Mount	106
Figure 49: Ag/AgCl pellets and cable	107

Figure 50: Ag/AgCl pellet into plug	107
Figure 51: Epoxy left to cure	107
Figure 80: The 10/5 System (Dan et al. 2007)	108
Figure 81: Visual checkerboard stimuli protocol.....	109
Figure 82: System Requirements and BioCapture Specifications	110
Figure 83: Modified electrode-amplifier interface	111
Figure 84: Recorded EEG signals with eye closed	112
Figure 85: Recorded EEG signals with eye open.....	112
Figure 86: VEP of channels PO7, O1, OZ, O2 and PO8.....	114

LIST OF TABLES

Table 1: Summary of the properties of different types of electrodes when used in combination with a chloride containing gel.....	21
Table 2: Skull Resistivity against Thickness	43
Table 3: Partial 10/10 System used for Head Profile Categorization.....	50
Table 4: Performance of the Polaris® Spectra®.....	60
Table 5: Accuracy of the Spline Curve Algorithm.....	62
Table 6: Subject's head profile vs. Commercial head cap size	63
Table 7: Regions of the subjects' head profile that is incompatible to the Commercial head cap	64
Table 8: Parameters for Spring Design.....	74
Table 9: SNR to visual stimulus.....	114

LIST OF SYMBOLS

$Z_{CPA(E)}$	constant phase angle impedance
R_{gel}	resistance of gel
R_{CT}	electrode-electrolyte resistance
Z_{Skin}	total electrode-skin impedance
Z_{α}	electrode-skin impedance of electrode α
Z_{β}	electrode-skin impedance of electrode β
Z_{IN}	amplifier input impedance
f	frequency of the magnetic field
R_P	skin's parallel resistance
C_P	skin's parallel capacitance
K_S	magnitude of $Z_{CPA(S)}$ when $\omega=1$
S_{eff}	the total effective skin area contacted with gel
S_O	electrode surface area
x	position along the 1D cylindrical volume
t	time moment
ρ	effective resistivity
$R(t)$	resistance at time t
$Z_T(t)$	total skin impedance at time t
C_T	steady state electrode-skin impedance
Z_0	initial value of skin impedance at reference initial time point ($t=0$)
Z_S	Impedance of Stratum Corneum
Z_A	Impedance of appendages
Z_k	Impedance of Stratum Corneum

ACRONYMS

EEG	Electroencephalogram
ECG	Electrocardiography
EMG	Electromyogram
SC	Stratum Corneum
RC circuit	Resistor–Capacitor circuit
Ag-AgCl	Silver- Silver chloride
DC	Direct Current
AC	Alternate Current
FEM	Finite Element Method
IPA	Isopropyl Alcohol
PU	Polyurethane
SDK	Software Development Kits
SVM	Support Vector Machine
GUI	Graphical User Interface
AWVT	Audio Working-Memory Vigilance Task
PMMA	Poly(Methyl methacrylate)
DXRL	Deep X-Ray Lithography

CHAPTER 1

INTRODUCTION

Scalp electroencephalography, commonly known as EEG, is the recording of electrical activities in the brain from the scalp surface, for which these electrical activities were produced by the firing of neurons within the brain. Neurons are electrically excitable cells that processes and transmits information by means of chemical and electrical signaling. Chemical signaling occurs via synapses, which are specialized connections that neurons have with other cells, and this connection allowed neurons to be vastly connected to each other forming networks which then form the core components of the human central nervous system consisting of the brain and spinal cord (Nieuwenhuys, Voogd and Vanhuijzen 2007).

Neurons are electrically charged by transport proteins that pump ions across their membranes which in the process consumes adenosine triphosphate (ATP). When a neuron receives a signal from its neighbor via an action potential, it responds by releasing ions into the space outside the cell. Ions of like charge repel each other, and when many ions are pushed out of many neurons at the same time, volume conduction occurs. When the wave of ions reaches the electrodes on the scalp, they can push or pull electrons on the metal on the electrodes. Since metal conducts the push and pull of electrons easily, the difference in push, or voltage, between any two electrodes can be measured by a voltmeter and this recording over time gives us the EEG (Tatum,

Husain and Benbadis 2008). The electric potentials generated by a single neuron are far too small to be picked by EEG or MEG (Nunez PL 1981).

EEG activity therefore always reflects the summation of the synchronous activity of a cluster of neurons, typically thousands of them, which have similar spatial orientation. If the cells do not have similar spatial orientation, their ions do not align to create waves that can be detected. Pyramidal neurons of the cortex are thought to produce most of the recordable EEG signal as they are well-aligned and have synchronous firing. Even so, it must be noted that these generated voltage fields fall off with the square of the distance, thus activities from deep sources are more difficult to detect than those that were located nearer to the skull (Klein and Thorne 2006). In order to perform EEG-based neuroimaging, the location of these sources must be determined and this is only possible by having a thorough understanding of the properties of brain circuits by performing a direct measurement of the neuronal activity real time using EEG and MEG as they are capable of measuring the neuronal cell assemblies' electrical activity on a sub-millisecond time scale.

Unfortunately, these techniques face the problem that the signals measured on the scalp surface do not directly indicate the location of the active neurons in the brain due to the ambiguity of the underlying inverse problem (Helmholtz 1853). Different source configurations can generate the same distribution of potentials and magnetic fields on the scalp (Gevins and Remond 1987), therefore maximal activity or maximal differences at certain electrodes do not unequivocally indicate that the generators were located in the area underlying it (Christoph, et al. 2004).

Capitalizing on the fact that different scalp topographies must have been generated by different configurations of brain sources, the identification of differences in scalp topographies is fundamental to the understanding of the dynamics of different neuronal populations although it does not provide any conclusive information about the sources' location and distribution.

The only way to localize these electric sources in the brain from that of the scalp potentials is through the solution of the so-called inverse problem (Christoph, et al. 2004), a problem that can only be solved by introducing a priori assumptions on the generation of these EEG and MEG signals. These assumptions include different mathematical, biophysical, statistical, anatomical or functional constraints; the more appropriate these assumptions are, the more accurate are the source estimations.

Moreover, after the application of the electrolyte gel, time is needed to achieve a stabilized impedance and this set-up time results in restricting the use of EEG outside the clinic and research institute, even though there is a significant need for them. An electrode system that does not require long preparation time and can be used immediately after the application of the electrode represents a major advancement in this technology and could significantly increase its utility.

Various inverse solution algorithms had been formulated and implemented, ranging from the single equivalent current dipole estimations to the calculation of three-dimensional current density distributions. However, the accuracies of all of these algorithms rely mainly on the amount and quality of the EEG signal that could be

collected and this collection brings with itself a set of challenges which must be overcome before EEG-based neuroimaging could find its way into clinical usage.

1.1 Motivation

With the advancement in signal processing methods and electronic technology, many EEG-based applications have undergone intensive research and development in order to obtain a better source estimation. However, the fundamental to obtaining as a more correct sampling of the spatial frequencies of the scalp electric fields should lead to a better resolution of the topographic features (Christoph, et al. 2004). Scalp potentials recorded at limited locations, are used to determine the potential of the whole scalp by means of interpolation. This would definitely induce information loss thus if we are able to obtain a larger number of recording channels, more information would be available and thus the source estimations would then be more accurate which could then lead to the better understanding the dynamics of the brain activation.

An increase in the number of recording sites would be a great contribution, but what is the limit of this increase in electrode density? It would be useless to increase the number of electrodes if the signals recorded from the added sites have very high correlation. In standard clinical practice, 19 recording electrodes are placed uniformly over the scalp using the International 10–20 System (Ernst and Fernando 2004). It must be noted that these electrodes record not only the EEG signals but also sweat artifacts as they are sensitive to changes in the chloride concentration due to the sweating of the subject as well as the drying of the electrolyte as the time of the experiment lengthens.

When a metal electrode contacts an electrolyte, ions from that metal will have a tendency to enter the solution releasing electrons that tend to combine with the metallic surface (Geddes 1989) and the minimization of this difference in the ion concentration is important for the collection of good quality EEG signals with high SNR (Dankers 1996). In order to minimize this artifact, conventional wet EEG electrodes are always equipped with a cavity large enough to contain sufficient electrolyte so as to make the chloride concentration change insignificant (Voipio, et al. 2003). The volume of this cavity sets a constraint on the size of the electrodes thus limiting the development of a high density electroencephalography (HD-EEG) measurement system.

The wet electrode system is not designed to be disposable and it does not allow immediate repositioning and reusability on the same user or subject. The components of the electrode system have to be cleaned and disinfected immediately after the EEG recordings (Ferree, Luu et al. 2001). There are two types of wet electrodes system that are currently available in the market, namely the (1) electrolyte paste wet electrode, and the (2) electrolyte gel wet electrode.

The first consists of a cup electrode to be used with a waxy electrolyte paste. To use this, one has to remove the Stratum Corneum (SC) layer by abrasion, with the use of abrasive stick which may exfoliate the skin which can cause bleeding and infection, and clean the scalp prior to applying the waxy electrolyte paste onto the cup electrode before placing the electrode on the measurement site. However, this has been widely accepted as a standard procedure in the clinical environment. as it could minimize the

motion artifacts and the power line interference which is mainly due to very high electrode-scalp impedance of the unprepared scalp.

The second type consists of a cup electrode, usually mounted onto an electrode cap, to be used with a large amount of low viscosity electrolyte gel, and in so doing eliminates the need to do skin abrasion. However, the electrolyte may evaporate over time and over injection of the electrolyte may cause cross-bridging between neighboring electrodes resulting in electrolyte shunt effect (Greischar, Burghy et al. 2004).

It is also important to have a uniform scalp impedance distribution so as to minimize the amount of noise that is being embedded in the signals recorded. As such, we first must have a thorough understanding of the impedance distribution before we could try to make it uniform. This scalp impedance is dependent on (1) the electrode-scalp contact which is then dependent on the curvature of the head, (2) the material property of the electrode, and (3) the amount of force exerted on the scalp by the electrode. As such, a headset that is capable of holding the HD-EEG in the optimized configuration for the maximizing of the HD-EEG measurement system must be designed for. Although signal processing can remove the noise prior to using it for EEG-based neuro-imaging; there is a limit as to how well this noise can be removed and that artifact removal may remove important signals unknowingly.

It must also be noted that the structural stability of the electrode plays an important role in ensuring a quality signal could be obtained. Knowing that the skull acts as a low-pass filter that only allows low frequency signals to pass through, the impedance

distribution of the skull is necessary in order to better understand the shunt effect on EEG due to the high impedance ratio between the skull, the brain and the scalp. This skull impedance distribution, which is highly dependent on the thickness of the skull and the porosity of the skull material, has to be fully understood thus making the understanding of the skull another challenge.

The brain machine interface applications that have been reported include rapid image triage system, fatigue detection, mental workload monitoring system, mind control gaming console (Gevins, Smith et al. 1998; Berka, Levendowski et al. 2004; Birbaumer and Cohen 2007; Yonghong, Erdogmus et al. 2008; Heingartner 2009; Pai-Yuan, Weichih et al. 2009), several of which possess extremely significant research potential with high market potential.

However, the major drawbacks with the current EEG technology of inaccurate source estimation, long preparation time and the requirement of specialized EEG-related skills result in the prolonged commercialization for the products and the restriction on the use of such technology.

1.2 Objective

The objective of this thesis is to provide a fundamental and comprehensive understanding of scalp electroencephalography measurement. The factors includes the study of the human skull's profile and its resistivity, and the effects of skin compression on electrode-skin impedance which was used for the development of a novel method to achieve uniform impedances across the scalp. With that, a gated

capillary action bio-potential sensor for a portable bio-potential recording system was patented, designed, developed and validated.

The research topic is divided into the following main steps:

- 1) Identify the requirements and design considerations of a portable bio-potential recording system
- 2) Study the effect of skin compression on the electrode-skin impedance.
- 3) Study the enhanced effect of skin compression with electrolyte gel.
- 4) Study the scalp impedance distribution on the human scalp.
- 5) Develop a novel method to achieve uniform scalp impedance across the scalp.
- 6) Propose, design, develop and validate the novel gated capillary action bio-potential sensor.

1.3 Organization of the Thesis

This thesis is organized as follows:

Chapter 1 serves as an introduction to examine the need of an evolutionary EEG electrode system that allows the EEG recordings to be commenced immediately after the electrode application and provides an overview of the past related work, followed by the description of the objectives of the present work.

Chapter 2 provides the relevant background information on EEG basis, EEG electrode, current bio-potential electrode technology, and the detailed review of the past related work on the factors affecting the electrode-skin impedance.

Chapter 3 describes the methodology used in this doctoral research for the study of the human skull resistivity, including the determining of the basic requirements and design considerations of the gated capillary action bio-potential sensor.

Chapter 4 presents the proposed head profile measurement and categorization system that was set up to determine the feasibility of using the current commercial head-caps for the gated capillary action bio-potential sensor on the Asian population.

Chapter 5 presents the study of the human scalp impedance distribution so as to develop a novel self-clamping headset design to be used with the gated capillary action bio-potential sensor.

Chapter 6 presents the principle and design of a novel gated capillary action bio-potential sensor which utilizes the combined effect of skin compression and electrolyte gel. This novel gated capillary action bio-potential sensor was integrated into the driving mental fatigue detection system and the performance of the developed bio-potential recording system presented.

CHAPTER 2

LITERATURE REVIEW

2.1 EEG Basics

2.1.1 Physiological Background of EEG

The discovery of the measurement of scalp EEG in 1929 by the German psychiatrist Hans Berger was a historical breakthrough that provided a novel neurologic and psychiatric diagnostic tool at the time, considering the lack of the other neurodiagnostic tools, such as CT and MRI, without which neurologic diagnosis and planning neurosurgical operative procedures would then be unconceivable. It was understandable that brain electrical stimulation produces contra-lateral motor response, but it was unknown then that a spontaneous brain electrical current could be recorded.

The discovery of EEG was a milestone for the advancement of neuroscience and neurosurgical everyday practice, especially for patients with seizures. The real nature of the disease was unknown at that time, and through Berger's persistent hard work he overcame the technical obstacles involved in the experiments. The discovery of EEG revolutionized modern daily neurologic and neurosurgical procedures, till the advent of computer tomography. Nowadays its importance is not as great as it was before, but it still has its place in the diagnostic work-up of seizures, brain tumors, degenerative brain changes, and other diseases.

2.1.2 Properties of EEG

Typical clinical EEG measured from the surface of the cortex has a frequency band that ranges from 0.1 to 100 Hz with amplitudes that can vary between $500\mu\text{V}_{\text{p-p}}$ to $1500\mu\text{V}_{\text{p-p}}$. However, when it is volume conducted to the scalp, the EEG is attenuated considerably and typically ranges below $50\mu\text{V}_{\text{p-p}}$ for adults. This measured amplitude is highly sensitive to the location of the electrodes and that of the inter-electrode distance (Niedermeyer 2005a). EEG is not only restricted to frequencies ranging from 0.1 to 100 Hz as there are some ultraslow EEG, that has its frequency band starting from DC, and ultrafast EEG that has a frequency range of 400 to 1000 Hz.

Conventional EEG is well known for its good temporal resolution on the sub-millisecond scale, but with also a poor spatial resolution that is affected by blurring due to volume conduction through the tissue of different conductivities. This poor spatial resolution can be improved by means of increasing the number of electrodes and by advanced algorithms to reduce blurring; however the former is always preferred as signal processing may lead to the loss of important EEG signals.

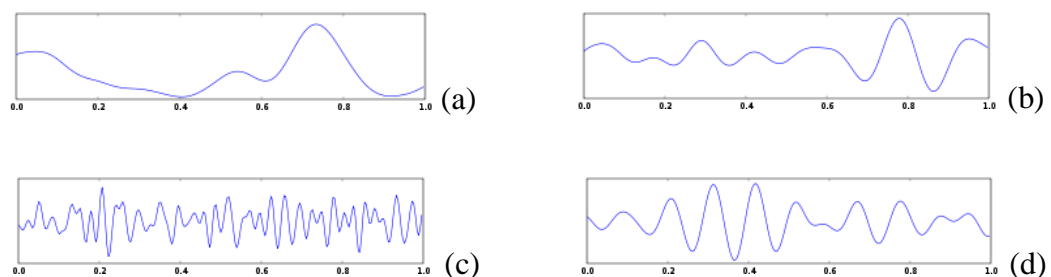


Figure 1: Typical EEG Waves

Brain waves have been categorized into four basic groups namely the (a) delta waves ranging from 0.5 to 4 Hz, (b) theta waves ranging from 4 to 8 Hz, (c) beta waves that

are greater than 13 Hz, and the (d) alpha waves ranging from 8 to 13 Hz as shown in Figure 1. The most extensively studied rhythm of the human brain is the alpha rhythm which can be induced by closing the eyes and by relaxation and it can be significantly observed in the posterior and occipital regions with typical amplitude about $50\mu\text{Vp-p}$. This wave can be abolished by opening of the eye or by increasing the alertness level by means of thinking, concentrating or calculating. Most subjects are remarkably sensitive to the phenomenon of “eye closing”, for which their wave pattern significantly changes from beta into alpha waves when they close their eye. Alpha waves are usually attributed to summated dendrite potentials but their precise origin has yet to be discovered. EEG is highly sensitive to a continuum of states ranging from stress, resting, and sleep. During normal state of wakefulness with open eyes beta waves are dominant, however when one is feeling drowsy or in the relaxation state, alpha activity rises (Bickford 1987).

2.1.3 Measurement of EEG

Standard EEG measurements employ a recording system consisting of (1) electrodes with conductive media, (2) amplifiers with filters, (3) A/D converter, and a (4) recording device. Electrodes read the signal from the head surface, amplifiers bring the microvolt signals into the range where they can be digitalized accurately, converter changes signals from analog to digital form, for storage and display of the obtained data. EEG allows for the measurement of potential changes over time in basic electric circuit conducting between the active electrode and reference electrode. An extra ground electrode is then needed to obtain the differential voltage by

subtracting the same voltages at both the active and reference electrodes. Current state-of-the-art allows for multi-channel configurations comprising of up to 128 or 256 active electrodes (Teplan 2002).

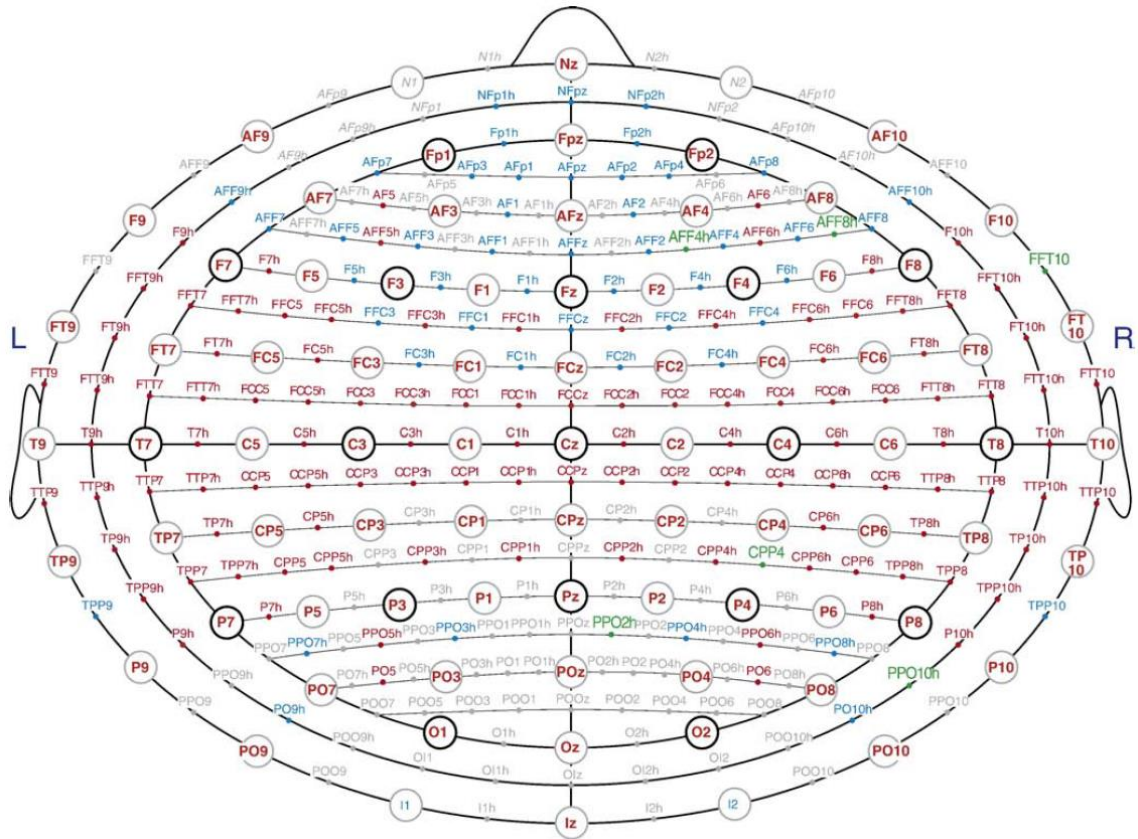


Figure 2: The UI 10/5 system (Valer, Daisuke and Ippeita 2007)

For the ease of communication between researchers the location of the EEG measured, the standard international 10-20 system is typically used (Jasper 1958). This system consisting of 21 electrode locations positioned at regular 10% and 20% intervals in accordance to 4 reference points namely the inion, the nasion, and the left and right pre-auricular points is still widely practiced in clinical settings. With technological advancement, better amplifiers were developed to satisfy the constant need to have an increased number of electrodes. This led to the birth of multichannel

arrays having more than 21 electrodes as determined by the standard international 10-20 system. The current state-of-the-art, as shown in Figure 3, showcases a 10-5 electrode system by Oostenveld and Praamstra (2001) that make use 345 electrodes for the recording of high resolution EEG.

EEG measurements were typically conducted by directly placing the electrodes individually on the scalp but the advent of multichannel array EEG systems made direct placement not feasible due to the long preparation time required prior to the recording of EEG. This led to the birth of EEG caps that can cater to a wide range of electrodes being placed on it ranging from 21 electrodes to 256 electrodes, as shown in Figure 3. The usage of EEG caps undermines the ability of the electrodes being precisely placed at standard locations but it can be overcome by the use of digitizers to register the locations of all the electrodes.

The nomenclature for the electrode locations follows a set of simple rules and they are as follows: (1) electrode names consist of a single or multiple letters, combined with a number, (2) electrodes on the left are numbered odd, electrodes on the right are numbered even, (3) electrodes on the midline are appended with the letter z representing zero to avoid confusion with the letter “O”, (4) electrodes near the midline have the smallest numbers, and they increase towards the side, and (5) the letter indicates the location on the head for which **Fp** represents the *frontal pole*, **F** represents the *frontal lobe*, **C** represents the *central lobe*, **T** represents the *temporal lobe*, **P** represents the *parietal lobe*, and **O** represents the *occipital lobe*. Combinations of two letters indicate intermediate locations such as **FC** representing

locations in between frontal and central electrode locations while **PO** representing locations in between parietal and occipital electrode locations.

Combining these rules gives straight forward labels for all electrode positions. The contour in between the frontal pole (Fp) and the frontal (F) electrodes is called “AF” (anterio-frontal). The electrodes overlying the temporal lobe are indicated with a T. In the original 21 channel 10-20 standard, the electrodes in the central contour that runs from the vertex towards the left ear are labeled Cz-C3-T3 with the intermediate locations C1 and C5 added in the extended system, and location T3 was renamed to T7.

Similarly, electrode T4 (old) has been renamed to T8 while the parietal-temporal electrodes T5 and T6 (old) have been renamed to P7 and P8. Electrode T7 and T8 would correspond to C7 and C8. The fronto-central (FC) electrode row and the parieto-central (CP) electrode row use the letter T for the electrodes overlying the temporal lobe. You only need to remember that “T” in the official extended 10-20 system always can be read as “C”. The electrode names T3, T4, T5 and T6 are still commonly used in clinical EEG with 19 or 21 channels, but they are not applicable in experimental ERP studies.



Figure 3: Standard EEG system with EEG caps

2.1.4 Distribution of EEG electrodes

The distribution of the EEG electrodes on the scalp can be categorized into two different types, namely the homogenous and the inhomogeneous. In the inhomogeneous model, the most famous of all is the 10/20 system. According to Suihko, Malmivou and Eskola (1993), this arrangement caused electrodes at the occipital lobe to be placed closer to each other.

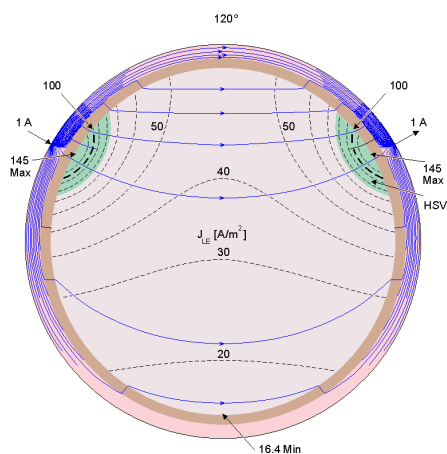


Figure 4: Effect on EEG by electrodes located within 120 deg

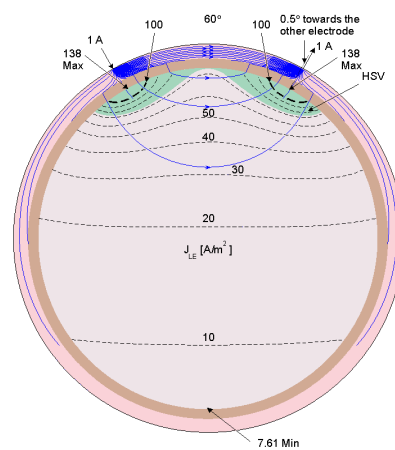


Figure 5: Effect on EEG by electrodes located within 60 deg

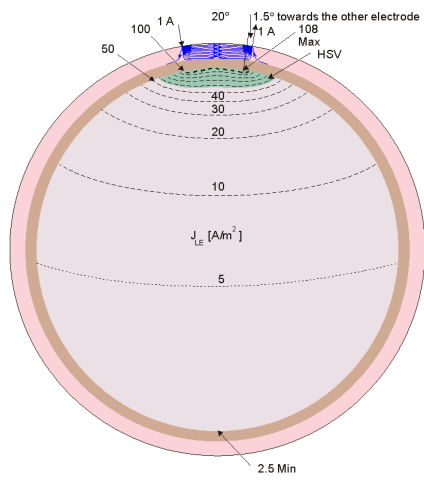


Figure 6: Effect on EEG by electrodes located within 20 deg

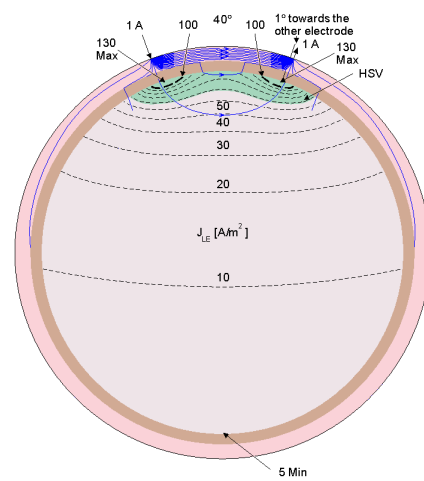


Figure 7: Effect on EEG by electrodes are located within 40 deg

They did a study on the electrode distribution in an inhomogeneous spherical head model and found that as the electrodes near, a greater lead field within the region was felt and as sensitivity decrease, the noise level increases. However, in the homogenous model where the electrodes are located within 180° , the sensitivity typically increases and the noise decreases.

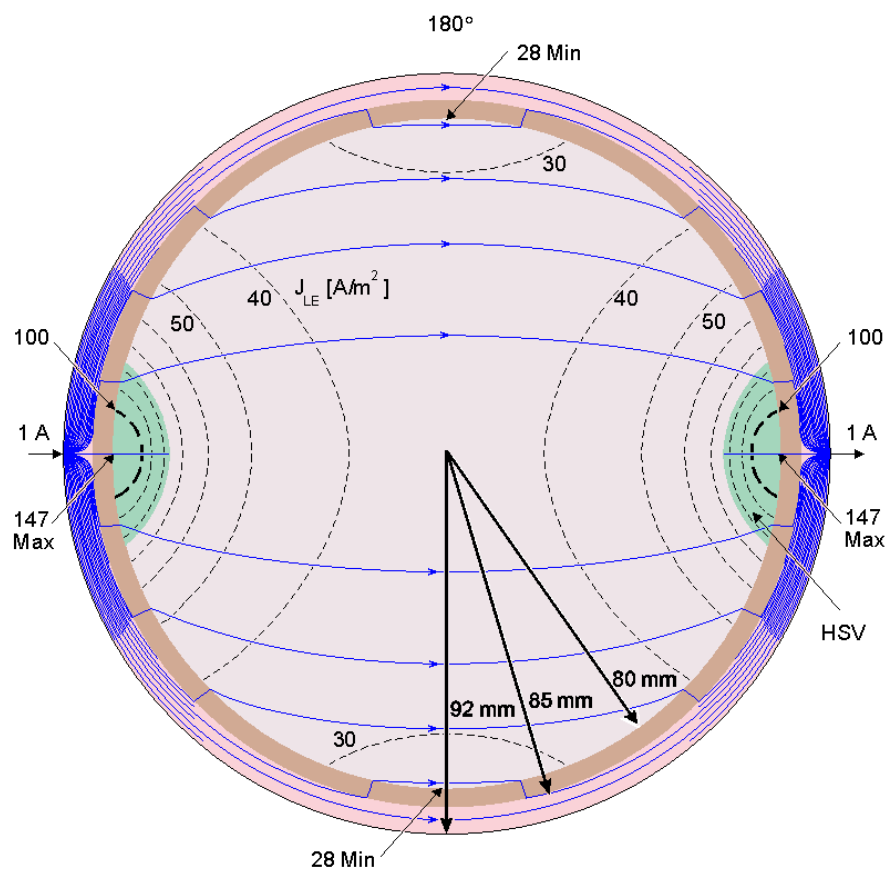


Figure 8: Effect on EEG by electrodes are located within 180°

2.2 Factors Affecting Electrode-Skin Contact Impedance

There are also other factors affecting the electrode-skin contact impedance that must be taken into account. For instance, the type of electrode used, intra and inter-human variations, the skin preparation technique used can affect the contact impedance to various degrees (McAdams, et al. 1996). Electrodes used for EEG recordings can either be of the wet or dry variety for which wet electrodes can be categorized as hydrogels or 'wet' gels.

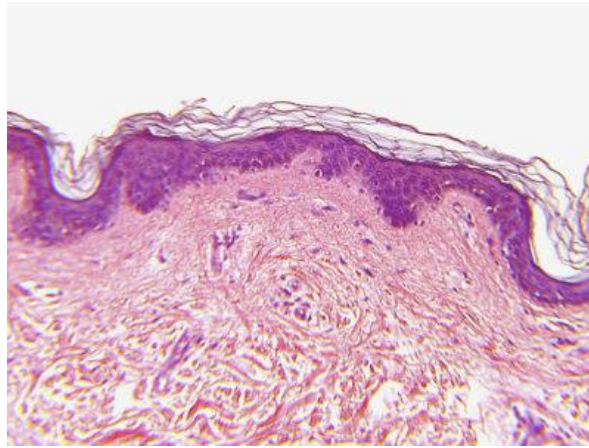


Figure 9: Cross-sectional view of the human skin

Standard 'wet' electrodes work by rapidly filling up the pores and wrinkles in the skin under the electrode and in the process ensuring maximum effective contact area (McAdams, et al. 1996). It was also found that the skin's resistance tended to decrease in an exponential manner as the ions in solution diffused through the skin to make it more conductive (McAdams, et al. 1996). On top of that, hydrogels have the disadvantage of being hydrophilic (McAdams, et al. 1996). It must also be noted that perspiration on the scalp, resulting in a release of an ionic salt solution, would in

effect reduce the electrode-skin impedance and this will cause an unstable impedance reading which will induce noise.

Dry electrodes are those that have metal in direct contact with the skin (Taheri, Knight and Smith 1994) and a key disadvantage of dry electrodes is that they result in higher contact impedances (Taheri, Knight and Smith 1994). This has been overcome by amplifiers that can pick up signals resulting from high impedances however as the experiment time lengthens and the subject sweats, impedance reading will become unstable inducing noise

Intra and Inter-human variations such as the density of sweat glands, density of hair follicles and variations in the thickness of the stratum corneum can affect electrode-skin contact impedance. For instance, it was found that skin impedance was higher for dark skinned subjects as compared to light skinned subjects due to a higher thickness of the stratum corneum in dark skinned subjects (McAdams, et al. 1996).

Additionally, while the thickness of the stratum corneum did not vary significantly with age or sex (Kligman 1984), slightly higher skin impedance values were reported for females as compared to males (Lawler, Davis and Griffith 1960). It was also noted that an increased density of sweat glands, hair follicles and an unsubstantial thickness of the stratum corneum on the scalp gave rise to skin impedances that were one of the lowest as compared to other sites on the body (McAdams, et al. 1996).

To ensure that all the electrodes have similar skin impedance, the method of scraping of the skin to reduce the electrode-skin contact impedance is often used. However, the usage of the traditional wet electrode appears to render the uncomfortable and time-

consuming scraping procedure less necessary as the electrolyte penetrates the skin within a few minutes (McAdams, et al. 1996).

2.2.1 Effect of Electrode Material on EEG Signal Quality

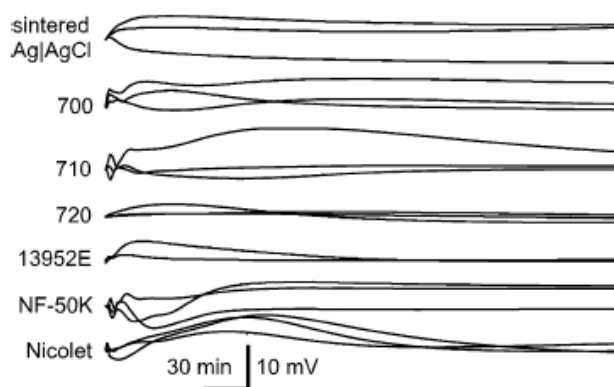


Figure 10: Long-term DC-stability of Ag/AgCl electrodes in continuous recordings

The impedance of the SC is the largest component in the overall skin impedance (Mcadams and Jossinet 1991) and there is a great demand for smaller EEG electrodes in bio-potential recording applications. Ag/AgCl clearly emerges as the best material in long-term DC-stability of Ag/AgCl electrodes in continuous recordings, as shown

Table 1: Summary of the properties of different types of electrodes when used in combination with a chloride containing gel

Electrode	Offset voltage, resistance and polarization	Rate of drift	Noise level	Suitability for DC-coupled recording	Suitability for long time-constant AC-coupled recording
Sintered Ag/AgCl	Very low	Very low	Low	Excellent	Excellent
Disposable Ag/AgCl	Low	Very low	Low	Good	Excellent
Silver	Variable	Variable	Low	Poor	Good
Gold-plated silver	Variable	Variable	Low	Poor	Good
Platinum	Very high	N.A.	Low	Poor	Good
Stainless steel	Very high	N.A.	Medium	Poor	Medium

in Figure 4, as other types of reusable electrodes suffered from diverse degrees of polarization, baseline drift, low-frequency noise, high resistance, and changes in properties due to wear and tear (Tallgren, Vanhatalo, Kaila, & Voipio, 2005).

2.2.2 Effect of Electrolyte on EEG Signal Quality

Electrolyte allow for a stable electrical contact to be established between the electrode and the skin on top of decreasing the high stratum corneum impedance. There exist two main types of electrolytes, namely the liquid gels and hydrogels.

The liquid gel comes in forms of different viscosity level, and may sometimes be in the form of a paste or cream. Standard electrolyte is usually made out of water, thickening agent, bactericide, fungicide, ionic salt and surfactant (Carim 1988). The ionic salt ensures the electrical conductivity of the gel by mimicking the major ions presented in bodily cells and fluids such as sweat are Na, K and Cl ions. Hence, the most commonly used salt in electrode gels are NaCl and KCl to ensure biocompatibility.

Hydrogels are 'solid' gels that incorporate natural hydrocolloids such as karaya gum or synthetic hydrocolloids such as polyvinyl pyrrolidone (Carim 1988). The use of hydrogels entails numerous advantages, such as its ability to be manufactured into a thin, lightweight and highly flexible electrode arrays with accurately defined electrode/gel areas, shapes and inter-electrode distances and to cause lesser skin irritation than liquid gels while being able to accommodate to the skin contours and irregularities, thus increasing the effective contact area with the skin.

However, hydrogels tend to be more resistive than liquid gels ranging from 800 to 8000 Ω /cm while liquid gels are in the order of 5-500 Ω /cm (McAdams and Jossinet 1991). As such, the liquid gel is preferred over hydrogels as high resistance results in a high voltage drop thus reduce the SNR of the EEG recorded.

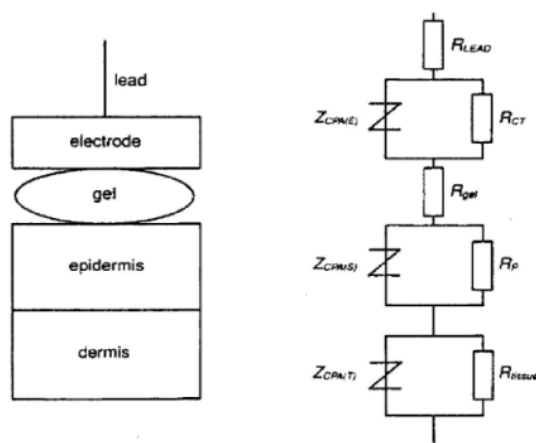


Figure 11: Equivalent circuit model of the electrode-electrolyte-skin interface

In EEG measurements, the use of low-impedance electrodes means that the electrode impedance may be ignored as the skin impedance is the dominant impedance. The skin impedance between the unprepared human skin and abraded skin with stratum corneum barrier layer removed can be very different when the electrolyte gel is used as a medium between the electrode and the skin. The skin is generally modeled as a parallel RC circuit as shown in Figure 11 (McAdams, et al. 1996). Over time, many other electrode-electrolyte models were developed for the different electrodes and they are as follows:

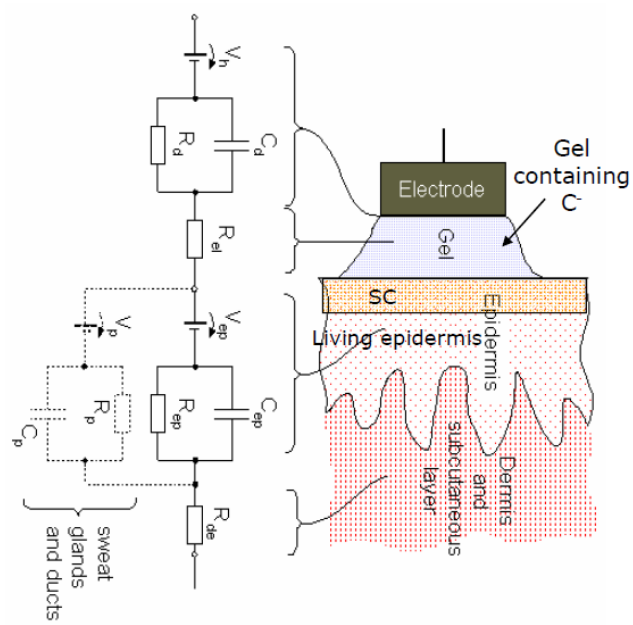


Figure 12: Equivalent circuit model for the conventional wet electrode

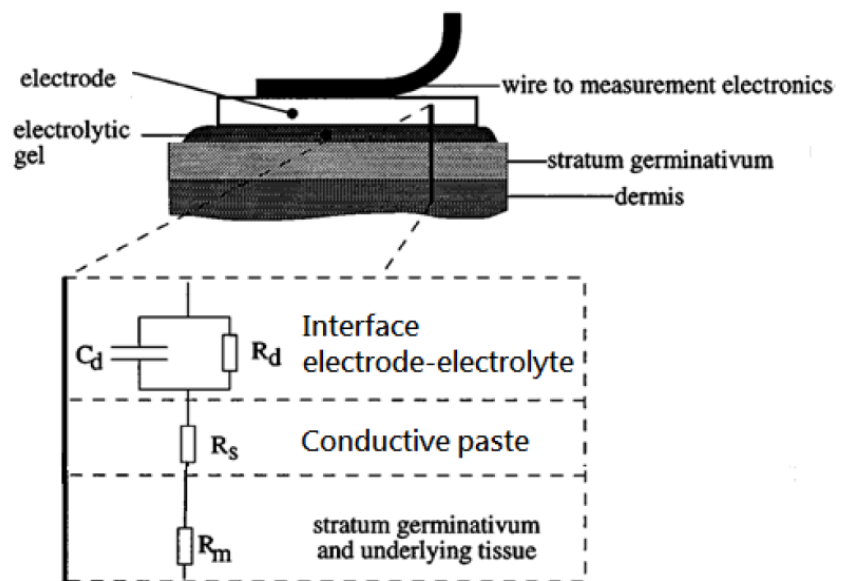


Figure 13: Equivalent circuit model for the cup electrode

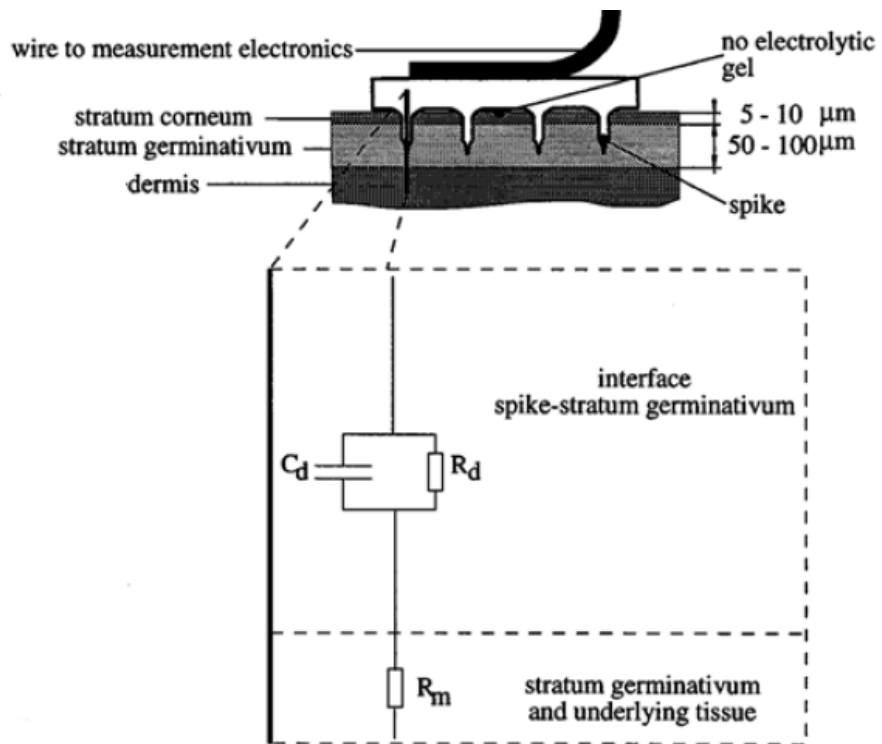


Figure 14: Equivalent circuit model for the spike electrode

2.2.3 Effect of Impedance on EEG Signal Quality

During EEG recordings, electric potentials are measured on the scalp surface and used to detect and localize the activity of the brain. Prior to computer based EEG recording, EEG signal quality was dependent on achieving a scalp-electrode impedance of less than 5k Ω in order to separate it from power line noise.

We know that a potential drop occurs whenever an electric current flows through impedance. A higher impedance value will result in a higher voltage drop at the scalp-electrode interface and some attenuation of signal amplitude, resulting in a loss of data quality (T. C. Ferree, et al. 2001).

One method that has been explored to overcome this voltage drop is through the design of amplifiers that have input impedance which is much higher than that off the scalp-electrode interface (T. C. Ferree, et al. 2001). Higher impedance values also tended to result in higher impedance mismatches (Jurcak, Tsuzuki and Dan 2007). Mismatched input electrode impedances can lead to noisy EEG and evoked potential recordings even if the electrode impedances are low (Legatt 1995).

It was observed that balanced input electrode impedances were particularly important during intra-operative monitoring, when ambient electrical noise levels are usually high (Legatt 1995). Thus, there is a clearly identifiable need to improve EEG signal quality by both reducing the scalp-electrode impedances and also by eliminating impedance mismatch to the greatest extent possible.

2.3 Electrical Impedance of the Human Head

2.3.1 Electrical Impedance of the Skull

Presently, there are many skull resistivity studies known from past research via in-vitro or in-vivo experiments and the range of the skull resistivity from these experiments varies greatly. The earliest in-vitro experiment attempts to acquire the bone resistivity used animal bone in in-vitro experiments (Kosterich 1983). These experiments has many drawbacks such as the taking of readings from animals bone sample would be insufficient and inaccurate, considering the large variation in density, homogeneity, thickness and directional properties that are characteristic of the human bone. Furthermore, the skull consists of 3 layers, the outer compact layer, the inner cancellous layer (spongiosum) and the inner compact layer (bulk layer) and each of these layers possess different resistivity,

Cancellous bone composes of a lattice or network of branching bone spicules or trabecular and is porous while compact bone appears as a mass of bony tissue lacking spaces visible to the unaided eye. Two outer layers for the human skull consist of the compact, dense tissue which surrounds the cancellous tissue. The resistivity of the skull is not uniformed and this is due to the inhomogeneous tri-layers in the skull (Law 1993). Furthermore, the thickness and density of the different layers varies with the different location on the human skull as seen from this study and experiments on compact and cancellous layers had been shown to give different resistivity value (Akhtari 2002).

Current flows from the brain through the skull and the scalp during an EEG recording. It is also commonly understood that the low conductivity and thickness of the skull affects both the amplitude and the current arising from cortical activity resulting in poor EEG data quality (Eskola, et al. 1998). Previous studies have identified the conductivity ratios between the brain, the skull and the scalp to be 1: 1/15: 1 (Oostendorp, Delbeke and Stegeman 2000). With the skull having the lowest conductivity, it is reasonable to assume that variations in the skull thickness would impact scalp impedance readings significantly. In fact, a finite element model of the skull incorporating features such as a hole in the skull and lesions suggested that the skull conductivity values would differ significantly from a skull without these features (Broek, et al. 1998).

Thus to ensure comparable readings it is important to ensure that subjects have not had any kind of surgery or major injury to the skull. The area on top of the head has generally been found to have lesser soft tissue and is bonier than at the sides and back of the head (Ustuner 2008). The electrical resistivity could be derived by injecting current and measuring the potential difference, also known as the EIT method. Nevertheless, the amount of information that could be extracted from the potential difference measurement is limited due to the isolating effect of the skull which causes a large amount of current to flow through the skin. To further extract information from the potential difference measurement, a realistic head model has been used to solve this forward problem (Gonçalves 2003).

In the BEM analysis, the realistic head model is taken from MRI and modeled as a volume conductor with 3 compartments, namely the scalp, skull and the brain as

shown in Fig 5. An assumed scalp to skull to brain resistivity ratio is used in the analysis thus it forms the limitations of the BEM method and this introduction of the ratio is bound to introduction errors for the BEM analysis.

2.3.2 Electrical Impedance of the Skin

Several studies have asserted the dominant effects of the electrode-skin contact impedance in determining the overall impedance values at a particular location on the scalp (Hua, et al. 1993) (Taheri, Knight and Smith 1994) especially at the frequencies associated with EEG recordings (McAdams, et al. 1996). Hence, reducing the electrode-skin contact impedance becomes a priority in reducing overall impedance values. It is thus advisable to first examine the impedance properties of human skin.

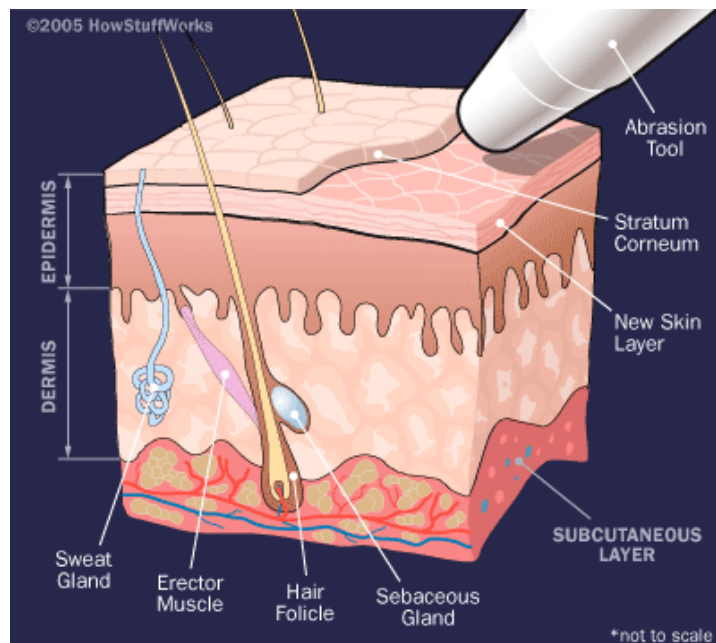


Figure 15: A cross-sectional view of the human skin

Studies identified that the largest obstacle to ideal electrical behavior of the electrode-skin interface is the horny layer of the epidermis, called the stratum corneum, which

acts as a barrier to ionic current and thus significantly increases the impedance of the interface, particularly at the low frequencies at which EEG measurements tend to be taken (Alba, et al. 2010). Typically in a standard EEG recording, the stratum corneum is removed by scraping prior to electrode application; an extremely time consuming process and also a potentially hazardous one (T. C. Ferree, et al. 2001). In a prior experiment, the electrical impedance values were measured at varying thicknesses of the stratum corneum which was removed through the application of sodium lauryl sulphate (Nicander, et al. 1995).

It was found that electrical impedance decreases with a reduction in the thickness of the stratum corneum (Nicander, et al. 1995). The same study also found that there is great individual variability in the barrier properties of the skin even for subjects of the same age and gender. In a study on the volar forearm, it was found that there was a decrease in local impedance in response to mechanical, electrical or thermal stimulation. It was also found that when pressure was continuously applied, the impedance drop peaked in about 15 to 25 seconds (Edelberg 1973).

In another experiment on skin relaxation after stretching, it was found that the impedance value dropped by 100% and this change occurred rapidly within 10 seconds from the time of relaxation (Odman 1981). It is thought that mechanical stress on the skin causes a reduction in resistivity of the stratum corneum hence leading to lowered impedance values (Odman 1981). It is thus reasonable to hypothesize that a similar drop in local impedance values should be expected for readings taken from the scalp.

2.4 Advantages and Limitations of EEG

EEG is widely used as it is able to provide good temporal resolution clinical diagnosis, on the order of milliseconds, with low hardware costs as compared to other neuro-diagnostic methods. On top of that, EEG machines are portable and can be deployed into a wider variety of environments and are relatively tolerant of subject movement as the artifacts can be removed by means of signal processing. Furthermore, usage of EEG is silent thus making it a better candidate for the study of the responses to auditory stimuli. In addition, the nature of its setup does not aggravate claustrophobia in subjects that may sometime induce unnecessary errors in the data collected.

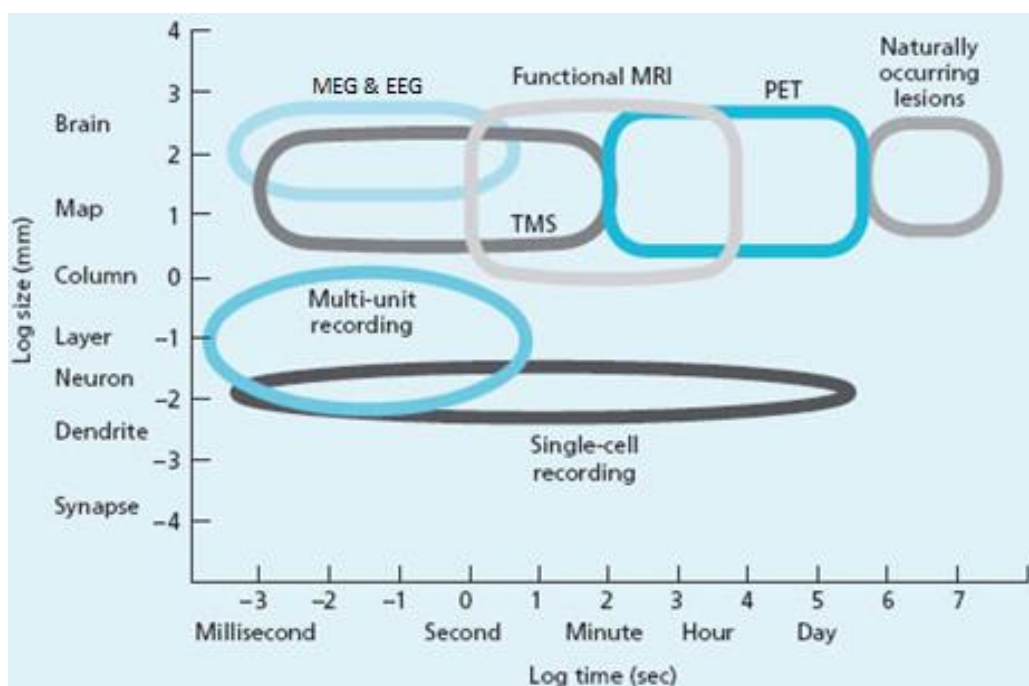


Figure 16: Spatial and temporal resolution of various neuro-diagnostic methods

EEG has several limitations and most importantly is its poor spatial resolution which is at least 100mm in size compared to that of the fMRI which is in tens of millimeters.

However, caveats have to be taken into consideration in the integration of the methods as EEG is a direct measure of the neuro-physiological activity but not fMRI. FMRI studies measure the change in blood oxygenation over time as blood oxygenation levels change rapidly following the activity of neurons in a brain region. As there is no direct correlation to brain activation, the images produced by fMRI must be interpreted carefully as brain processes are complex and often non-localized.

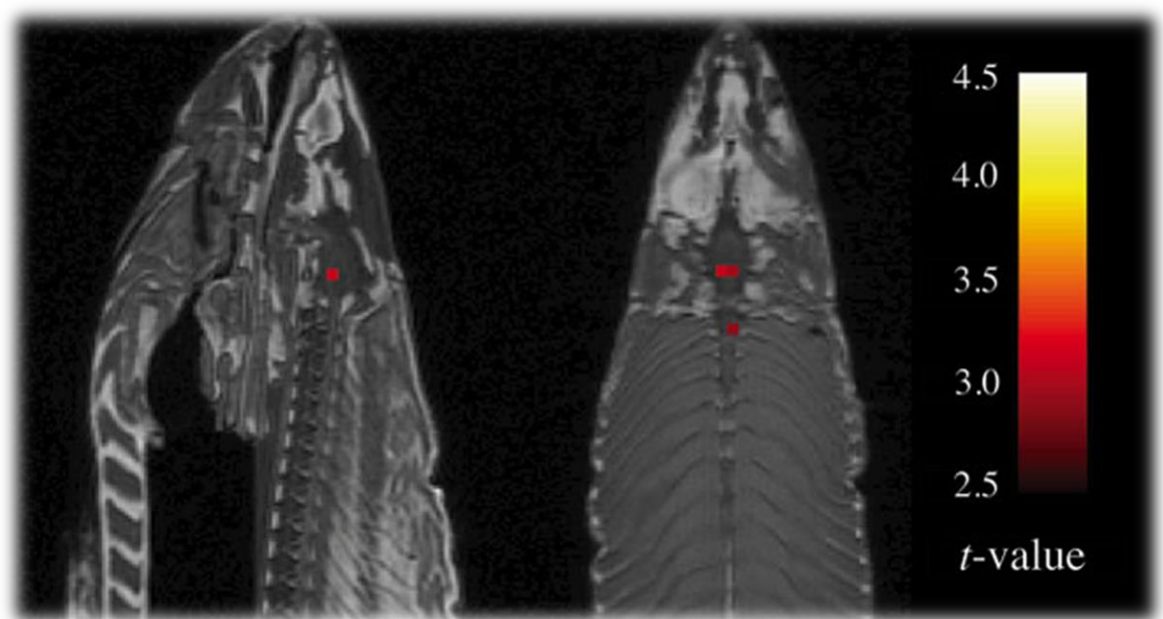


Figure 17: fMRI results on a dead salmon

On top of that, statistical methods used in the interpretation of fMRI data must be used carefully because they can produce false positives. This is evident in an experiment aimed at the studying of the reactions by a dead salmon to pictures of human emotional expressions. In this experiment, it was reported that there are a few activated voxels in the brain of a dead salmon when no correction for multiple comparisons was applied, illustrating the need for rigorous statistical analyses when considering the use of fMRI (Craig, et al. 2010).

CHAPTER 3

IN-VITRO STUDY OF THE HUMAN SKULL RESISTIVITY

Presently, many skull resistivity values are known from past research via in-vitro or in-vivo experiments (Oostendorp, Delbeke, & Stegeman, 2000), the range of the skull resistivity from these experiments varies greatly. The earliest in-vitro experiment attempts to acquire the bone resistivity used animal bone in in-vitro experiments (Kosterich, 1983). These experiments hold many drawbacks, taking reading from animals bone sample would be insufficient and inaccurate, considering the large variation in density, homogeneity, thickness and directional properties that are characteristic of the human bone. Furthermore, the skull consists of 3 layers, the outer compact layer, the inner cancellous layer (spongiosum) and the inner compact layer (bulk layer). These layers possess different resistivity (Akhtari, 2002), and they differ from animals and humans.

The human skull consists of 3 layers and composed of two types of tissue, which are the compact and cancellous (spongy) tissue. Cancellous bone composes of a lattice or network of branching bone spicules or trabecular and is porous while compact bone appears as a mass of bony tissue lacking spaces visible to the unaided eye. Two outer layers for the human skull consist of the compact, dense tissue which surrounds the cancellous tissue. The resistivity of the skull is not uniformed and this is due to the inhomogeneous tri-layers in the skull (Law, 1993). Furthermore, the thickness and

density of the different layers varies with the different location on the human skull as seen from this study and experiments on compact and cancellous layers had been shown to give different resistivity value (Akhtari, 2002).

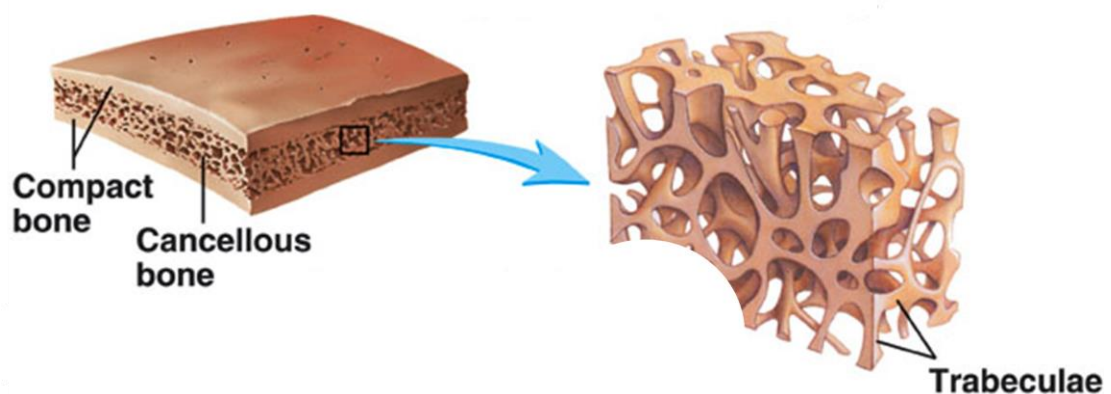


Figure 18: Layers of Different Bone Tissue of the Human Skull

The skull to brain resistivity ratio is an important parameter used in BEM and EEG analysis, thus an accurate ratio is necessary to reduce errors in calculating the extracranial magnetic fields and electric potentials produced by intracranial sources of activity. In the past, several studies to obtain the skull resistivity are based on a combination of EIT and BEM analysis. These methods mainly use a resistivity ratio of brain, skull, and scalp, which differs from different studies, 1:15:1 (Oostendorp, Delbeke, & Stegeman, 2000) and 1:20-50:1 (Gonçalves, 2003).

The use of BEM method is susceptible to errors in the introduction of the ratio (Gonçalves, 2003). Thus, the past experiments have not produced skull resistivity of dependable values with respect to microstructure and thickness. EIT method utilizes the 10-20 head positioning system for electrode placement. In principle, the information about one's electrical resistivity could be derived by injecting current and

measuring the potential difference, this is also known as the EIT method. Nevertheless, the amount of information that could be extracted from the potential difference measurement is limited due to the isolating effect of the skull which causes a large amount of current to flow through the skin. To further extract information from the potential difference measurement, the BEM analysis using a realistic head model is used to solve this forward problem of EIT.

In the BEM analysis, the realistic head model is taken from magnetic resonance scan and molded as a volume conductor with 3 nested compartments, mainly the scalp, skull and brain (Gonçalves, 2003) as shown in Figure 20. The downside of the BEM method is that it uses an assumed scalp to skull to brain resistivity ratio, therefore introducing errors into the BEM analysis.

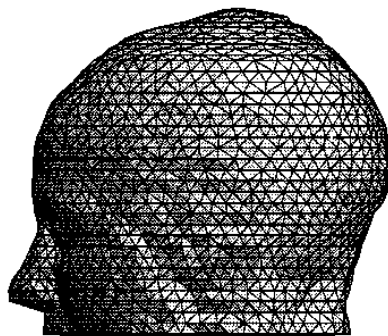


Figure 19: Magnetic Resonance Image of
Realistic Head Model

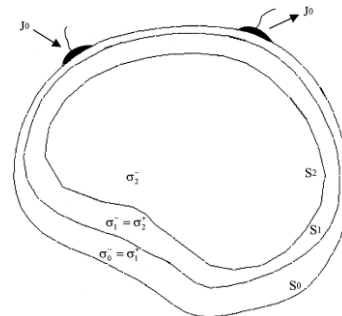


Figure 20: Schematic Representation of BEM
model

3.1 Regions of Interest for Skull Impedance Measurement

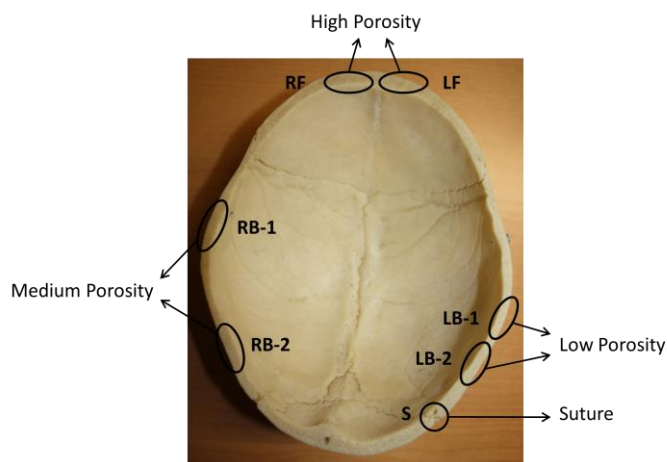


Figure 21: Locations for which readings were taken

An experiment on different locations of the human cadaver was done so as to study the feasibility of having a correlation between the skull's impedance and that of the scalp's impedance distribution obtained. As such, the experiment was conducted on particular points of the standard international 10-20 system (Jasper 1958) with the locations measured are as labeled in Fig 22. Measurements from the front, middle and rear portion of the skull with different thickness would be taken.

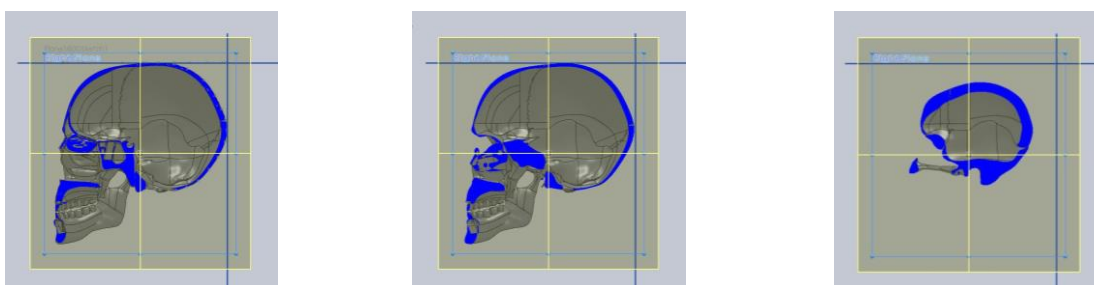


Figure 22: Skull Model Constructed from MRI scans

To allow us to understand the effect of skull impedance to its thickness, the skull model was reconstructed from a MRI scan. With the MRI scan, we are able to determine the thickness and the exact profile of the skull.

3.2 Experiment Setup

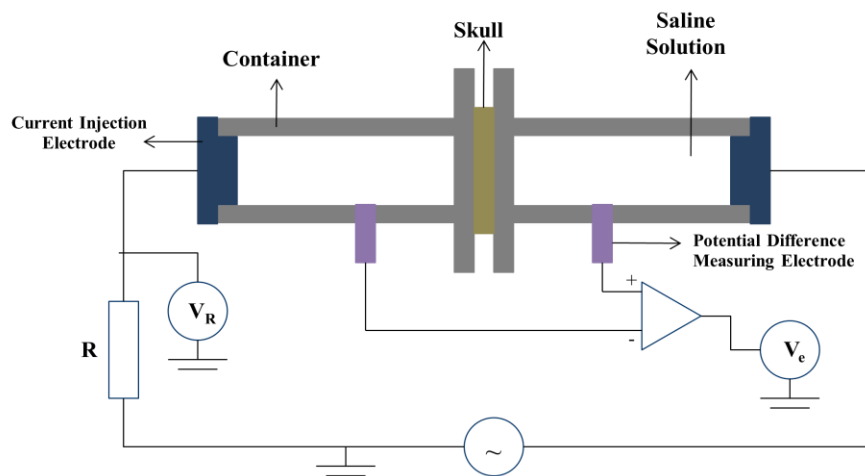


Figure 23: Schematic of the In-Vitro Experiment Setup

The skull sample would be placed in between the experiment main body and the holder clamped with the use of G-clamps which varied according to the different skull thickness. To measure the resistivity of the human skull, a current is passed through the skull and the potential difference measured, as shown in Figure 23. Current from a source with a 5Vp-p was passed through the setup from the pair of electrodes positioned at both ends of the setup. The resulting potential difference is then measured at frequencies of 20Hz, 50Hz and 100Hz.

3.2.1 Saline Solution

Saline solution of 1.3 S/m, similar to the cerebral-spinal fluid was used as the electrolyte. It was made by mixing 0.7 grams of sodium chloride in one liter of distilled water. Studies have shown that the amount of fluid that permeates the bone structure and its dielectric properties primarily account for electrical properties of the

tissue and the conductivity of live skull tissue is expected to be due to the most abundant and most mobile electrolytes such as Na^+ and Cl^- (Law, 1993). Such fluids are cerebral spinal fluid which has conductivity of 1.54s/m and blood which has conductivity of 0.606s/m (Geddes, 1989), this equates to a similar saline conductivity of 1.3s/m to be used on the cadaver human skull.

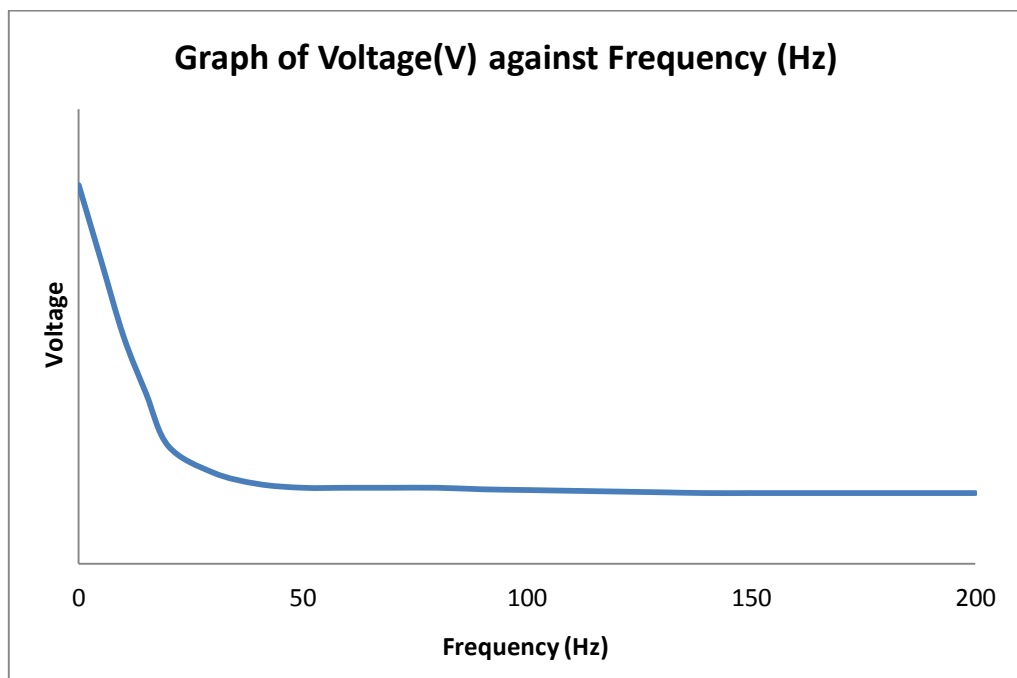


Figure 24: Characteristic of Frequency Respond of the Saline Solution

The experiment was performed over a low frequency range of 20Hz, 50Hz, and 100Hz. Low frequency were chosen as the effects of permittivity can be ignored and consider only conductivity. In general, at low frequency (below 1kKz), the potential difference between the voltage electrodes only varies slightly or is constant, and the linear dependence of the potential difference of the different skull sample would be obeyed. At higher frequency, other parameters of the system other than the skull sample evidently influence the measured potential difference. Moreover, the skull has

low pass frequency characteristic, therefore if high frequency is used, they would be omitted, and in this process, the calculated resistivity would not be accurate.

The frequency of 20Hz, 50Hz and 100Hz were chosen for this experiment due to the characteristic of the frequency responds curve, as shown in Figure 24. At 20Hz the graph is seen with a downward slope and it stabilizes at around 40Hz. Readings were taken at 50Hz and 100Hz as the stabilized readings do not differ much after 100Hz and also to keep within the low frequency range. To ensure that the volume of saline in the main body remains the same throughout the experiment, it is performed with the human cadaver skull soaked in saline.

3.2.2 Setting up of the Skull Sample

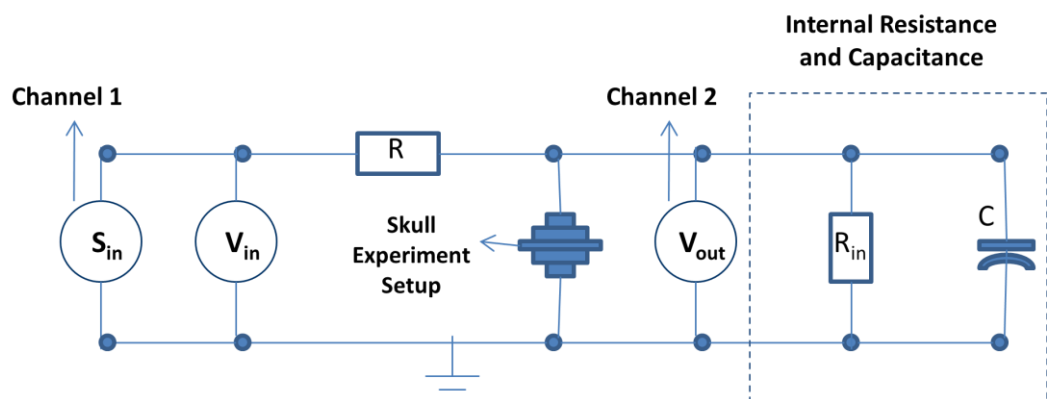


Figure 25: Schematic Drawing of Electric Circuit

The setup was designed according to the diagram in Fig 25 using Ag/AgCl as the electrodes with a saline that has a conductivity of 1.3S/m, which is similar to that of the CSF. The injection source and potential difference measurements were made by the Agilent 36670A Dynamic Signal Analyzer. Prior to the measurement, the

system's impedance was measured so as to ensure that the impedance measured is that of the skull only.

The impedance of parallel RC circuit is as

$$Z_{RC} = \sqrt{\left(\frac{R \cdot X_c^2}{R^2 + X_c^2}\right)^2 + \left(\frac{R^2 \cdot X_c}{R^2 + X_c^2}\right)^2}, \quad \text{where } Z_e = \frac{R \cdot V_{out}}{V_{in} - V_{out}} \text{ and } X_c = \frac{1}{2\pi f C}$$

By subtracting the system's impedance (Z_S) from that of the skull experiment's impedance (Z_E), the skull impedance could then be found by $Z_m = Z_E - Z_S$. With that, the resistivity of skull could be calculated by $\rho = \frac{1}{\sigma}$, where $\sigma = \frac{1}{Z_m} \cdot \frac{d}{\pi r^2}$.

The output voltage of the setup without the human skull attached to it would be taken first in order to provide the potential difference of the saline solution within the setup. Next, the output voltage of the setup with the human skull in place would be taken. This reading provides the potential difference of the skull and the saline solution. The impedance is then calculated base on the potential difference measured. To do so, the calculated impedance of the setup without the skull in place is removed from the setup with the skull in place, thus the giving the localized resistivity of the skull.

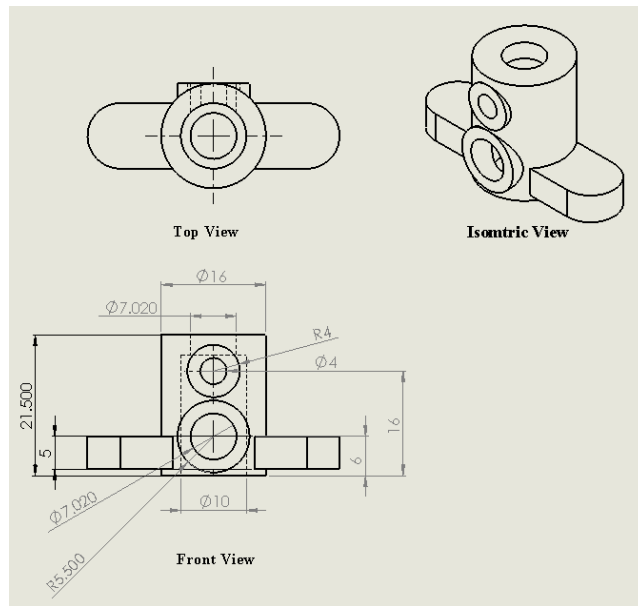


Figure 26: CAD drawing of the Holder

The holder is necessary to ensure that during every setup, a fixed distance is maintained between the measuring electrode and the skull; a skull of 5mm thickness has a clamping distance of 20mm and a skull of 7mm thickness would have a clamping distance of 22mm, the distance in between skull and clamp is always maintained at 15mm. The holder, as shown in Figure 26, was made to hold skull of thickness from 4mm to 7mm. To conform to the curvature of the skull, sponge is attached to the holder, giving the holder its functionality yet not exerting too much stress on the skull during the measurement.

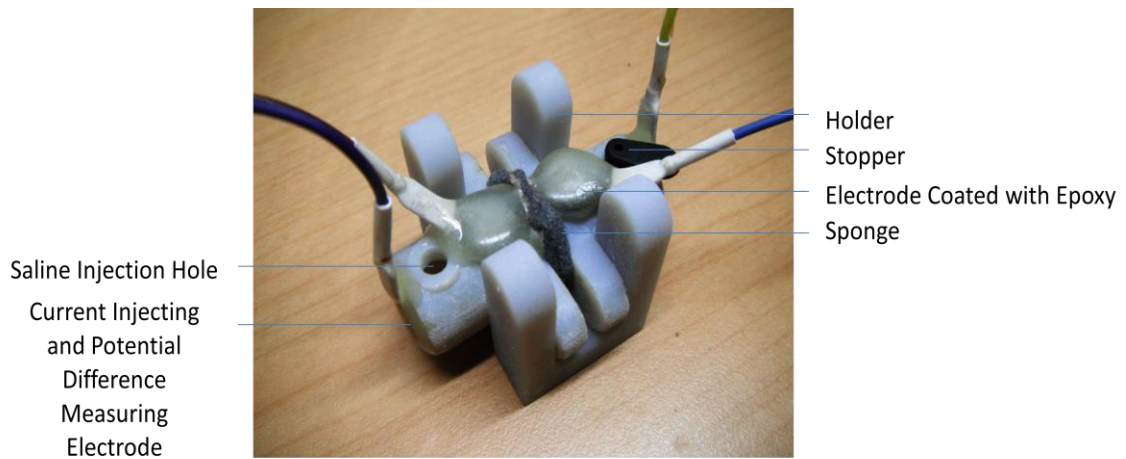


Figure 27: Experiment setup

The saline injection hole is created to allow for injection of saline into the holder, and to allow bubbles to escape from the holder prior to the start of the experiment. A stopper is then used to seal the saline injection hole. Subsequently, the experiment will be conducted with the skull fully soak in a container of saline solution. To prevent corrosion of the Ag wires that were attached to the AgCl electrode during contact with the saline, resulting in unstable impedance reading, the soldered connections were coated with epoxy.

3.3 Results and Discussions

Table 2: Skull Resistivity against Thickness

	Thickness (m)	Resistivity ($\Omega.m$)	
FREQUENCY: 20Hz	Low Porosity Region		
	Location: LB-1	0.0035	74.78
	Location: LB-2	0.0038	88.00
	Medium Porosity Region		
	Location: RB-1	0.005	54.44
	Location: RB-2	0.0045	56.25
	High Porosity Region		
	Location: LF	0.00535	52.00
	Location: RF	0.0055	53.74
	Sutures		
Location: S	0.005	3.18	
FREQUENCY: 50Hz	Low Porosity Region		
	Location: LB-1	0.0035	84.96
	Location: LB-2	0.0038	97.36
	Medium Porosity Region		
	Location: RB-1	0.005	73.36
	Location: RB-2	0.0045	63.28
	High Porosity Region		
	Location: LF	0.00535	55.07
	Location: RF	0.0055	61.76
	Sutures		
Location: S	0.005	9.68	
FREQUENCY: 100Hz	Low Porosity Region		
	Location: LB-1	0.0035	71.14
	Location: LB-2	0.0038	88.63
	Medium Porosity Region		
	Location: RB-1	0.005	71.91
	Location: RB-2	0.0045	56.51
	High Porosity Region		
	Location: LF	0.00535	48.32
	Location: RF	0.0055	54.83
	Sutures		
Location: S	0.005	3.88	

The results produced patterns in the resistivity with respect to the thickness of the human skull. The experiment was conducted on 7 locations of the skull, it consist of the low porosity region, medium porosity region, high porosity region and on the suture.

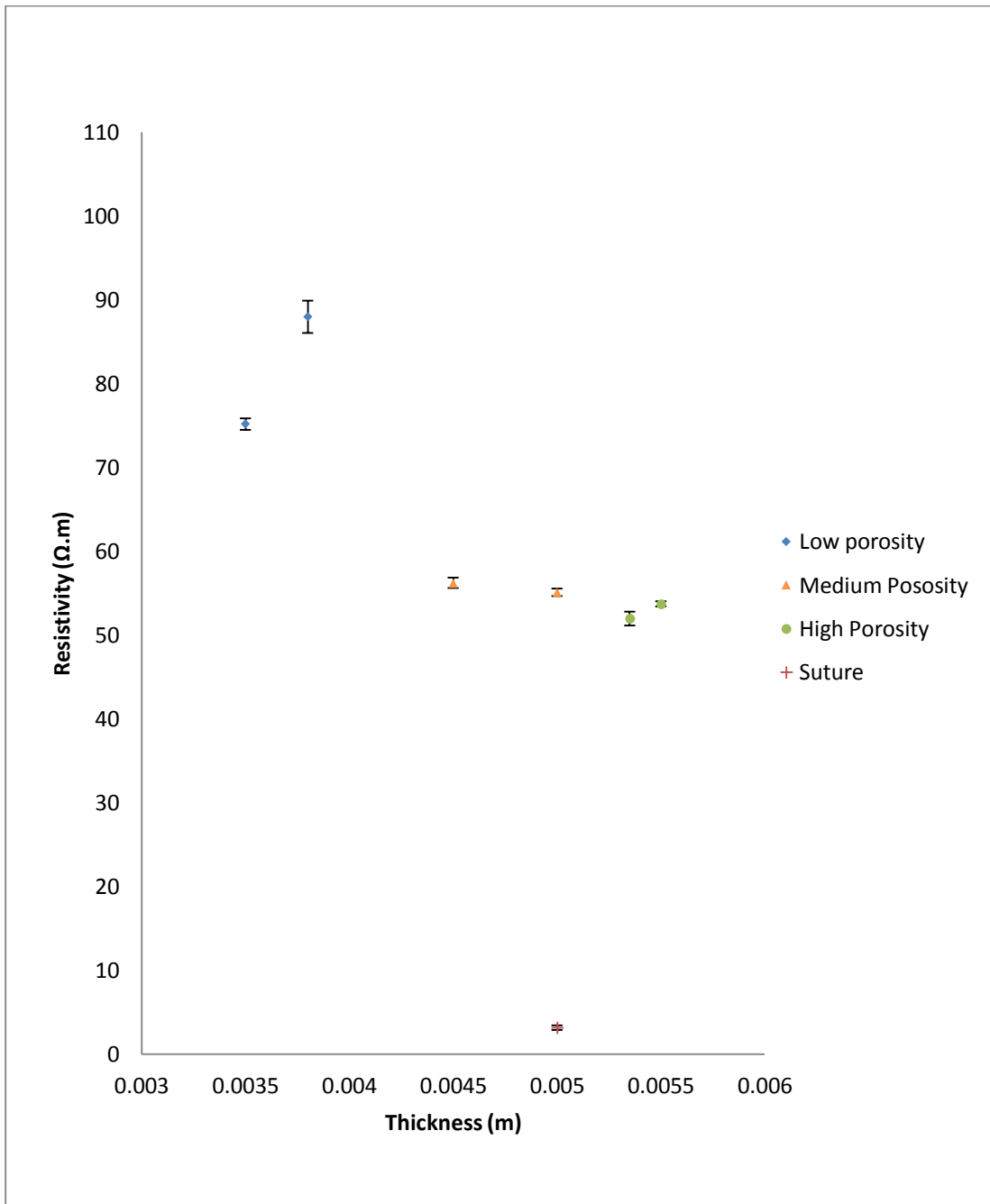


Figure 28: Skull Resistivity vs Thickness at 20 Hz

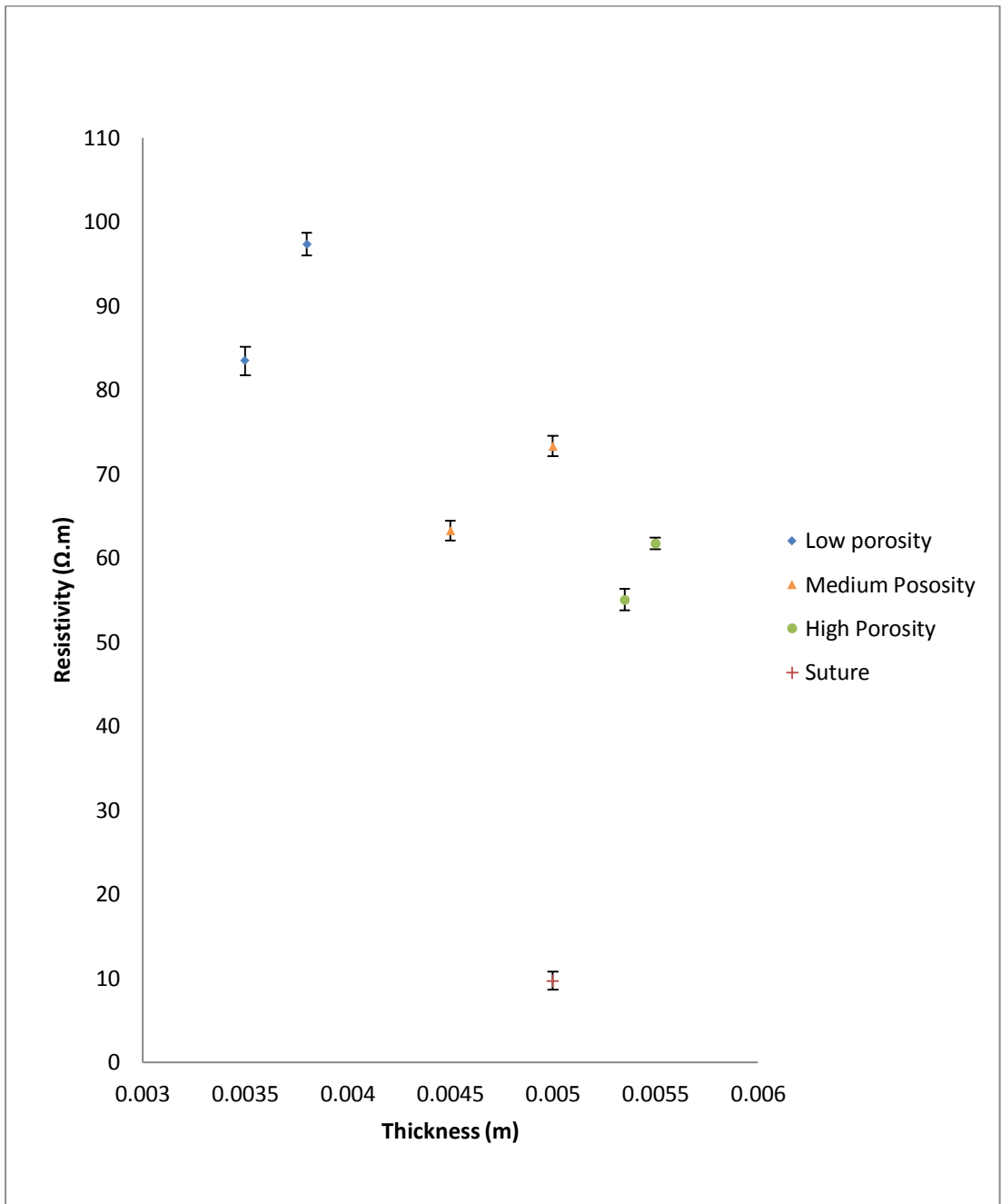


Figure 29: Skull Resistivity vs Thickness at 50 Hz

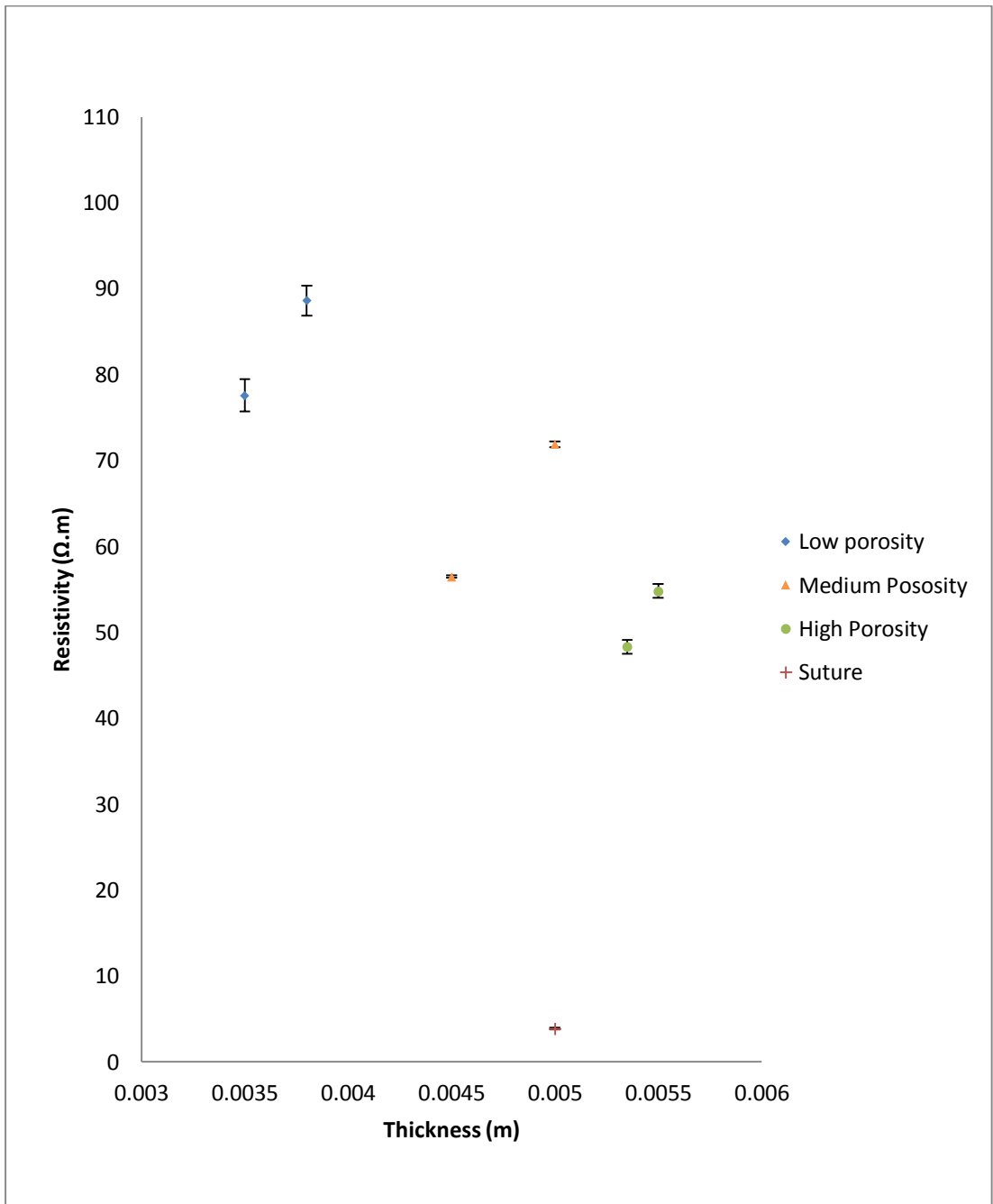


Figure 30: Skull Resistivity vs Thickness at 100 Hz



Figure 31: Close-up views of locations for which readings were taken

The locations where the readings were taken are along the perimeter of the skull. The purpose for this is that the microstructure of the skull region tested could be easily distinguished visually and the thickness easily obtained. Furthermore, it is inaccessible for the equipment to reach the inner skull and impossible to distinguish the microstructure of the inner skull region with the equipment at hand. It can be observed that the resistivity of the skull shares a relationship with its microstructure and thickness.

For the low porosity region, a dense microstructure can be seen in Figure 31. In this region, the spongiosum and sandwiching compact layers is hardly distinguishable, holding much resemblance to that of a fully compact microstructure. This fully compact microstructure inevitable translate to a higher resistivity value. As shown in the graph, the skull thickness of 3.50 mm and 3.80 mm gives a resistivity value of 84.96 Ω .m and 97.36 Ω .m respectively. In regions of high porosity, the skull thickness of 5.35mm and 5.50mm gives a resistivity of 55.1 Ω .m and 61.8 Ω .m respectively.

The impedance values of samples with thickness of 3.50 mm and 3.80 mm (low porosity region) consisting of the minimal porous microstructure shows the highest resistivity values while the thickest samples of 5.35 mm and 5.50 mm (high porosity

region) with the most porous microstructure shows the lowest resistivity value (not taking into account the readings from the suture region). It shows that in the absence of the spongiosum layer, the skull resistivity increases with its thickness.

From the analysis of these 3 regions, the resistivity of the skull could be concluded to be greatly influence by its microstructure and that the resistivity of the skull is not uniformed due to the inhomogeneous tri-layers of the skull. Conclusively, the resistivity of the skull is the combination of the resistivity of the upper compact, lower compact and spongiosum layers skull and cannot be measured base on the geometric factor alone unless the relationship between porosity and thickness is established.

The resistivity of the lambdoidal suture was also measured in this experiment, giving a resistivity value of $9.7\Omega.m$. This shows that the dense, fibrous connecting tissue between the sutures has a lower resistivity value. The microstructure of the suture is not considered, therefore only the relationship that regions with sutures generally have much lesser resistivity can be established.

Although the cadaver skull used in this experiment is soaked in saline solution, which provides free moving electrons that simulate the actual conductivity of a cerebrospinal fluid, the resistivity of live human skull compared to the cadaver skull is expected to be affected by the frequency and input current. This is due to actual live human skull having numerous charged molecules such as proteins in live cells and blood components. Therefore, the dielectric behavior of biological tissues is dependent on its nature and on the frequency of interest.

CHAPTER 4

HEAD PROFILE MEASUREMENT AND CATEGORIZATION

Understanding of the head profile is of great importance as mechanical loading is used to equalize the impedance across the scalp, too large a curvature may cause a high level of discomfort to the subject thus a program to characterize the head profile is being written. On top of that, better understanding of the Asian head model is necessary as the current EEG caps that can be purchased off the market are products arising from anthropometry research from the European market and may not be relevant in the Asian context given that the head profiles may differ to quite an extent.

4.1 Protocol Design

A group of 50 Asian subjects were recruited for this study in order to better understand the difference in head profiles between the Asians and the Europeans. Actual measurements of the individual segment lengths were performed prior to the digitizing of the electrode locations based on the 10/10 system. This study has been approved by the Institutional Review Board.

Points on the subject's head are being digitized with the use of the Xensor 3D Electrode Digitizer system that is based on the NDI Vira™ system for which infrared light is being used to track the digitizer pen and the head tracker. The system takes care of the electrode digitization procedure and records, visualizes and stores the

digitized electrode positions. Positions are acquired by locating the respective electrode at the scalp, placing the digitizer pen at that location and pressing a button. Markers (nasion, left pre-auricular point and right pre-auricular point) are digitized in order to transform the locations to the nasion-ear coordinate frame.

To keep the subject's head from movement that could potential induce errors in the gathering of head profile's information, an optician headrest was modified to keep the subject's head in place. The support structure consisted of a space that allows the subject to be seated inside as well as a supporting structure for the various head measurement components. The system provides real-time feedback on the current location of the digitizer pen and acquired electrode position by displaying them in the MRI and head surface. Digitized electrode positions are immediately marked on the head surface and can be visualized in the MRI for inspection. With that, the data collected are based on the partial international 10/10 system is as follows:-

Table 3: Partial 10/10 System used for Head Profile Categorization

Curve 01	NZ, FPZ, AFZ, FZ, FCZ, CZ, CPZ, PZ, POZ, OZ, IZ
Curve 02	T9, T7, C5, C3, C1, CZ, C2, C4, C6, T8, T10
Curve 03	FPZ, FP1, AF7, F7, T7, TP7, P7, PO7, O1, OZ, O2, PO8, P8, TP8, T8, F8, AF8, FP2
Curve 04	AF7, AF3, AFZ, AF4, AF8
Curve 05	F7, F5, F3, F1, FZ, F2, F4, F6, F8
Curve 06	FT7, FC5, FC3, FC1, FCZ, FC2, FC4, FC6, FT8
Curve 07	TP7, CP5, CP3, CP1, CPZ, CP2, CP4, CP6, TP8
Curve 08	P7, P5, P3, P1, PZ, P2, P4, P6, P8
Curve 09	PO7, PO3, POZ, PO4, PO8
Curve 10	T9, FT9, F9, AF9, NZ, AF10, F10, FT10, T10, TP10, P10, PO10, IZ, PO9, P9, TP9, T9

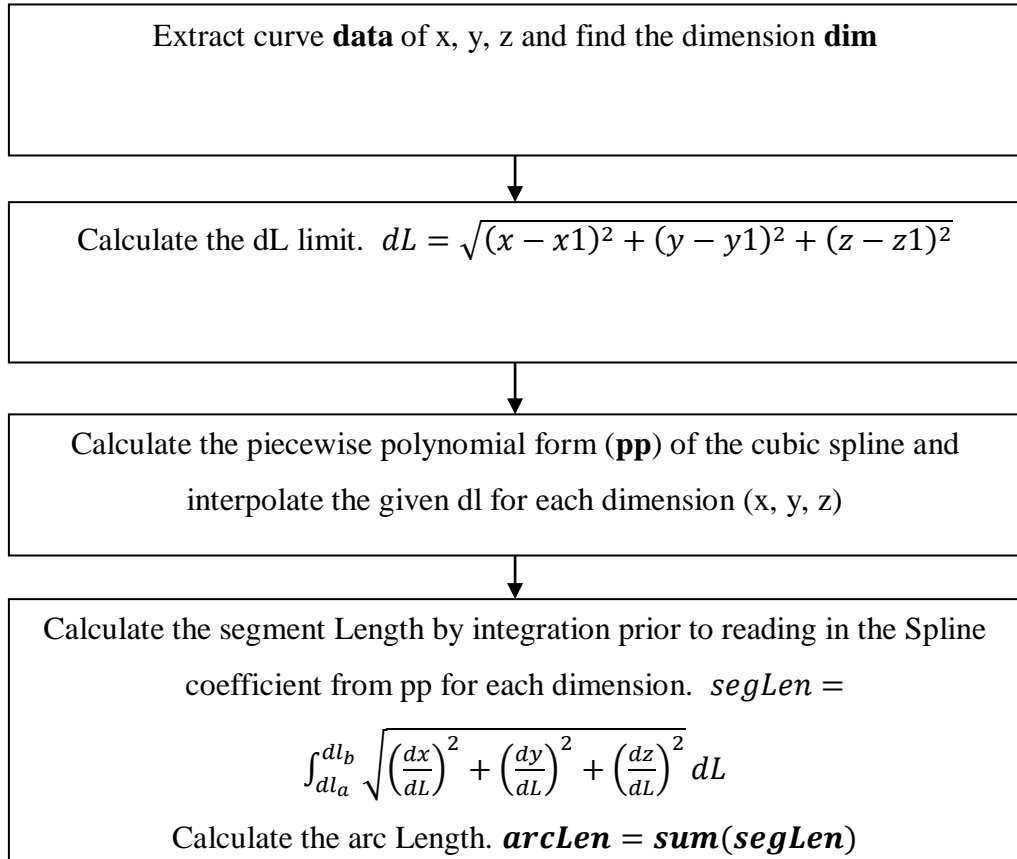
4.2 Material and Methods

4.2.1 Segment Length and Arc Length Calculation

The segment length is calculating by using integrating approach on spline curve while the arc length is total length of all curves.

$$\text{segLen} = \int_{dl_a}^{dl_b} \sqrt{\left(\frac{dx}{dL}\right)^2 + \left(\frac{dy}{dL}\right)^2 + \left(\frac{dz}{dL}\right)^2} dL$$

The spline curve algorithm is used to calculate the piecewise polynomial form of the cubic spline, thereafter the value for the given dL for each coordinate (x, y, z) are interpolated as shown in the flowchart. Thereafter, the spline curve is being used to find the curvature of the location of interest.



A Matlab program has been written to perform the calculation and the GUI interface could be seen in Figure 34. This allows the user to automatically input the data file recorded from the Polaris® Spectra®, which will be discussed later, for the analysis of both its segment and arc length of every individual curve.

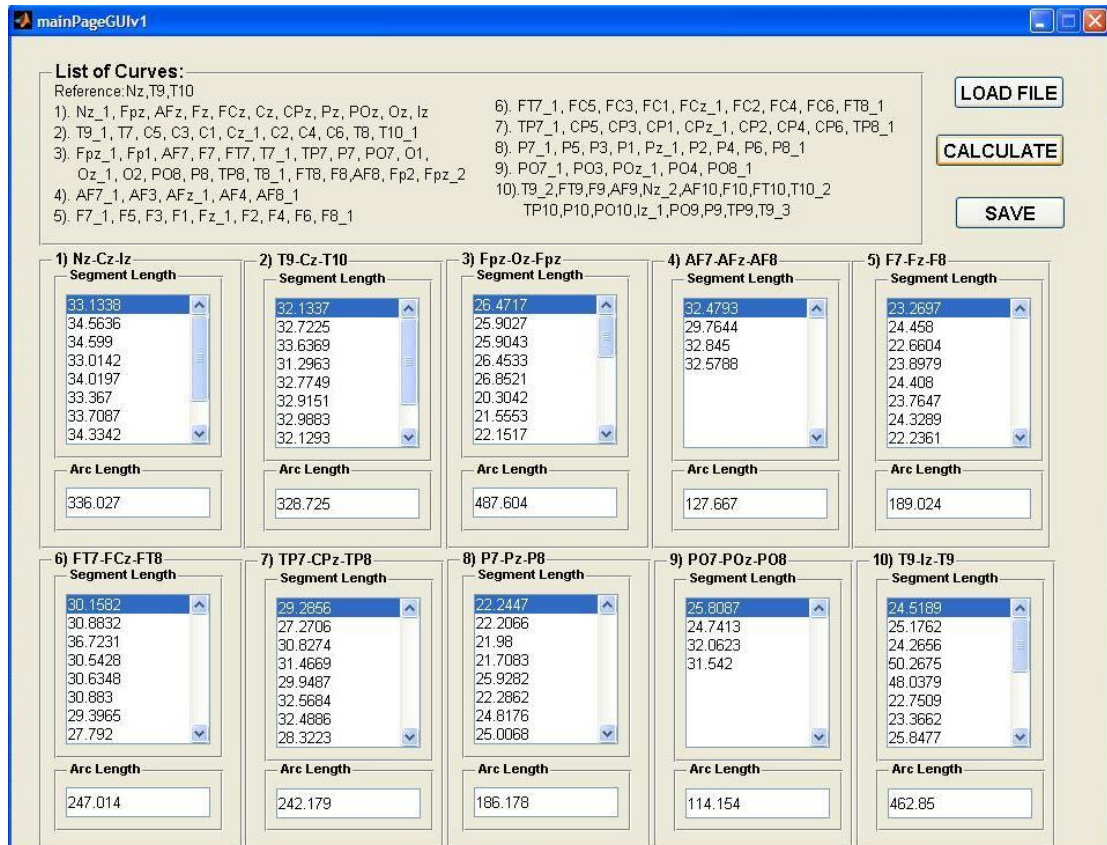


Figure 33: Overall database model

4.2.2 Database for Human Head Shape Data Collection

With so much information on hand, an efficient way to manage these data must be in place so that universal headbands could be designed for with the data collected analyzed according to categories such as race, region and physical appearances. The database was designed with the aim of completing the following tasks:-

1. Store larger quantity of data
2. Easily accessible from anywhere in the world my many users
3. Provide options such as filter, analyze, extract and view function
4. Able to produce visual users

With factors like availabilities, number of users able to access, performances, intelligence processing, easier of handling, security and integration with other databases, the following choices were analyzed:-

Microsoft SQL

It is very compatible with windows based environments. MS SQL is easily available and score high on all factors mention above however there is a major disadvantage attached to it is price. It is very expensive and not available for free of charge.

MySQL

The MySQL database is world's most popular open source database because of its consistent fast performance, high reliability and ease of use. It is easy to handle and widely popular among education and nonprofit organization as well as individuals as it is free of charge and offers a lot of online supports.

PostgresSQL

PostgreSQL is perceived as more powerful, more focused on data integrity, and stricter at complying with SQL specifications, but correspondingly slower and more complicated to use.

Oracle

Highly secured and one advance database model today's market however most of its applications are attached with advanced and highly secure environments. Given this advantages, Oracle intend to be more expensive and not possibly acquirable by individual users in simple application

After going through all of the above and considering their advantages and disadvantages also our project requirements, MySQL was selected to be used as our project database.

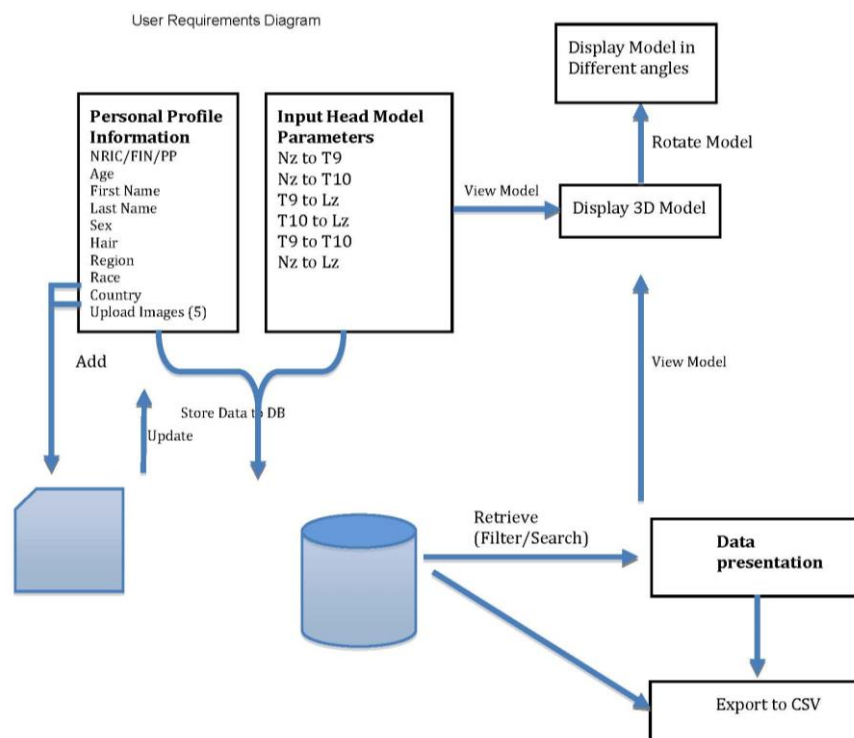


Figure 34: Overall database model

4.2.3 User Input Graphical User Interface (GUI)

This is the communication interface with users and it allows end users to

1. Input Personal Information / Head measurements Data
2. View 3D model and
3. Store data into Database.
4. To use Analyzing tools and using of filter tools

Since this part was done using Flex Builder 3.2 for development which allows developers a lot of flexibilities, it can be changed according to user requirements and easily customizable give any basic requirements.

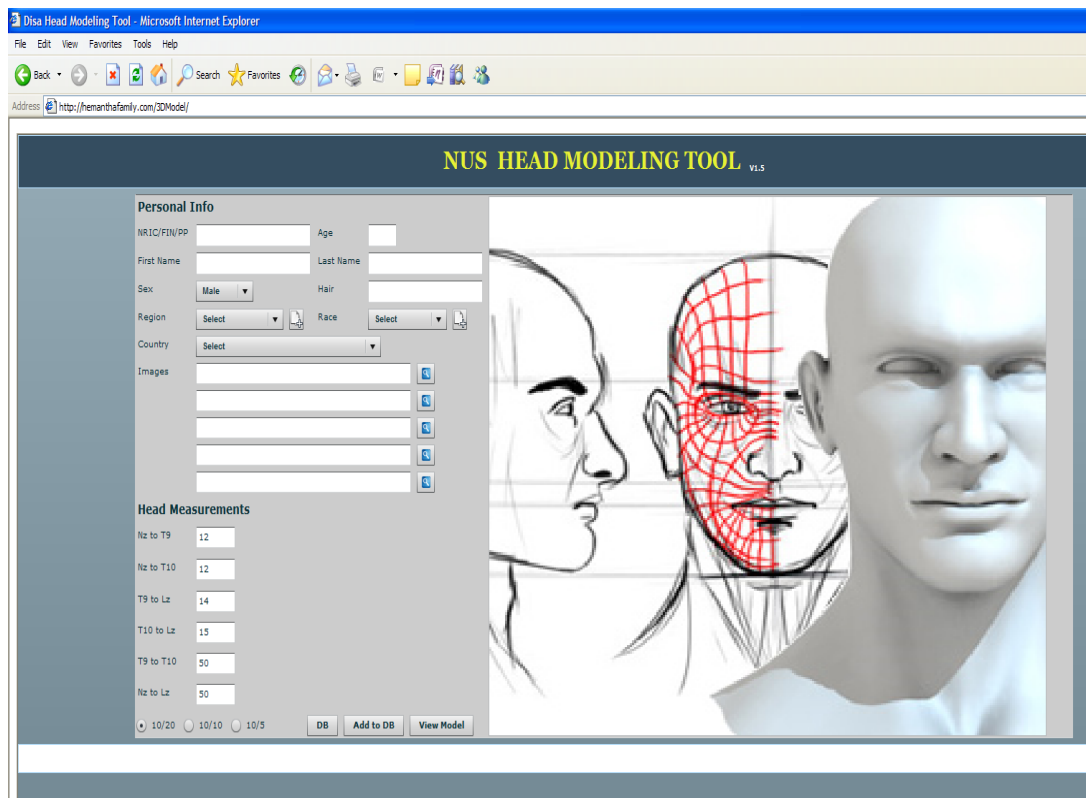


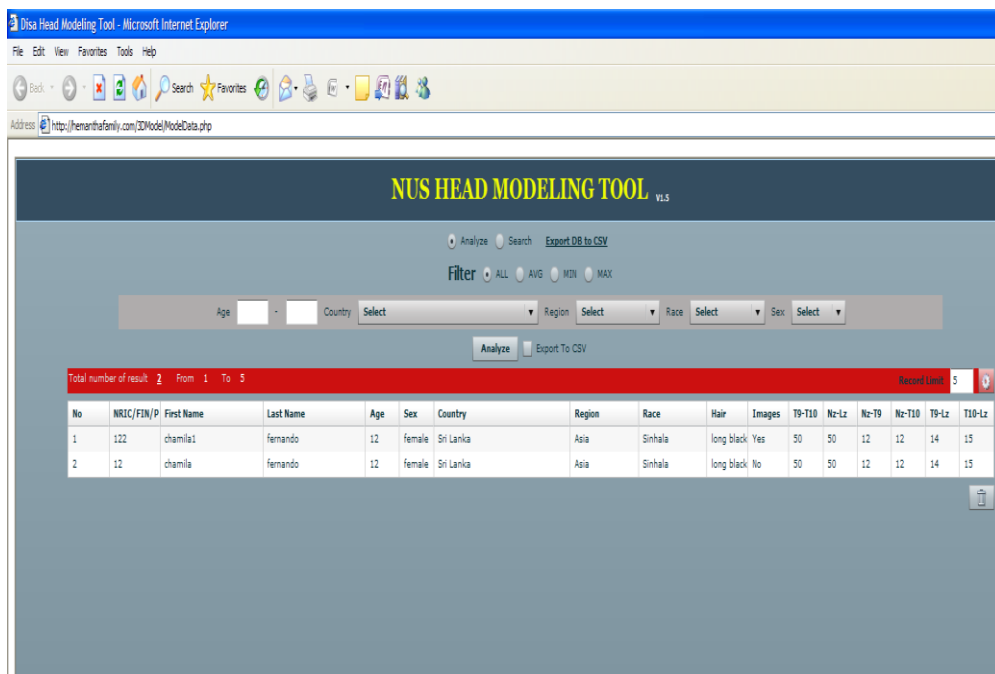
Figure 35: User interface design

Data Communication

Since the Flex programme itself is unable to handle database interactions, we have to use certain web language to handle the database interactions such as PHP, ASP and JSP. Those web languages are readily available and most of them are free of charge to use as well. Once the end-users input were recorded, Flex will then pass these values to the Server Backend for the storing of data into database, updating of information into data the processing, and refreshing files.

Data Presentation

The main purpose of this GUI is to showcase data from database to end users in user friendly manner. This GUI would pull data from the database and displays it to the users in table format.



The screenshot displays the 'NUS HEAD MODELING TOOL v1.5' web application. The interface features a search and filter section with options for 'ALL', 'AVG', 'MIN', and 'MAX'. Below this, there are dropdown menus for 'Age', 'Country', 'Region', 'Race', and 'Sex'. A table below the filters shows the results of a search, with a total of 2 records. The table columns include 'No', 'NRIC/FIN/P', 'First Name', 'Last Name', 'Age', 'Sex', 'Country', 'Region', 'Race', 'Hair', 'Images', and various measurements (T9-T10, Nz-Lz, Nz-T9, Nz-T10, T9-Lz, T10-Lz). The data is as follows:

No	NRIC/FIN/P	First Name	Last Name	Age	Sex	Country	Region	Race	Hair	Images	T9-T10	Nz-Lz	Nz-T9	Nz-T10	T9-Lz	T10-Lz
1	122	chamila	fernando	12	female	Sri Lanka	Asia	Sinhala	long black	Yes	50	50	12	12	14	15
2	12	chamila	fernando	12	female	Sri Lanka	Asia	Sinhala	long black	No	50	50	12	12	14	15

Figure 36: Data presentation graphical format

Custom database fields

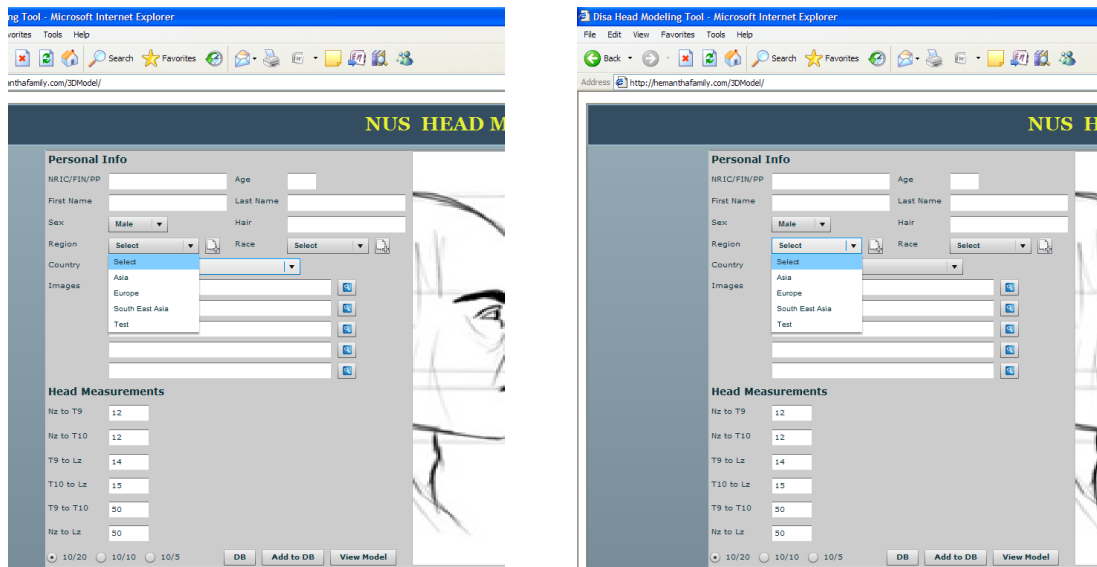


Figure 37: Customable database fields

Database utilities

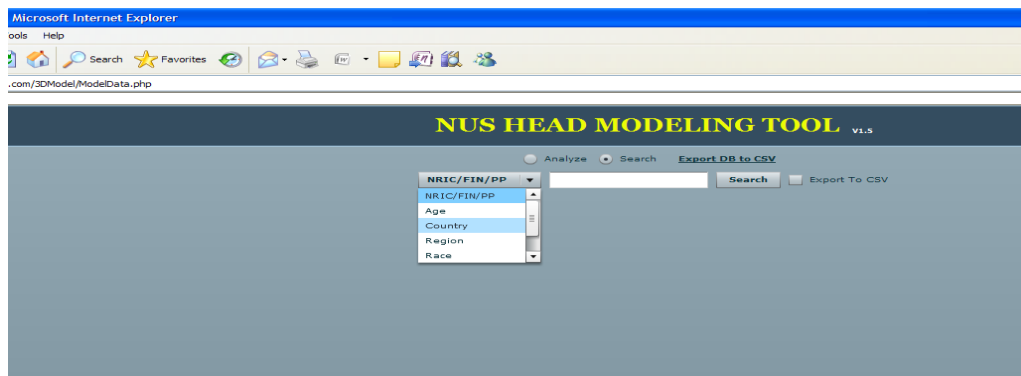


Figure 38: Filter/search option

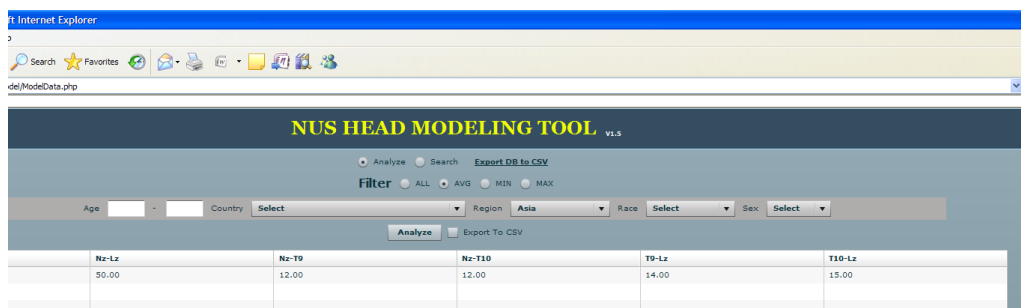


Figure 39: Data analysis option

4.2.4 3D model planning

This type of programming is very different from the conventional 3D programming which allows the use of special concepts such as Cameras, Views and Scenes. As such, Flash/Flex libraries were good alternatives with sound knowledge of Action Script programming. Flash/Flex libraries do not make things easier in 3D programming prospective however it allows greater convenience during the GUI creation. A basic 3D Model was modified to be used in 3D Max and this model could be changed and loaded onto the web browser after the end users finished inputting the required values.

Logic of creating the 10/20 system

1. The basic 3D model will be loaded using the default 3D library
2. In order to do the changes to the model, I have divided model into 2 major parts: (1) Head ($Z > +25$), and (2) Face ($Z \leq +25$)
3. The head was divided into 4 parts, namely the (1) Front Right, (2) Front Left, (3) Back Right, and the (4) Back Left, as sectioning the head into small sections would help to make changes easier.
4. Appropriate changes would be applied to each section of the head section during the runtime of the program.
5. Identifying the points of the model would be handled by 3D Engine with some programming logics.

4.2.5 Optical Measurement System - Polaris® Spectra®

The Polaris® Spectra® is an optical measurement system that measures the 3D positions of either active or passive markers affixed to application-specific tools. Using this information, each Polaris System is able to determine the position and orientation of tools within a specific measurement volume. Optical tracking uses a position sensor to detect infrared-emitting or retro-reflective markers affixed to a tool or object.

The position sensor calculates the position and orientation of the tool based on the information the position sensor receives from those markers. The measurement volume is the area in which the tool is tracked and the Polaris® Spectra® comes equipped with the Pyramid Volume, as shown in Figure 40.

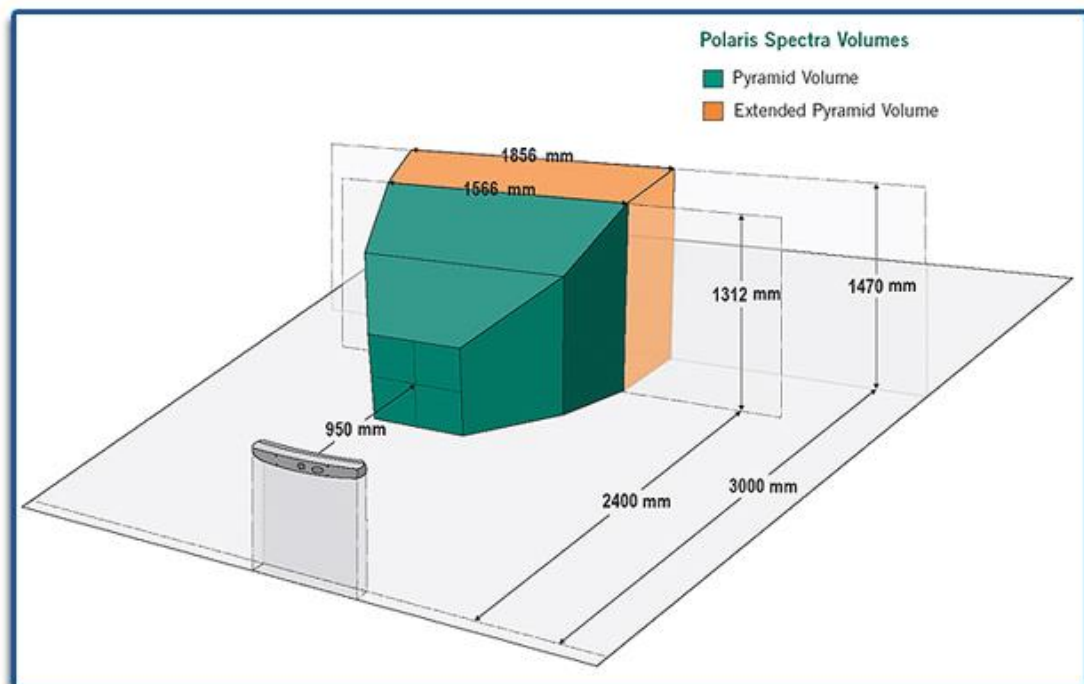


Figure 40: Spectra Pyramid Volume

There are two types of markers that can be used in optical tracking, including (1) Active markers which are infrared-emitting markers that are activated by electrical signal, and (2) Passive markers which are spherical, retro-reflective markers that reflect infrared light, emitted by illuminators on the position sensor. The Polaris® Spectra® allows for the following advantages:-

- Large working volume
- Very small, portable solutions
- Ability to track either or both active and passive markers
- High degree of measurement accuracy (up to 0.3mm RMS↑)
- Measures accurately within a large operating temperature range
- Ability to perform quick in-field accuracy assessment

Table 4: Performance of the Polaris® Spectra®

	Hybrid Polaris Spectra®	Passive Polaris Spectra®
Performance		
Accuracy:		
Volumetric ^{1,2}	Pyramid: 0.25 mm RMS Extended Pyramid: 0.30 mm RMS ²	
AAK	0.35 mm RMS	
95% Confidence Interval	Pyramid: 0.5 mm Extended Pyramid: 0.6 mm	
Maximum Update Rate ³	60 Hz	
Operating Temperature ⁴	10C° to 40°C	
Measurement Volume	Pyramid and Extended Pyramid	

Before any recording, the experimenter will perform a series of calibration on the system to ensure its accuracy. This is also to allow the experimenter to correctly place the subject in the Spectra Pyramid Volume so as to obtain an accurate measurement reading.

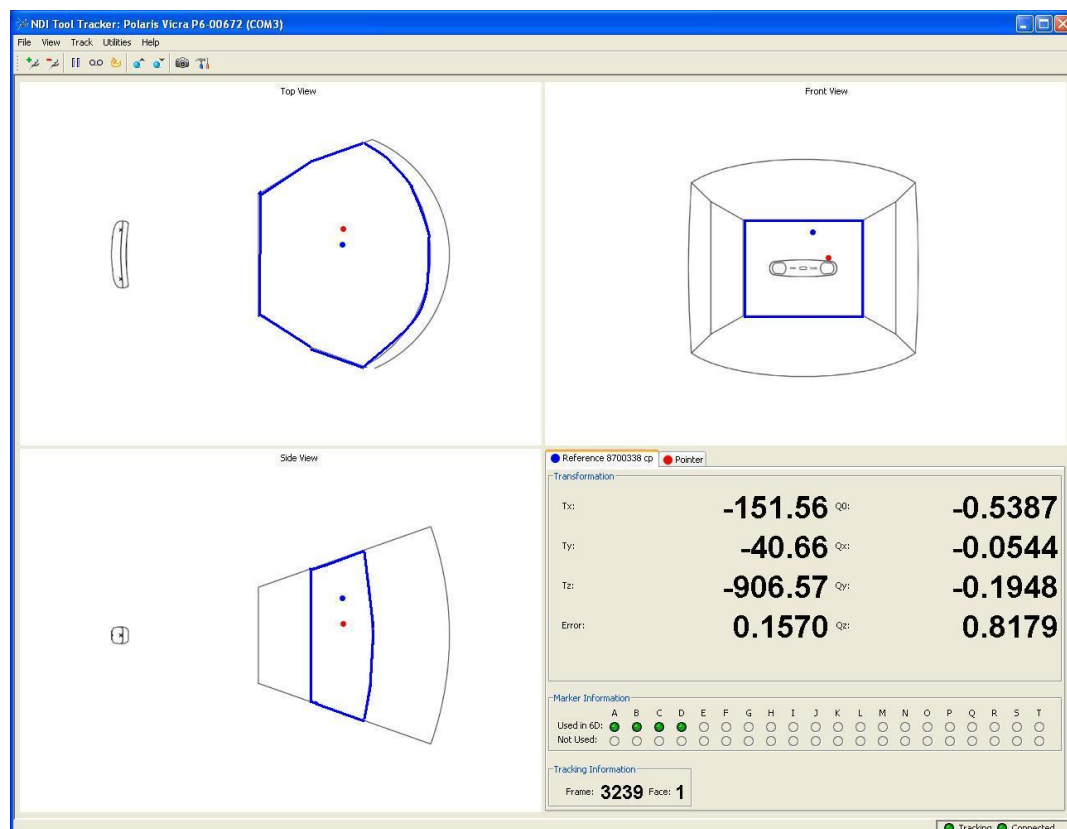


Figure 41: Reference pointers ranges

4.2.6 Subjects

A total of 50 subjects (25 males and 25 females) were recruited for this study. All participants provided written informed consent that was approved by the University Institutional Review Board.

4.2.7 Procedures

The head profiles were measured using the Polaris® Spectra® and the recorded data processed using the Spline Curve Algorithm. Thereafter, the processed data is being used to be compared with commercial EEG head caps. This allows us to determine the feasibility of using EEG head caps that were built using the European anthropometry on Asians.

4.3 Result and Discussion

Table 5: Accuracy of the Spline Curve Algorithm

	Measured Results	SolidWorks Results	% error	Program Results	% error
Nz-Cz-Iz	336	335.98	0.01	336.027	0.01
T9-Cz-T10	328	328.73	0.22	328.725	0.22
Fpz-Oz-Fpz	487	487.58	0.12	487.604	0.12
AF7-AFz-AF8	127	127.83	0.13	127.667	0.26
F7-Fz-F8	189	189.02	0.01	189.024	0.01
FT7-FCz-FT8	247	247.01	0.00	247.014	0.01
TP7-CPz-TP8	242	242.18	0.07	242.179	0.07
P7-Pz-P8	186	186.18	0.10	186.178	0.10
PO7-POz-PO8	114	114.18	0.16	114.154	0.14
T9-Iz-T9	463	463.32	0.07	462.851	0.03

To ensure that the spline curve algorithm is able to correctly provide the segment length, a study was done on the mannequin and results show that our program has an error of about 0.26%. This is compared with SolidWorks, a 3D CAD software which aims to deliver powerful design functionality with the intuitive SolidWorks user interface to speed your design process and make you instantly productive (Dassault Systemes, 2013). Noting that the maximum difference between our programs with the commercially available software being 0.13%, the spline curve algorithm program is being used to calculate the segment lengths of the head profiles of all our subjects.

Table 6: Subject's head profile vs. Commercial head cap size

	Males		Females		Head Cap Size	
	Mean	SD	Mean	SD	Medium	Large
FPz-Cz-Oz	29.85	0.71	28.73	1.25	28	33
T7-Cz-T8	30.04	0.80	28.89	1.22	24	29
FPz-Fz-Cz	14.89	0.34	14.35	0.63	14	16
Cz-Pz-Oz	14.96	0.4	14.35	0.60	14	16
M1-Cz-M2	37.16	1.7	35.52	2.56	34	39
P7-Pz-P8	22.84	0.83	22.01	1.02	19	21
P7-Oz-P8	18.41	0.74	17.61	0.49	16	17
FPz-Oz-FPz	58.49	1.53	55.61	1.48	58	59
T7-P7-Oz	15.46	0.73	14.36	0.70	13	14
T8-P8-Oz	15.36	0.53	14.43	0.5	13	14
T7-F7-FPz	13.88	0.72	13.46	0.44	15	15
T8-F8-FPz	13.97	0.64	13.36	0.40	15	15
F7-FPz-F8	17.01	0.73	16.21	0.69	19	20
T7-FPz-T8	27.95	1.31	26.86	0.81	29	30
T7-Oz-T8	30.54	1.23	28.85	1.15	28	29

Table 7: Regions of the subjects' head profile that is incompatible to the Commercial head cap

	Percentage Difference	
	Males	Females
T7-Cz-T8	11.199	10.271
P7-Oz-P8	9.822	11.248
F7-FPz-F8	6.462	6.808
T7-FPz-T8	6.15	6.217
T7-Oz-T8	5.718	7.541

The various segments on the scalp was analyzed and compared with the individual segments of the recommended size of the commercial head caps which is based on the circumference of the subject's head. Table 7 shows regions on the subjects' head that has more than 5% difference when compared to the segment lengths of the commercial head caps. As such, this difference is being taken into consideration during the design of the head cap for the mounting of the patented sensor (to be discussed in Chapter 6).

CHAPTER 5

STUDY TO ACHIEVE UNIFORM SCALP IMPEDANCE

In this chapter, the effect of a non uniform scalp impedance would be discussed and a method being put forward to achieve uniform scalp impedance. Dry electrodes has been widely researched and developed for ease of use and long term bio-potential measurement such as EEG, ECG and EMG. Compression of the skin during the use of the dry electrode is essential to ensure maximal contact area to lower electrode-skin impedance and minimize electrode movement relative to skin, which would otherwise result in large signal noise.

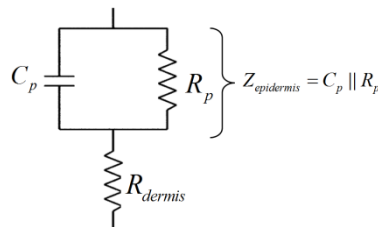


Figure 42: Equivalent circuit of the skin

The skin impedance has been one of the key performance indices for bio-potential electrode. An equivalent circuit of the skin is shown in Fig. 42, with resistance R_p and capacitance C_p as the constituent elements of the stratum corneum (SC). Factors that can cause changes in the human skin impedance are found to be complex and could be affected by the subject's emotion, duration of use, electrode-skin interface,

electrolyte's content and environmental condition. However, the relationship between compression and the electrical properties of the SC has yet to be established.

The skin barrier function is found to be correlated to the skin impedance and the major contributor is found to be the SC, the outermost layer of the skin (Y. N. Kalia, 1998). The integrity of the barrier function was often accessed by means of trans-epidermal water loss and skin capacitance. Studies have found that the skin hydration state can be measured by low-frequency susceptance measurement of the skin (R. Darlenski, 2009) as differences in the epidermal water concentration level has an effect on the skin capacitance. It is also known that the barrier function of the skin can be affected by the application of mechanical stress to the skin (L. Pedersen, 2006).

It was found that the skin compression has a great influence on the skin admittance when measured at 100 kHz (Y. Yamamoto, 1986), and suggested that the change in skin admittance might be attributed to the change in contact area between the electrode and skin. However, there are other possible influencing factors which have not been comprehensively investigated since. It is hypothesized that there might be causal relation between the change in skin impedance and the skin compression as the latter could potentially weaken the skin's barrier integrity.

In this present study, an indentation-impedance measurement method was established to investigate the influence of skin compression on skin impedance, accompanied by standard SC removal to investigate the influence of SC thickness on the compression induced skin impedance change. Furthermore, to investigate whether the change in contact area caused by compression contributes to impedance change, adequate

electrolyte is applied initially to maximize the contact area, and it is kept constant throughout the compression process with the use of electrolyte that does not smear.

$$Z_{Skin} = Z_{Epidermis} + Z_{Dermis} \quad (1)$$

5.1 Design Considerations

Compression-induced Impedance Change on the Hand

Doing the compression experiment on the hand prior to moving to the scalp would minimize the risk of over applying pressure at the measurement site resulting in damage of the subject's skull. Thus a compression-induced impedance change study on the hand was performed to determine the effect of compression on the impedance at the skin-electrode interface and also the maximum force that can be applied.

Compression-induced Impedance Change on the Scalp

To determine the relationship between the load and the corresponding impedance values of the scalp, a novel electrode with a tip of 5mm was design for. It was decided that the load would be varied between 50 grams and 150 grams. The lower limit of 50 grams was chosen to ensure that the electrode tip was in full contact with the scalp and the upper limit of 150 grams was chosen as it was felt that any value higher than that would cause discomfort to the subject.

5.2 Materials and Methods

5.2.1 Subjects

Male, Chinese subjects within the age range of 18 to 26 and having a head circumference had to be between 54cm to 62cm in order to accommodate the medium size Neuromedical Supplies head cap available. 50 subjects were selected for the experiment to determine the relationship between the load and impedance on various points on the scalp all participants provided written informed consent that was approved by the University Institutional Review Board.

5.2.2 Experiment Procedures

Compression-induced Impedance Change on the Hand

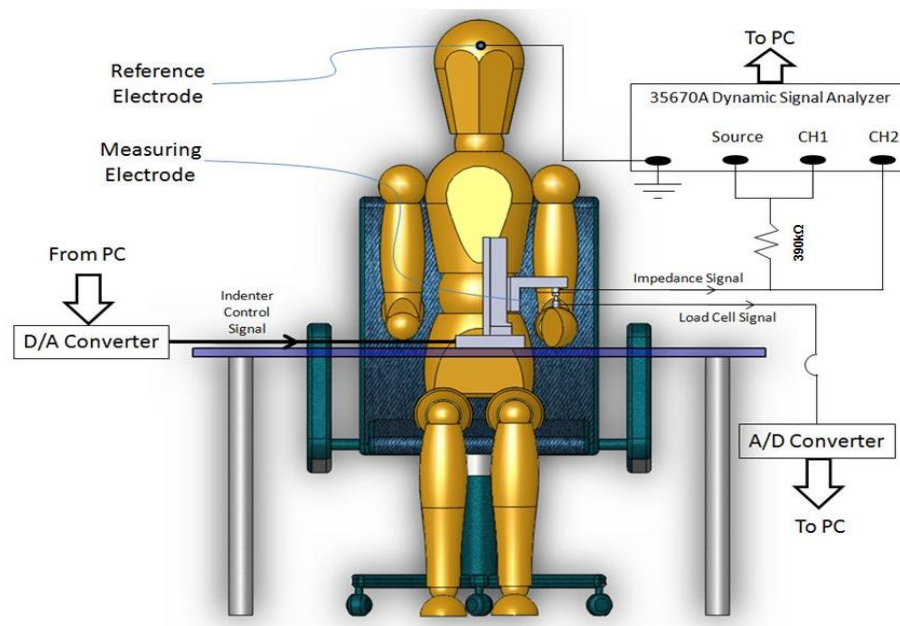


Figure 43: Setup for impedance and indentation measurement

The indentation-impedance measurements in this study were conducted using a specially designed indenter and the 35670A Dynamic Signal Analyzer (Agilent, Santa

Clara, CA, USA), which was connected to LabView (National Instruments, Austin, TX, USA) to obtain the force on the indenter and its corresponding impedance recorded from the Dynamic Signal Analyzer at 25 Hz. To minimize the variation in results caused by the change in both the environment and the subject's skin condition, the measurements were carried out simultaneously within the same session for every subject at the same ambient conditions.

In-vivo experiments were carried out using a two-electrodes measuring system, consisting of a Ag/AgCl EEG cup (reference electrode), and a brass electrode (measuring electrode) attached on the indenter system for the measurement of the skin impedance. Before the experiment, the measurement site was cleaned with cotton cloths saturated with distilled water and the SC layer of the reference site (forehead) is removed by scrubbing. The indentation experiments use a flat cylindrical brass tip electrode of 5 mm diameter. Indentation were done up to a depth of 12 mm in order to measure the human skin impedance of both the inner and outer forearm. There are two different variations in the experiment set-up and they are as follows:

1. Dry electrode coated with a thin layer of high viscosity electrolyte paste (Ten20 Conductive EEG Paste) being used in order to maintain the contact area throughout the indentation. This is to exclude the influence of the change in contact area on the result. The electrolyte paste is selected because it has limited diffusion through the skin in a short duration to ensure minimal impedance change by the electrolyte during the experiment. There is no electrolyte smearing so that the contact area remains constant throughout the experiment.

2. To compare the performance with conventional Ag/AgCl cup electrode filled with electrolyte gel (One-step Clear gel), the brass electrode is also coated with the same electrolyte gel. To eliminate the smearing effect, both electrodes are restricted to a 5mm diameter exposed area by masking with a circular cut-out 3M Scotch tape. In either experimental, a thin layer of electrolyte paste/gel was evenly applied on the dry electrode tip by stroking with cotton bud. The schematic diagram of the experimental setup for impedance-indentation measurement and the circuit diagram of the skin impedance measurement are depicted in Figure 43.

To measure the effect of skin impedance under compression, it was initially studied under fixed indentation. The forehead of the subject was being scrubbed in order to remove the SC prior to attaching of an Ag/AgCl cup electrode as reference. Thereafter, commercial electrolyte gel (OneStep Clear Gel) was used at the reference electrode-skin interface to minimize the influence of the skin impedances on the reference site to the total measured impedance.



Figure 44: Indentation positions (a) Outer (extensor) forearm, (b) Inner (volar) forearm

A thin layer of electrolyte paste (Elefix paste for EEG test, Japan) was applied on the flat-top brass dry electrode before the experiment to maintain the effective contact surface area throughout the experiment. This paste is chosen as it (1) has limited diffusion through the skin within a short duration thus ensuring minimal impedance change by the electrolyte throughout the duration of the experiment, (2) will not evaporate easily at room temperature, (3) does not smear which allows the contact surface area to be kept constant, and (4) has negligible impedance change over time. The indenter will then be manually placed in contact onto the measurement site – the inner and outer forearm areas as shown in the Figure 44. These sites were chosen for this study because of its relative flatness thus allowing for maximum contact with the flat indenter surface.

The indenter moves downward until the first load cell reading of 10 g, equivalent to 3 to 4.5mm of displacement depending on the subjects, is reached and this represents

the starting point for the load-indentation curve. Once the 10g was obtained, the indenter was held for 5 minutes before the next indentation so as to ensure that the brass electrode contacts the skin fully and the effective skin area under the indenter was kept constant stabilizing the impedance reading.

The indenter then moved 20 steps downwards, totaling a distance of 0.6 mm at a rate of 1.5 mm/s, prior to the recording of averaged impedance value processed by the Dynamic Signal Analyzer. There is a 10 s interval between every 20 steps for this recording and this cycle is being repeated for another 7 times. Once the loading cycles were completed, a similar unloading cycle mimicking that of the loading process was conducted for 8 times.

Compression-induced Impedance Change on the Scalp

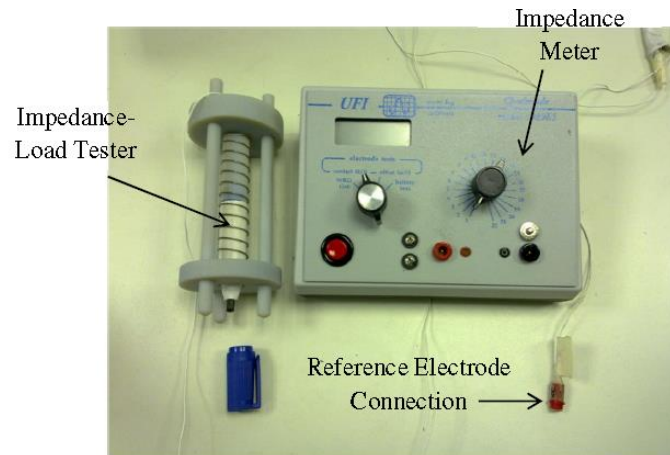


Figure 45: Experiment Setup

The subject's head circumference is measured and recorded using a measuring tape prior to putting on the head-cap on the subject's scalp and adjusts for good fit. The reference electrode location was exfoliated using scrub gel and a cue tip. Thereafter, the site is cleaned using an alcohol swab making sure to remove all debris. Both the reference and ground electrodes were adhered firmly on the subject and conductive gel being slowly injected using a syringe taking care not to leave air gaps within the electrodes. The electrodes were then connected to a multi-meter and the connections tested. The main principle behind the initial method was to use a spring loaded impedance-load tester to apply a variable force on the scalp. The experimental setup, as shown in Figure 45, includes the Impedance-Load Tester which varies the load using a compression spring, a ceramic reference electrode at the nasion and a multi-meter to measure the impedance at 20Hz between the two points on the subject's scalp. The impedance load tester has been designed to operate on a compression spring mechanism.

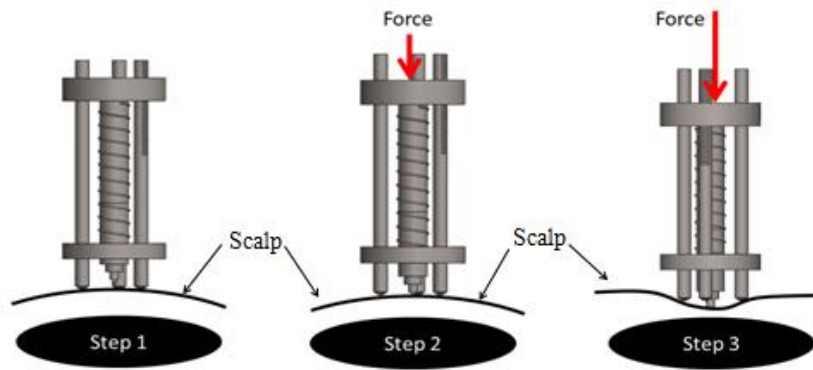


Figure 46: Procedure for using the spring based impedance-load tester

The notches on the tripod are for assessing the depth to which the electrode has been depressed on the scalp. Each notch is a millimeter in width and is spaced by the same distance. The tester is first positioned over that point of interest on the scalp before some force should be applied slowly on the cap of the tester in order to bring the electrode tip just into contact with the scalp, as shown in Step 1 and 2 of Figure 46. The notch number was noted at this point before additional more force being applied in order to depress the skin on the scalp. The amount of force applied can be ascertained by the change in the notch number as the spring is designed to compress proportionally to the force applied. In this design, the spring is a critical component and the following parameters, as shown in Table 8.

Table 8: Parameters for Spring Design

Parameters for Spring Design	
Material	314 Stainless Steel
Spring Diameter	16.5 mm
Maximum Compression	15 mm
Maximum Force	1.47 N
End Criterion	Squared & Ground

5.2.3 Novel Self-Clamping Headset Design

To ensure that the electrode is capable of obtaining quality EEG signals, the electrode-skin impedance must be minimized. This can only be done when sufficient force is being applied on the electrode so as to ensure good contact thus a headset, made out of reconfigurable self-clamping module as shown in Figure 47, and has been designed for the testing of the electrode. The modules can be reconfigurable in length to allow the headset to suit different head shapes and sizes.

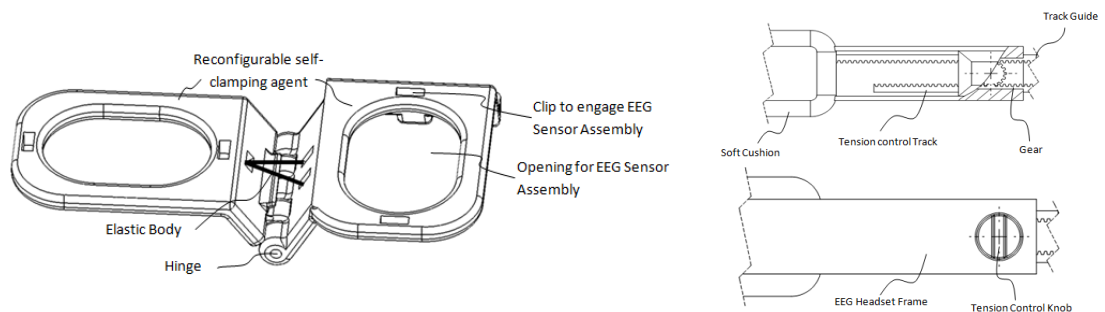


Figure 47: Reconfigurable self-clamping module (Left) and Tensioning mechanism (Right)

The shape of the reconfigurable self-clamping agent is configured to have at least one of the edges bent at an angle, and is connected to the end of similar bent part of another agent by a hinge joint so as to allow the agents to rotate smoothly within a certain range in relation to the each other. On the bend of the agent, an elastic body connects the two agents and can be tightened sufficiently to pull the two reconfigurable self-clamping agents toward each other. A tensioning mechanism on the headset allows for the securing of the headset assembly firmly and comfortably on the subject's head of different shapes and sizes, and also to customize the force to be exerted on the individual sensor so as to achieve a uniform scalp impedance at all the measuring locations.

5.3 Results and Discussion

5.3.1 Impedance-indentation on the hand

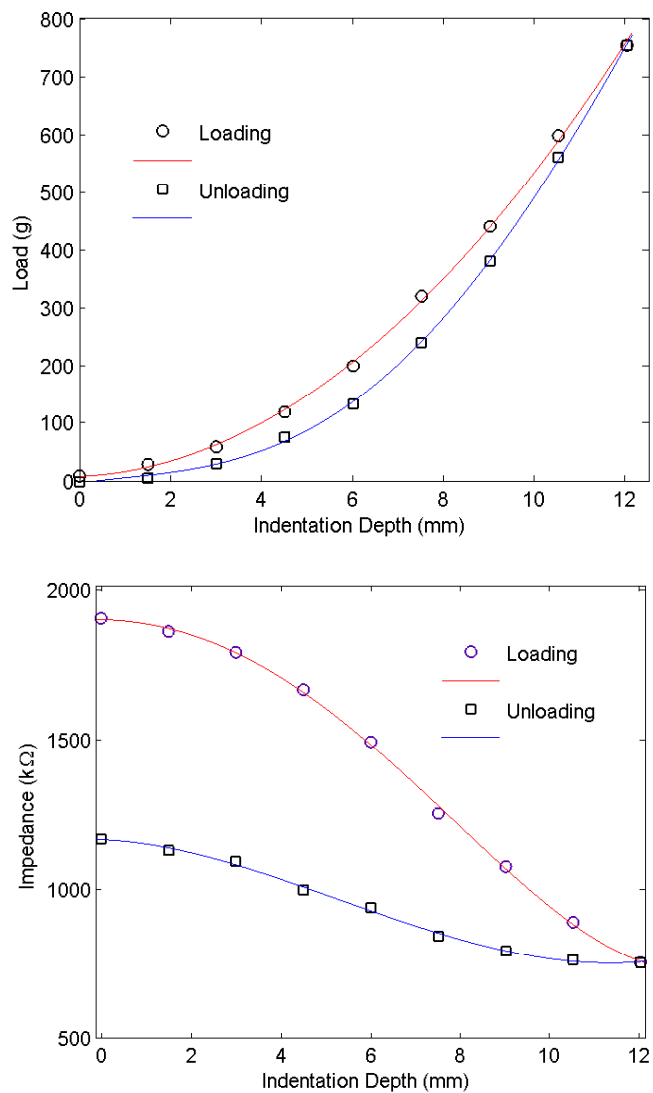


Figure 48: (a) Load-indentation and (b) Impedance-indentation curves on the volar forearm

Figure 48a shows a typical force-indentation curve of the skin due to compression and a lower load reading was observed during the unloading process while Figure 48b shows the corresponding impedance-indentation characteristic of a subject, at 25 Hz, due to the loading in Figure 48a. It could be seen that the skin impedance decreases

slowly during initial loading and a more drastic fall in impedance follows thereafter as indentation increases.

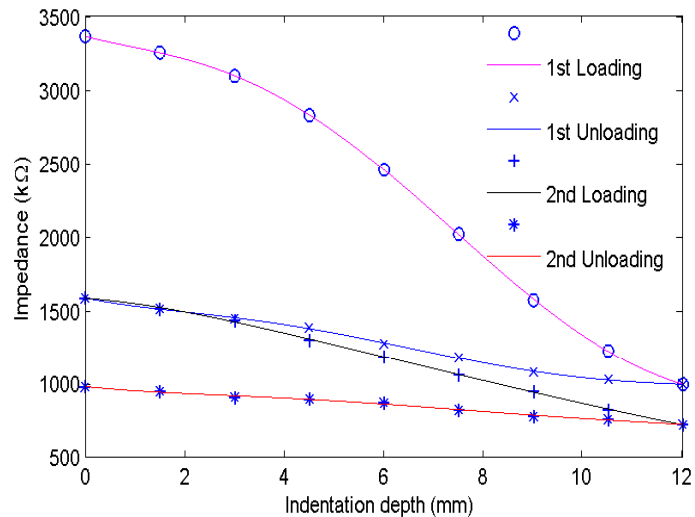


Figure 49: Two consecutive cycles of the impedance-indentation curve of on the volar forearm

The skin impedance during the unloading phase portrays a similar trend with lesser intensity to that of the loading condition. When the indenter is completely unloaded (indentation depth, $d=0$ mm), the resultant skin impedance is much smaller than that at the start of the experiment. When indentation is repeated, the subsequent cycle exhibits trends similar to that of the first cycle for both the loading and unloading process and lower resultant skin impedance could be achieved by repeated loading, as shown in Figure 49. This impedance at 12mm reduces from 996 kΩ to 723 kΩ in the subsequent cycle. The relationship between compression induced skin impedance change against indentation depth and their corresponding load are shown in Figure 50. Normalization has been done so as to negate the variations across subjects having different skin thickness layers and hydration levels, thus allowing underlying characteristics of the data sets to be comparable.

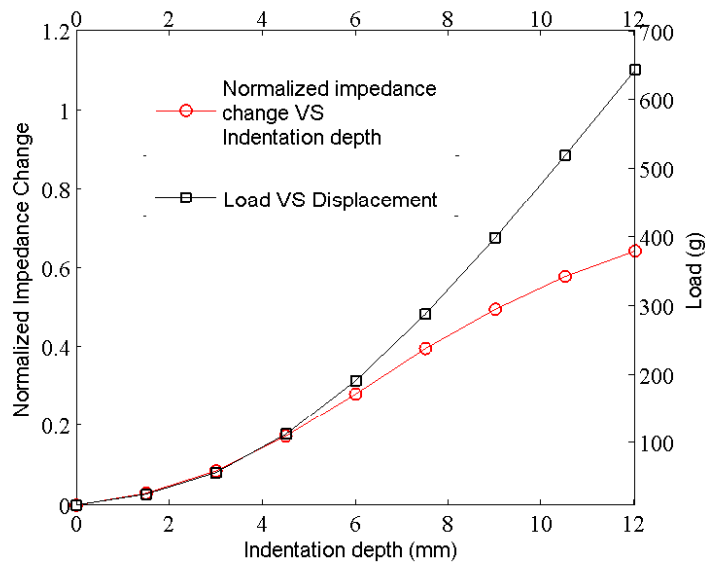


Figure 50: Changes in normalized skin impedance (‘o’) and load (‘□’) in relation to indentation depth

The curve of normalized impedance change vs. indentation depth portrays a sigmoid behavior. It starts with slow increase followed by drastic increase and subsequently slowly approaches a steady value. From the averaged results in Figure 50, it depicts that the change in skin impedance has a linear relationship with the load applied up to 125 g resulting in an indentation depth of 4.5 mm. Thereafter, divergence occurs between the load-displacement curve and the change in normalized impedance-displacement curve. It can also be seen that the rate of impedance change reduces after a critical value (approx.125 g), thus after achieving this critical load, a larger load is required to further decrease skin impedance. It is also found that the impedance change-displacement curves and the load-displacement curves on different body sites are different, but displayed similar characteristic.

This could be due to the load having caused a structural change in the “brick-and-mortar” configuration of the SC that weakens the barrier function of the skin thus

allowing better permeability of the electrolyte into the SC hence reducing the skin impedance. As the skin gets saturated with electrolyte, its impedance would then approach steady state thus diminishing the linear relationship between that of the normalized skin impedance and the compression load. The skin's parallel capacitance C_p value increases with increasing load applied, whereas the skin's parallel resistance R_p decreases with increasing load. Similar to skin impedance, they both approach a steady state after a critical value and recover partially after the load being removed.

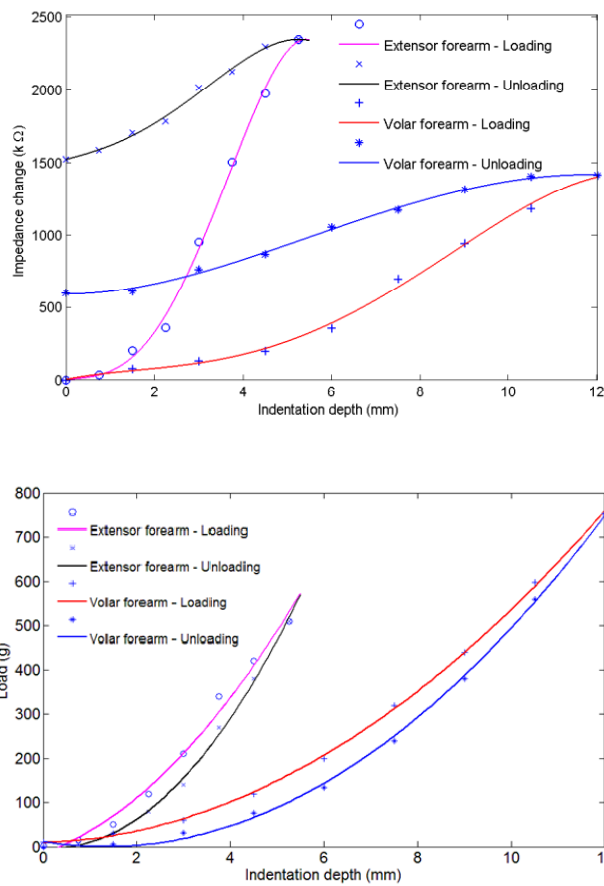


Figure 51: (a) Comparison of impedance change with indentation depth on volar forearm and extensor forearm. (b) Comparison of load-displacement curve between these two sites.

The measurement on the extensor and volar forearm, as shown in Figure 51, reveals that the rate of change in skin impedance on the extensor forearm is faster than that obtained on the volar forearm. This reduction approaches a steady state value for which is highly variable across different subjects and different body sites even on the same subject. According to Edsberg et. al., prior pressure loading may cause damage to the initially randomly oriented tissue collagen fiber bundles, thus causing a decrease in the stiffness of the tissue in subsequent loading, this compressive-pre-load-induced strain softening is also known as the Mullins effect.

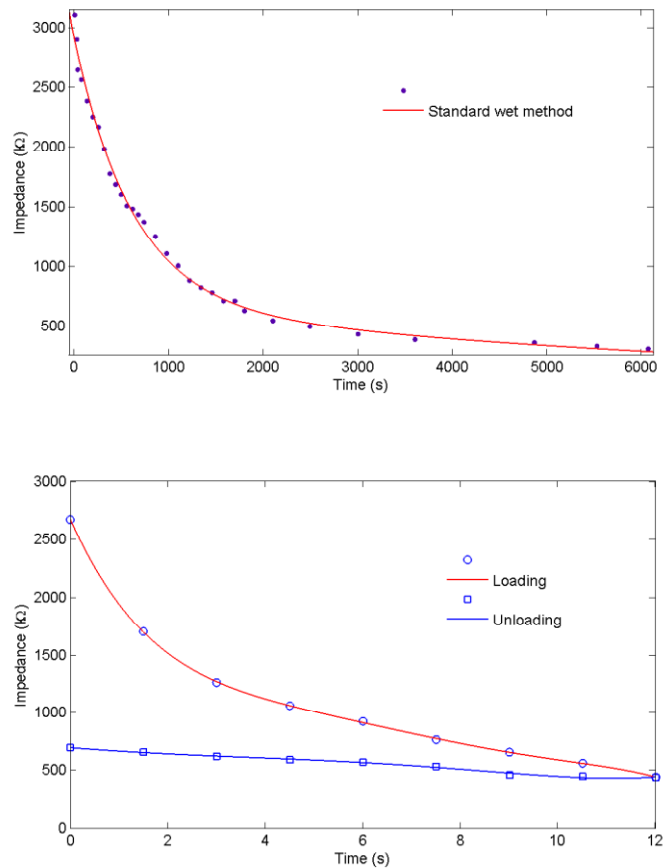


Figure 52: Enhancement method by coupling compression and gel penetration. (a) Variation of skin impedance with time for conventional wet electrode method on inner forearm of the same subject (b)

Variation of impedance with indentation depth on inner forearm with electrolyte gel

Figure 52 (a) shows the variation of skin impedance over time for an Ag/AgCl cup electrode filled with low viscosity gel on the subject's inner forearm, requiring a time interval of about 3500 s, approximately equivalent to an hour, for the skin impedance to stabilize. This electrolyte gel has a long stabilization time but when coupled with compression at a rate of 1.5mm/s, with 10 s intervals between every 2 mm of indentation for the recording of the impedance value, the skin impedance decreases rapidly towards the steady state value of 500 k Ω as shown in Figure 52 (b) in under 90 s. It can also be seen that this drop in impedance due to compression is significant right from the start of the indentation and that the resultant impedance remains relatively stable during and after unloading.

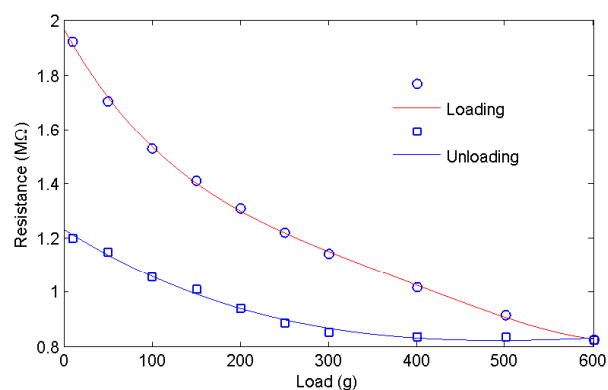


Figure 53: Skin resistance variation with indentation on the inner forearm

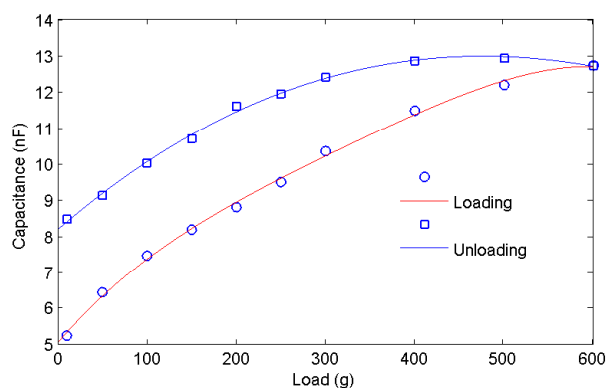


Figure 54: Skin capacitance variation with indentation on the inner forearm

5.3.2 Impedance Variation along T7-C3-CZ-C4-T8

The impedance was measured to be highest at the location CZ and fell subsequently for the other locations along the T7-T8 Line. In all three loading cases shown in Figures 55, 56 and 57, the impedance was lowest at points T7 and T8. The values peak at the top of the head as the hair follicle density is a lot higher on top of the head than at the sides. Additionally, it can also be seen that the impedances are similar on either side of the scalp.

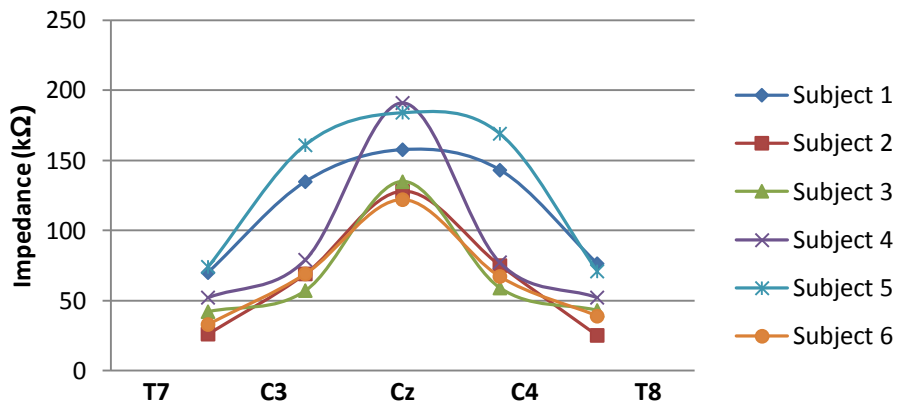


Figure 55: Graph of impedance with respect to position at 50 grams

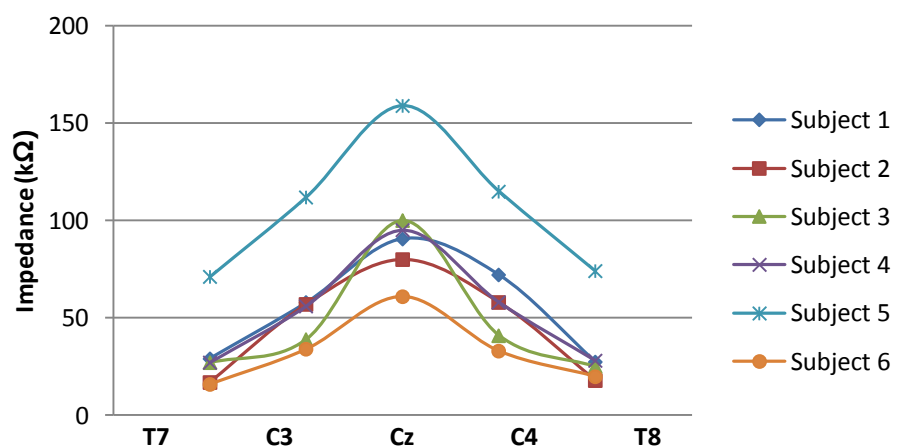


Figure 56: Graph of impedance with respect to position at 100 grams

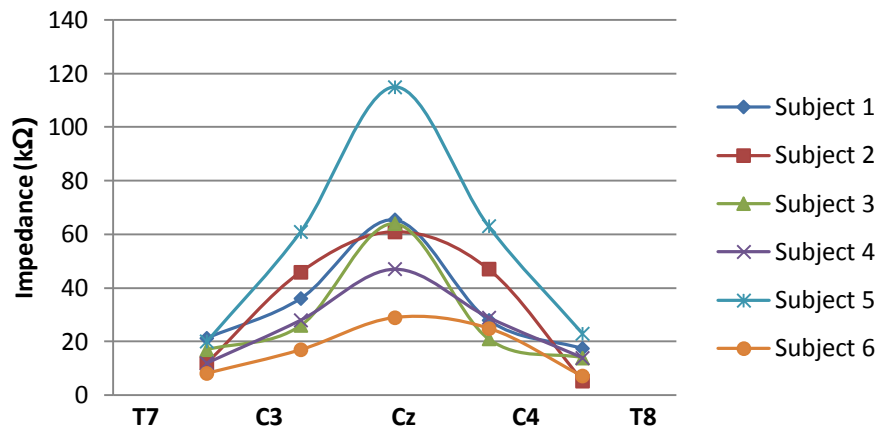


Figure 57: Graph of impedance with respect to position at 150 grams

5.3.3 Impedance Variation along FPZ-FZ-FCZ-CZ-PZ-OZ

CZ was observed to have the highest impedance reading under all three loading conditions for all subjects. Additionally, the point FPZ generally has the lowest impedance, even lower than point FZ. This could be explained by the fact that all the subjects had lower hair follicle density around the FPZ point and some did not even have hair there.

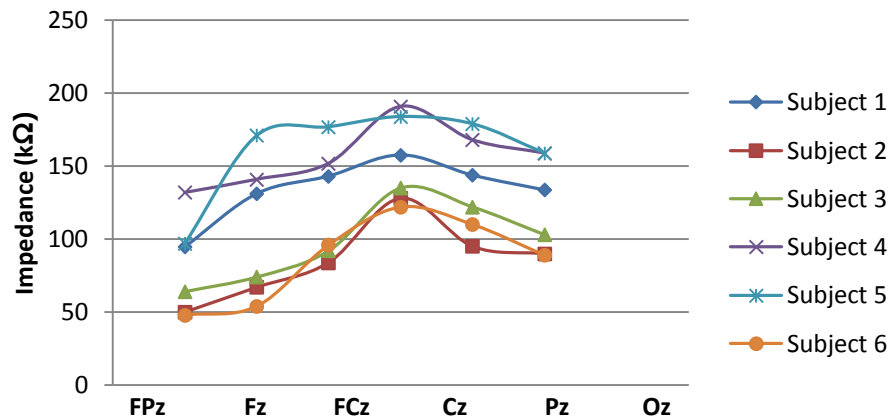


Figure 58: Graph of impedance with respect to position at 50 grams

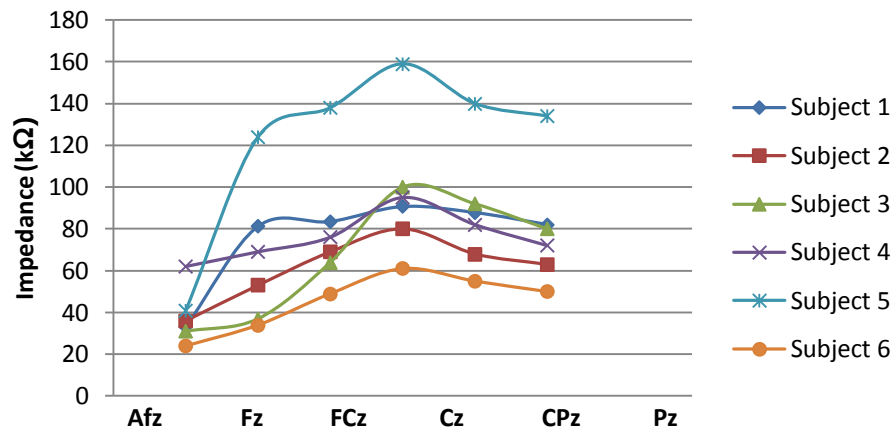


Figure 59: Graph of impedance with respect to position at 100 grams

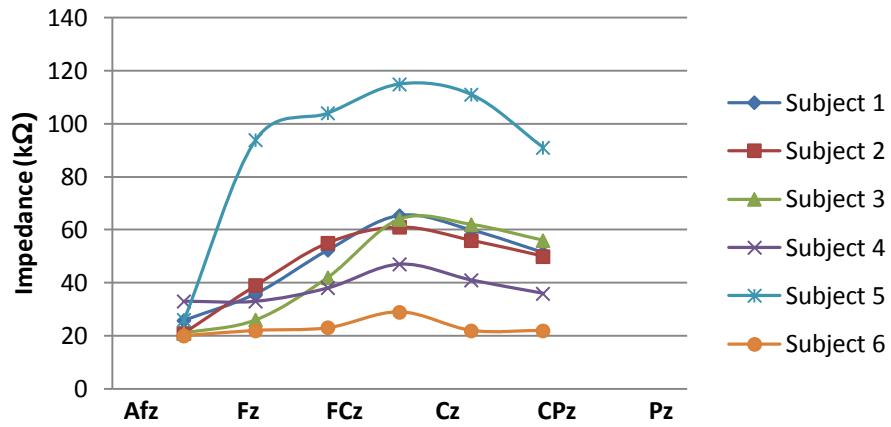


Figure 60: Graph of impedance with respect to position at 150 grams

5.3.4 Load Variation for Constant Impedance

As the impedances were only read for loading values of 50, 100 and 150 grams, it was necessary to interpolate the data to achieve constant impedance at all points and the linear curve fitting and exponential curve fitting were employed and compared. In the linear curve fitting method, the least squares method was used. The equation for the

slope of the regression line is:

$$m = \frac{\sum (x - \bar{x})(y - \bar{y})}{\sum (x - \bar{x})^2}$$

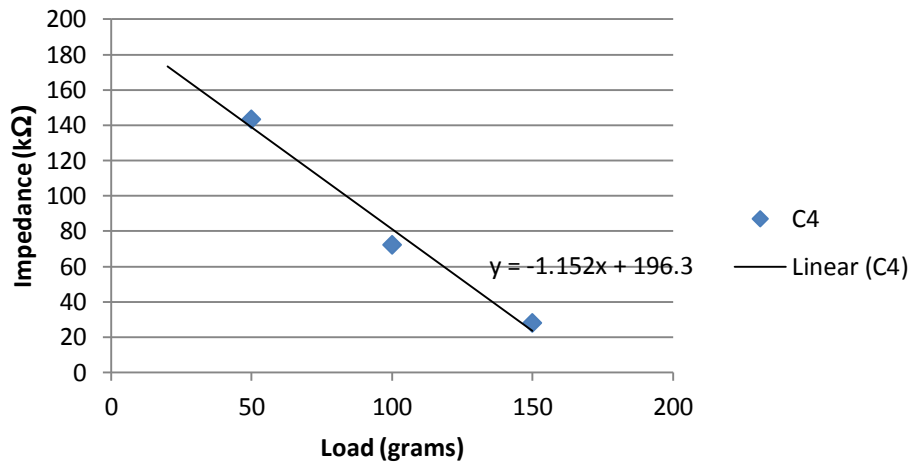


Figure 61: Sample best fit linear regression line

In the exponential curve fitting method, the data points at each scalp position for all subjects are fit to the functional form: $y = Ae^{Bx}$

The best fit values then become:

$$a = \frac{\sum_{i=1}^n \ln y_i \sum_{i=1}^n x_i^2 - \sum_{i=1}^n x_i \sum_{i=1}^n x_i \ln y_i}{n \sum_{i=1}^n x_i^2 - (\sum_{i=1}^n x_i)^2}$$

$$b = \frac{n \sum_{i=1}^n x_i \ln y_i - \sum_{i=1}^n x_i \sum_{i=1}^n \ln y_i}{n \sum_{i=1}^n x_i^2 - (\sum_{i=1}^n x_i)^2}$$

Where $B \equiv b$ and $A \equiv e^a$.

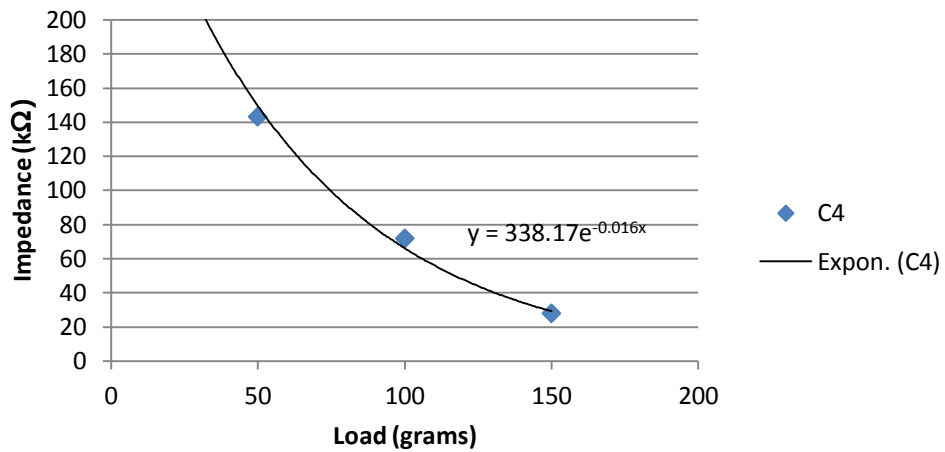


Figure 62: Sample best fit exponential regression line

The interpolated data from both methods was plot on the scalp as shown in Figure 63. Figure 63A and 63B show how the load has to vary across the profile of the scalp in order to maintain constant impedance via the linear curve fitting method and the exponential curve fitting method respectively. A minimum load of 10g was set though the interpolation data suggested a smaller load in order to ensure that the electrodes made sufficient contact with the scalp. Figures 24C and 24D show the resultant impedances for the 24A and 24B respectively.

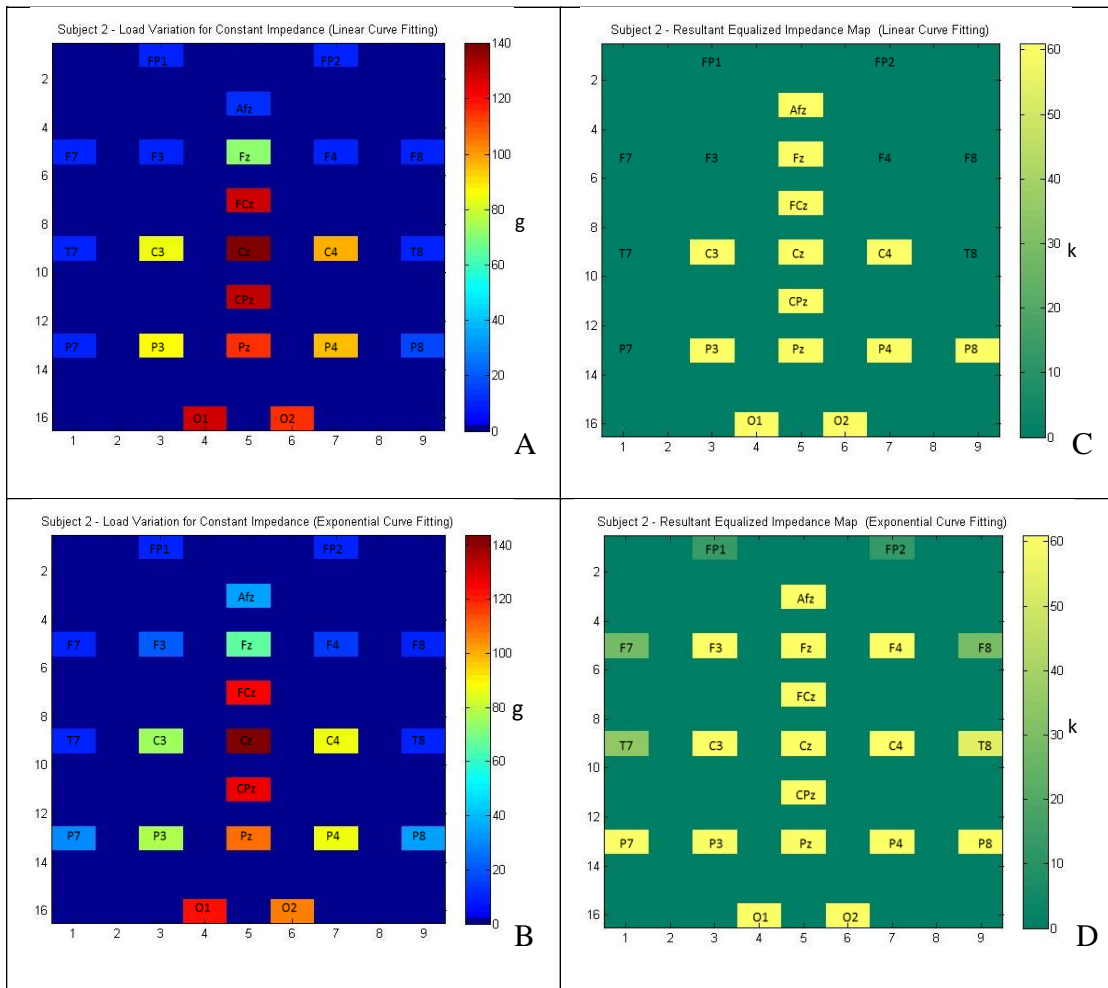


Figure 63: Load variation to minimize impedance mismatch. A and B shows values determined by linear and exponential curve fitting respectively. C and D show resultant impedances for linear and exponential curve fitting method.

From Figure 24, it can be seen that using the linear curve fitting method, causes most of the extrapolated data to be fall below the 10g lower limit which in turn causes significant impedance mismatch across the scalp profile. Figure 24B and 24D suggest that the load profile is more distributed and that the resultant impedances even at the extreme points FP1, FP2, F7, F8 and T7 while having a degree of impedance mismatch do not differ significantly from the intended impedance value of 61 k Ω . As

potential variations of the skin are non-linear with mechanical stress, it is reasonable to assume that the impedance would vary non-linearly with loading.

5.3.5 Optimized Loading Index for Constant Impedance

Figure 64 shows the optimized loading index to maintain constant scalp impedance. The impedance values were normalized for each subject and the average of the normalized indexes was calculated and plotted against each position on the scalp. This loading index allows the construction of an EEG headset designed to minimize impedance mismatch and noise and also allow better signal quality. Any such headset would have to vary the contact force of its electrodes on the scalp and the loading index would be very useful in that context.

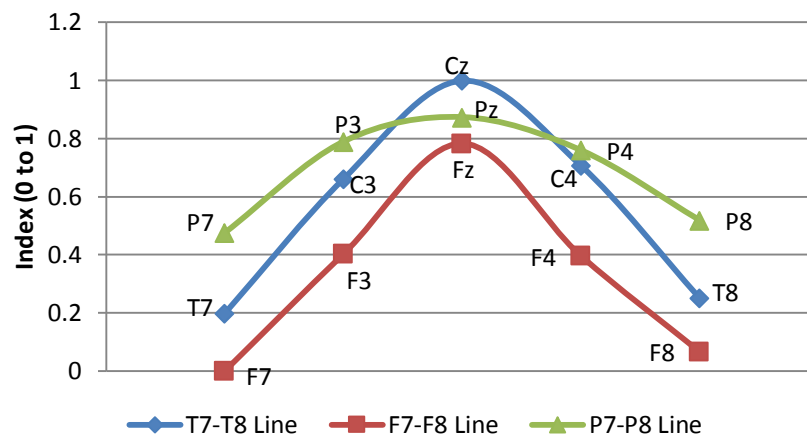


Figure 64: Graph showing optimized loading on at different locations

With the calculated load using both the linear and exponential curve fitting method, the scalp impedance of the subjects were taken with these loadings and normalized in Figure 65 and 66 respectively. It can be shown that by using the exponential curve fitting method, the resultant scalp impedance distribution has a lower standard

deviation than that of the linear curve fitting method which allows for more uniform scalp impedance for EEG to be recorded.

		91.8%				83.7%			Mean	89.80 %
									Std Dev	5.90 %
				96.1%						
88.2%		83.1%		93.8%		83.2%				81.3%
				82.1%						
93.0%		92.0%		100.0%		81.8%				82.6%
				92.8%						
90.1%		86.6%		99.8%		90.0%				99.5%
				85.1%		89.1%				

Figure 65: Impedance variation on the scalp by Linear Curve Fitting

		98.9%				90.1%			Mean	96.38 %
									Std Dev	2.66 %
				98.6%						
97.5%		98.3%		91.6%		98.1%				93.7%
				93.3%						
96.6%		98.7%		100.0%		97.8%				95.8%
				92.5%						
97.9%		95.8%		95.1%		97.7%				99.3%
				96.9%		96.1%				

Figure 66: Impedance variation on the scalp by Exponential Curve Fitting

5.4 Impedance checks

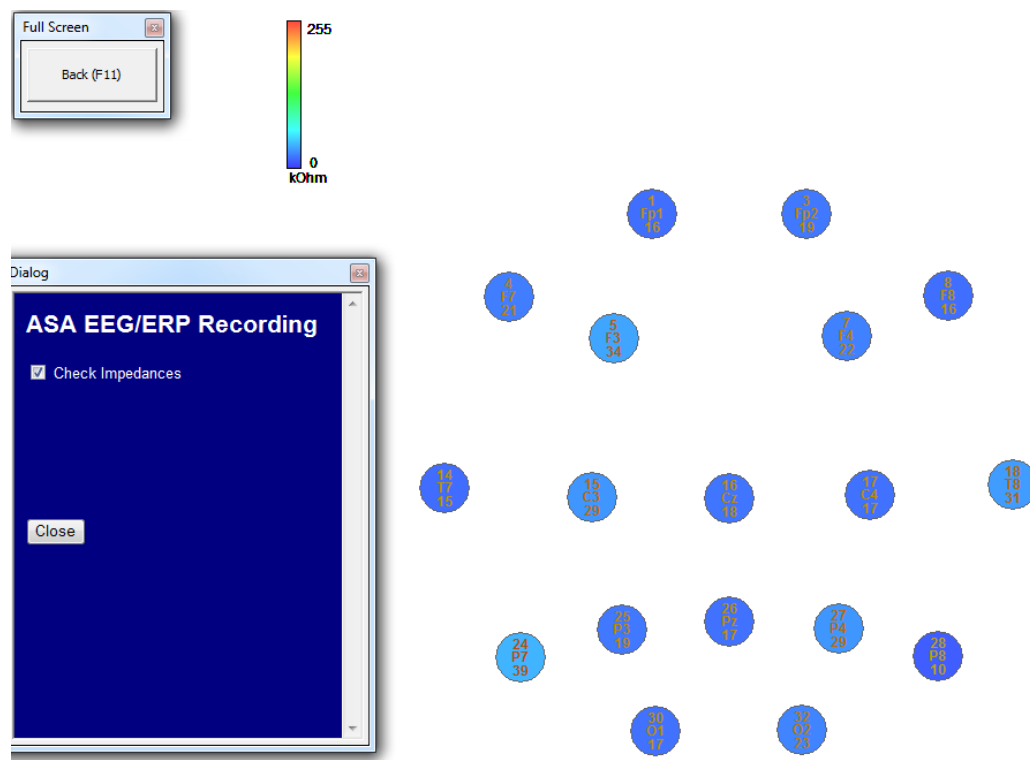


Figure 67: Impedance Test on the Novel Dry Electrode with the EEG Headset

Impedance checks using commercial EEG systems developed by Advanced Neuro Technology (ANT) were conducted to ensure that all electrodes have good contact, as shown in Figure 67. It shows that the impedances were relatively constant with an average of 21.77 and a standard deviation of 7.62.

CHAPTER 6

GATED CAPILLARY ACTION BIOPOTENTIAL SENSOR FOR A PORTABLE BIOPOTENTIAL RECORDING SYSTEM

With the rapid development of the world's economy, healthcare issues related to long working hours for the adults and age related problems for the elderly people have been plaguing societies that are so focused on squeezing that extra bit of gross domestic product growth. The Ministry of Health, Labour and Welfare of Japan reported that the sudden death of any employee who works more than an average of 65 hours per week for more than 4 weeks or more than an average of 60 hours per week for more than 8 weeks may be cause death due to overwork (Hiyama and Yoshihara 2008).

For aged cardiovascular patients living at home, a routine and repetitive electrocardiography measurement is often a basic vital monitoring parameter and is one of the commonly used techniques in modern clinic and biomedical applications, which records the electrical activities of the heart over time and yields important diagnostic information (Yu et al. 2009). This illustrates the need for effective monitoring of one's health, by means of electrophysiological monitoring, so that ample time could be catered for medical intervention should the need arises.

Electrophysiology is the study of the electrical properties of biological cells and tissues, involving measurements of voltage change or electric current on a wide variety of scales from single ion channel proteins to whole organs like the heart. In neuroscience, it refers to the measurements of large-scale electrical activity of the neurons particularly that of the action potential activity from the nervous system (Scanziani and Hausser 2009). This can be done by means of electroencephalography (EEG) which is the recording from the scalp, the voltage fluctuations resulting from ionic current flows within the neurons in the brain.

EEG has been widely used for both medical diagnoses and neurobiological researches as it is a non-invasive tool that provides a high temporal resolution (Gevins et al. 1994). One of the keys to recording good EEG signals is the type of electrodes used and electrodes that make the best contact with a subject's scalp and contain materials that most readily conduct EEG signals provide the best EEG recordings.

6.1 Types of EEG measuring electrodes

Some of the types of electrodes available include (1) reusable disks that are electrodes placed close to the scalp with a small amount of conducting gel used under each disk (made of tin, silver or gold) and held in place by a washable elastic head band, (2) adhesive gel electrodes that works together with a conductive paste that sticks to the scalp upon application, and the (3) sub-dermal sterilized, single-use needles with permanently attached wire leads, where the whole assembly is discarded, after every use so as to eliminate the risk to cross contamination between subjects. It must also be

noted that in some situations, regulatory committees need to approve the use of these sub-dermal needle electrodes before they are used.

As such, the most commonly used electrode for the recording of EEG is that of the reusable disks as the cost is low and does not require approval in its use. These disks usually comes with an electrode made out of Ag/AgCl and the characteristics of the widely used Ag/AgCl conventional wet electrode for EEG have also been thoroughly studied and it has been found that EEG signal quality is excellent with proper skin preparation and conductive gel usage.

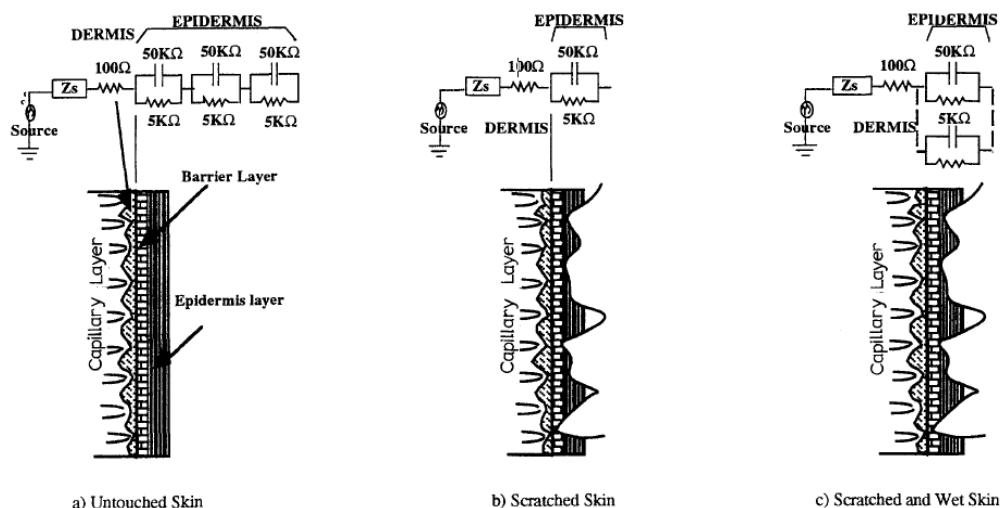


Figure 68: Skin model with typical impedance values at 10Hz (Taheri et al. 1994)

However, the use of conventional wet EEG electrode requires proper skin preparation and the use of conductive gels so as to reduce the impedance on the electrode-skin interface. Skin preparation involves the need to remove the stratum corneum by means of abrasion and that may be uncomfortable or even painful for the user. With skin preparation does not imply a good EEG signal quality throughout the whole

recording as this quality will degrade over extensive time period due to the regeneration of the skin or the drying of the conductive gel (Ferree et al. 2001).

Furthermore, repeated skin preparation may cause infections as the role of the stratum corneum is to form a barrier to protect underlying tissue from dehydration, infection, chemicals and mechanical stress. On top of that, these conductive gels would leave residues on the scalp thus requiring the user to have to wash their hair after every use. These processes are not only troublesome but also time consuming to the user, especially when it is to be used daily.

To overcome the issues with the use of the conventional wet EEG electrodes, various types of electrodes have been proposed and they range from dry-contact sensors (Lin et al. 2011) to the use of exotic technologies such as carbon nano-tubes (Ruffini et al. 2006). The impedance from these alternative electrodes may be comparable to the conventional wet electrodes after some time due to sweat and moisture buildup but they are highly susceptible to motion artifacts due to the high electrode-skin impedance and the lack of a hydro-gel or wet foam between the electrode and the skin to buffer against mechanical motion thus they work well for quick measurements but suffer in normal clinical applications(Sullivan et al. 2008).

A similar finding was reported showing that the EEG signal obtained can be largely comparable to wet electrodes, for stationary subjects. However, the high skin contact impedance results in a much larger motion artifact with the dry sensors with the TiN-based fingered dry electrode having reported impedance ranging from 14–55 k Ω / finger to around 10 M Ω / finger (Chi et al. 2009).

6.2 Design Consideration

The first consideration of the novel sensor is the bridging of the electrodes; sufficient amount of electrolyte is to be provided for yet without causing any cross-bridging, in which the electrolyte is confined such that it is kept totally inside the sensor when the sensor is not in bridging electrically the electrode and skin, and is totally confined within the sensor and sensor probe-skin interface when the sensor is in bridging electrically the electrode and skin.

The second consideration of the novel HD-EEG sensor is to have a design that allows for controlled scalp compression in order to reduce skin-electrode impedance hence obtaining good signal quality. However, this must be achieved by means of controlled compression of the scalp by the HD-EEG sensors as it must not achieve good EEG signals at the compromise of the comfort level of the user.

The third consideration is the setting up time of the HD-EEG measurement system. With the vast amount of sensors to be placed on the subject, the reduction of this time is crucial in ensuring that the subject's alertness level is still optimal for the experiments. Furthermore, the amplifier design is also of great importance as the amount of data to be captured is immense.

It is well-known that different neural imaging methods have their advantages and disadvantages and researchers have also started in the engaging of multi-modality sensing so incorporate the advantages of the different techniques, the novel HD-EEG sensor is designed with the ability of multimodal neural sensing with optical apparatus to obtain EEG-fNIR recordings.

As the dry HD-EEG sensors requires compression of the sensors so as to achieve a uniform scalp impedance which is crucial in the obtaining of good low impedance for good quality EEG signals, a self-clamping reconfigurable headset for the locating and securing the HD-EEG sensors in which the sensors and apparatus are properly placed on human heads of different shapes and sizes must be designed for.

The human scalp skin is physiologically very similar to non-palmoplantar skin of the rest of the body, except for its high concentration of sebaceous glands. There are about 250 hair fibers per cm^2 , which results, for a typical individual, in a hair surface area of $50,000 \text{ cm}^2$ relative to the scalp surface area of 600 cm^2 (James 2005). With a target number of electrodes set at 1024, each electrode can have a maximum surface area of 0.58 cm^2 , which results in the centre to centre distance between the electrodes having a distance of 8.59mm.

Knowing that there is a possibility of the electrodes touching each other in HD-EEG recording due to the touching of the sensors resulting in cross-bridging, each electrode is limited to a maximum diameter of 5mm. Electrode placement simulations were done on SolidWorks, 3D CAD and simulation software developed by Dassault Systèmes SolidWorks Corp, to determine the feasibility of the HD-EEG arrangement on the scalp, as shown in Figure 69. However, further studies have to be done to prevent cross-bridging due to contact between the wetted surfaces.

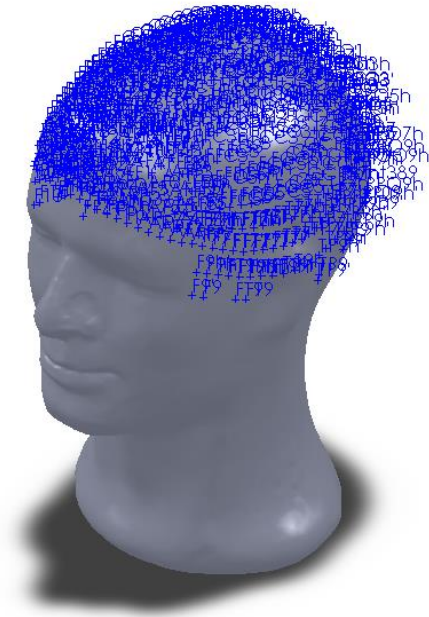


Figure 69: Feasibility study of HD-EEG measurement system

With the force required to have uniform scalp impedance obtained, this force is analyzed with the curvature of the head profile captured using the Xensor 3D Digitizer so as to ensure that the force is not too high so as to cause discomfort to the subject. Too high a force will not only cause discomfort but also cause the blood beneath that of the electrode to stop flowing and thus affecting the EEG signals.

With the maximum allowable sensor's diameter determined to be 6mm, a novel EEG sensor has to be developed as commercial EEG sensors, having sizes of about 50mm in diameter, are far too big in size so as to reduce artifacts due to chloride concentration change. Current state-of-the-art dry EEG electrodes can be grouped into two main categories for which the first is an invasive electrode having the purpose of penetrating the stratum corneum, and the second being a non-invasive electrode.

Two recently proposed solutions of the skin invasive category are the micro tip electrodes coated with iridium oxide (Dias, et al. 2010) and the carbon nano-tubes (Ruffini, et al. 2007). Both methods lead to high signal quality and are well suited for EEG recording. However, the possibility of the micro tips breaking and getting stuck inside the skin cannot be completely ruled out. For the case of the carbon nano-tubes, safety concerns have to be raised on the issue of the risks of infection by the carbon nano-tubes electrodes upon penetrating the tissue.

Although sterilization of the electrodes can be utilized to rule out transfer of infectious diseases such as Human Immunodeficiency Virus and Hepatitis C Virus, other diseases such as the Creutzfeldt-Jacob Disease may deem sterilization as inadequate as it is unable to destroy the prion that transmits. These risks speak against the use of skin-invasive dry EEG electrodes other than in disposable version, irrespective of production cost (Grozea, Voinescu and Fazli 2011). Risks of the transferring of infectious diseases clearly throw the invasive EEG sensors out of consideration leaving us with only the choice of using non-invasive electrode.

Non-invasive electrodes can then be categorized into the wet and dry electrodes. The use of the wet electrodes has the risk of having nearby channels being short-circuited due to the risks of cross-bridging. The use of dry electrodes then again is also not without problems; dry electrodes typically have high skin-electrode impedance as the stratum corneum is a layer of high impedance. However modern engineering principles suggest that excellent EEG signals can still be collected with high scalp impedance that are greater than $40k\Omega$ without scalp abrasion (T. Ferree, et al. 2001), thus the dry EEG electrodes is preferred.

This paper will present a new type of electrode for a wearable head cap for biopotential measurements which could be used in remote monitoring setting the foundation for telemedicine. The use of this new electrode allows EEG monitoring to be done remotely as the setting up of the conventional wet electrode by a trained technician is no longer necessary. First, a description of the new electrode design and its integration onto commercialized EEG head caps would be made. Then the new electrode would be tested against the conventional wet electrode for both the detection of standard EEG waves and the ERP of a visual protocol, with their respective results discussed.

Biopotential recording systems are used to record the various physiological signals so as to better understand the state of the human body, particularly of interest for applications such as detection of abnormal heart rhythms, diagnosis of epilepsy and brain-computer interface. Conventional biopotential measurement requires conductive gel to be applied at every measured location thus making the procedure lengthy and uncomfortable for the subject.

This work presents a novel electrode that allows for the recording of biopotential signals without the need for manual conductive gel application and whose technology principle leads to a portable biopotential recording system that retains the advantages of using the conventional wet electrodes while allowing the system to be portable for use in remote monitoring setting the foundation for telemedicine.

Experiments were performed to evaluate the impedance properties and signal quality obtained by the electrode to that of the conventional wet electrodes by means of both

a dynamic signal analyzer and a standard visual protocol. The results have shown that the new electrode has adequate sensitivity and records signals with a higher signal-to-noise ratio (SNR), making the electrode an eligible candidate for use in portable biopotential recording system.

6.3 Material and Methods

6.3.1 Novel Electrode Design

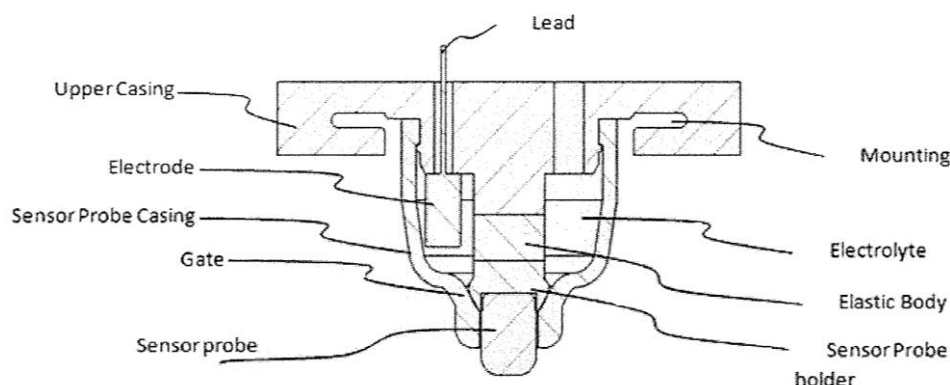


Figure 70: A cross-sectional view of the novel electrode

The proposed confined capillary action electrode, as shown in Figure 70, was designed and fabricated to contact the scalp surface using the sensor probe with a radius of 6mm, which may be a solid absorbent material that is made of either an electrically conductive or non-conductive material such that the electrolyte confined in the sensor would release only the right amount of electrolyte by means of capillary action, and confined at the probe-skin interface when the probe is in contact with the skin.

The elastic body behind the sensor probe holder has a spring rate of 50g/mm so as to maintain good electrode-skin contact without causing a painful sensation to the subject, and to ensure that the gate is always closed restricting the release of electrolyte to the sensor probe when the sensor is not in use. To allow for an extended use of the capillary action electrode, an opening in the upper casing allows for the injection of the electrolyte even when the confined capillary action electrode is in use.

In order to acquire quality EEG signals even on hairy sites, the sensor probe is designed to pass through the hairs, that grows out of the scalp surface at an average angle of 75 degrees (Pinkus 1958), without it being trapped beneath the probe impeding the obtaining of a good electrical contact with the scalp. The electrolyte reservoir is filled with a sponge-like material to dampen the motion of the electrolyte which could cause motion artifacts and to ensure a good bridge of the electrode to that of the scalp. In this design, the Ag/AgCl electrodes are used to have a better frequency characteristic which is required for DC recordings.

The electrolyte used in this electrode has high conductivity with low viscosity and it consists of Optrex Eye Lotion (Distilled Witch Hazel 13% v/v, Benzalkonium Chloride 0.0005% w/v in a solution buffered with Borax and Boric Acid) with 0.5% w/v Sodium Chloride. With the need to replace only the sensor probe assembly, consisting of the casing, probe and its holder, prior to every use to avoid cross contamination between subjects; this brings about the ease of use on the subject by reducing setting up time which is necessary when one is using the conventional wet electrodes.

On top of that, the use of conductive gel with the conventional electrode will require the subject to wash their hair after every recording and this can be done away with the use of the novel electrode. The design of the sensor probe was based upon that of the model developed by Clague (Clague et al. 2000) who used the lattice Boltzmann method on both the D3Q15 and D3Q19 lattice to simulate creeping flow through fully three-dimensional random fibre networks, in which free overlapping of the fibres was allowed.

In this model, the unbounded media were considered with the effect of the wall on the overall permeability of the fibrous media investigated using a scaling analysis to develop a phenomenological relationship between permeability and porosity for both the bounded and unbounded fibrous media and it was found that:

$$\frac{K}{a^2} = b_1 \left(\sqrt{\frac{1 - \phi_c}{1 - \phi}} - 1 \right)^2 \cdot e^{b_2(1 - \phi)}$$

where K , a , ϕ and ϕ_c are the permeability tensor, fibre radius, porosity and the critical value of porosity below which there is no permeating flow (the percolation threshold) respectively with b_1 and b_2 being the curve fitting parameters. With the novel electrode design, the effective model as shown in Fig.3 is that of the untouched and wet skin which could effectively lower the skin's impedance so that EEG measurement is feasible. The equivalent circuit model of the dry EEG sensor skin-electrode wet interface is shown in Figure 71.

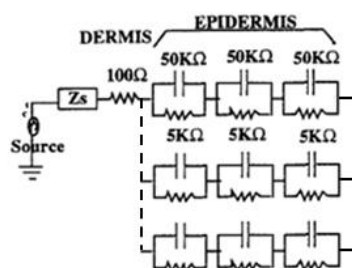


Figure 71: Effective skin model with typical impedance values at 10Hz

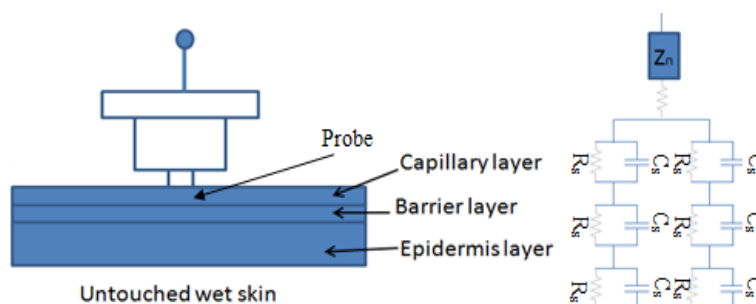


Figure 72: Effective skin model with typical impedance values at 10Hz

6.3.2 Novel EEG Headset Design

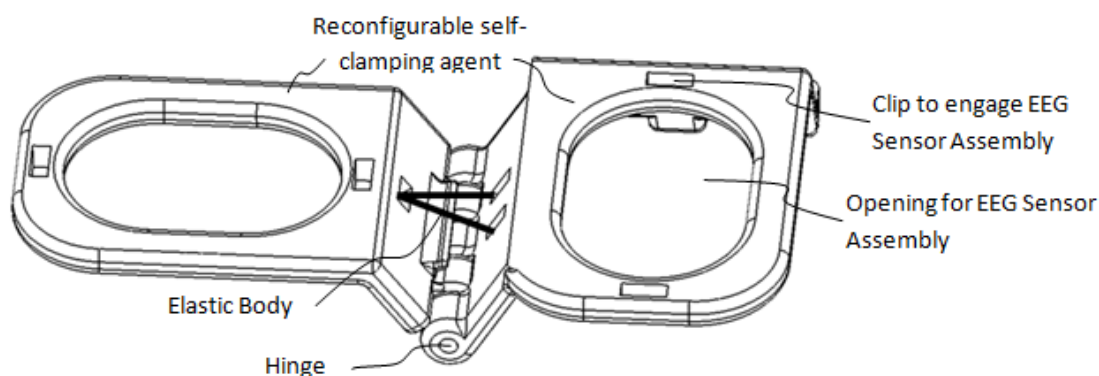


Figure 73: Design of the Reconfigurable self-clamping assembly

Figure 73 illustrates the reconfigurable self-clamping assembly, having two or more re-configurable self-clamping agents. Each agent is reconfigurable in length to allow the headset to suit different head shapes and sizes. The shape of the re-configurable self-clamping agent is not limited to thin rectangular or square sheet form, and is configured to have at least one of the edges bent at a certain angle. The end of the bent part is connected to the end of similar bent part of another reconfigurable self-clamping agent by a hinge joint so as to allow the reconfigurable self-clamping agents to rotate smoothly within a certain range in relation to the each other. On the bend of the reconfigurable self-clamping agent, an elastic body connects the two reconfigurable self-clamping agents and can be tightened sufficiently to pull the two reconfigurable self-clamping agents toward each other at a certain angle in the initial form. The self-clamping mechanism is realized by the tension between the re-configurable self-clamping agents, which may have an opening and a clip for the accurate positioning and mounting of the EEG Sensor Assembly.

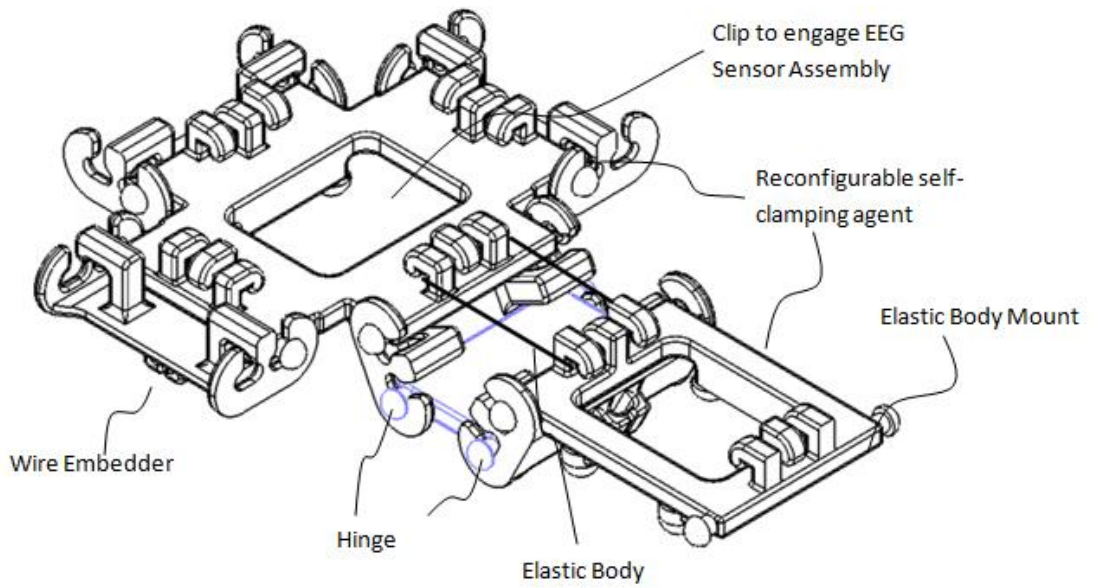


Figure 74: MRI compatible configuration of the self-clamping assembly

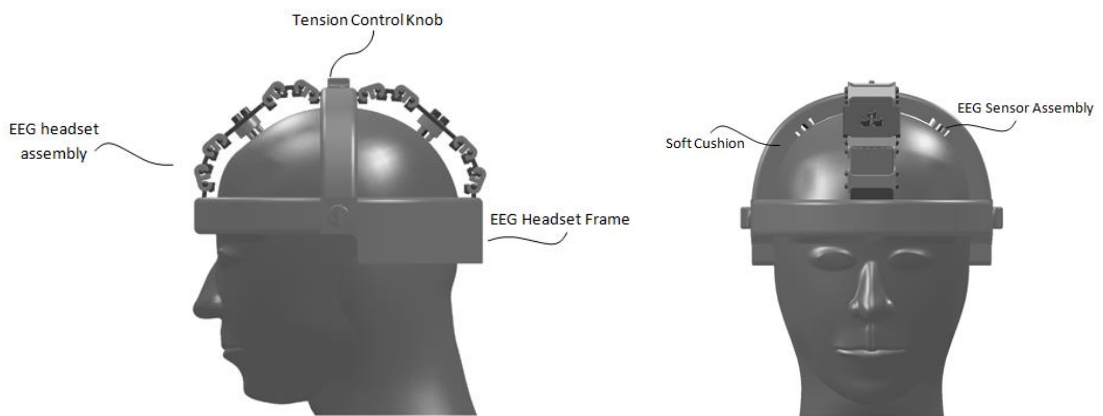


Figure 75: Full Reconfigurable self-clamping assembly

Figure 74 shows another embodiment of the re-configurable self-clamping assembly that is MRI compatible as the first design uses a metal rod as the hinge, which induces artifacts during a MRI scan. These modules are then mounted onto an EEG headset frame as shown in Figure 75. Soft cushion is being added in between the subject scalp and the frame for comfort.

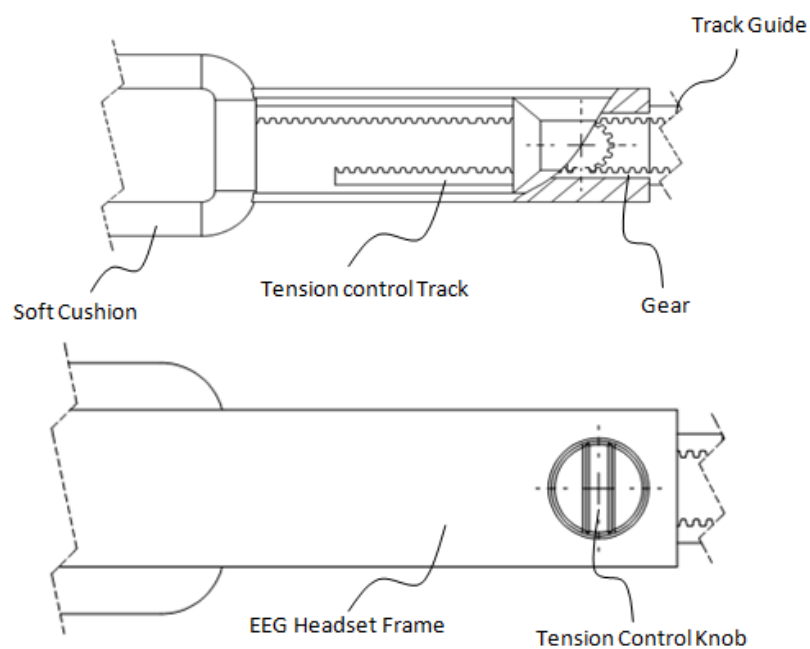


Figure 76: Tensioning Mechanism of the EEG Headset Mount

Figure 76 illustrates a tension adjustable headset apparatus that is to secure the EEG headset assembly or/and EEG sensor firmly and comfortably on the subject's head of different sizes. The apparatus may be formed by a headset frame that contains a tension control mechanism that includes the tension belts with track, tension control knobs, gears, and track guides. The mechanism allows the length of the tension belts to be adjustable by turning the tension control knobs. Soft cushions that covers around the tension belts providing moderate tension and comfort to the subject. The soft cushion may be an air-pump activated cushion. After the apparatus being worn on, the air-pump is activated to provide tension and at the same time providing comfort to the subject.

6.3.3 Fabrication process of a electrode

Each electrode consists of an Ag/AgCl pellet encase in a PVC plug. In this section, the fabrication process of an electrode shows how the steps of making an electrode.

1. Ag/AgCl pellet electrode is being soldered onto the 20 way flat cable.

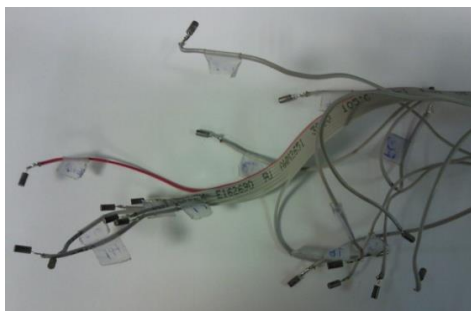


Figure 77: Ag/AgCl pellets and cable

2. Next the Ag/AgCl is placed into a PVC plug.

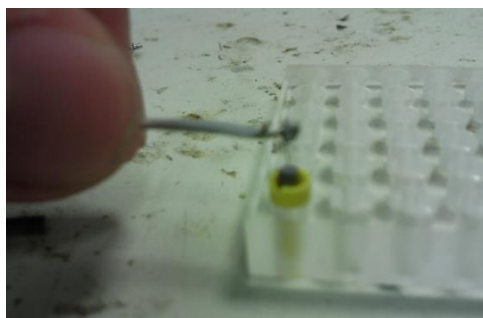


Figure 78: Ag/AgCl pellet into plug

3. The PVC plug and Ag/AgCl is then filled with epoxy¹ to cure.

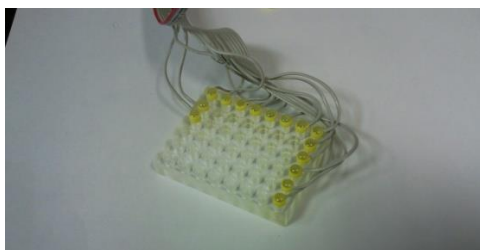


Figure 79: Epoxy left to cure

¹ Technical sheet of the Epoxy attached in Appendix B

6.3.4 Experiment Protocol for the Testing of the Novel Electrode Design

To evaluate the capability of the electrode, a thorough ERP and SNR analysis was done on the recorded EEG signals by the electrode and the commercialized wet EEG developed by Advanced Neuro Technology (ANT). As the core activation of the visual experiment lies in that of the occipital region of the brain, the channels over the occipital region such as PO7, O1, OZ, O2 and PO8 were selected. Channels PO7, OZ and PO8 from the 64 channels WaveGuard Cap from ANT were pitted against the gated capillary action electrode placed on O1 and O2.

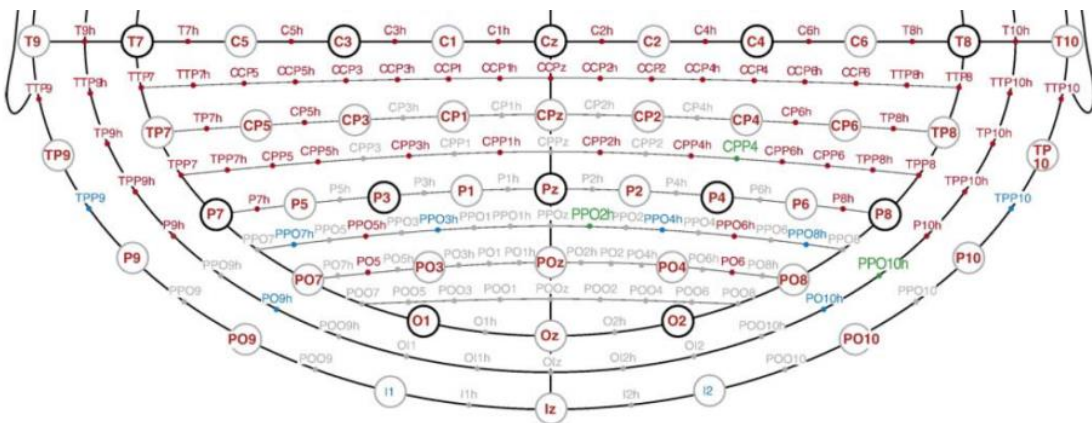


Figure 80: The 10/5 System (Dan et al. 2007)

A static checkerboard stimulus will be shown, a square of lateral 5° visual angle to a 9° visual angle from the inner margin of the square to the central fixation cross, randomly either on the left or the right side. The subject is asked to keep his eyes fixed on the central cross, with the help of a chin rest mounted on the experiment stage, so that if the stimulus appears on the left side, it will activate the right visual cortex and if it appears on the right side the left visual cortex will be mainly activated.

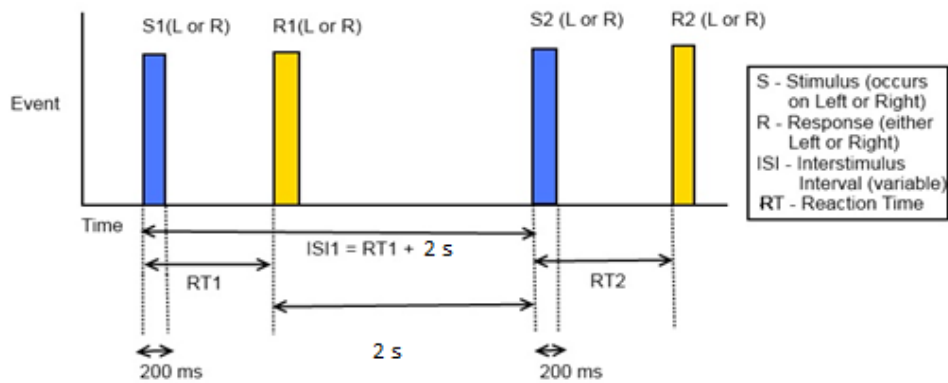


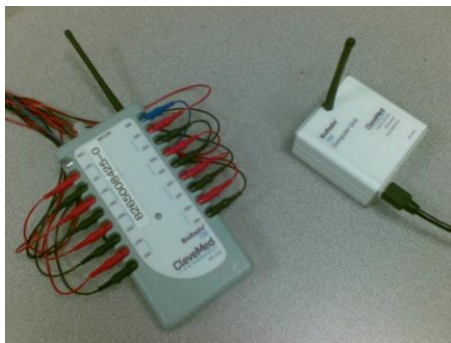
Figure 81: Visual checkerboard stimuli protocol

Each visual checkerboard stimulus, on either the left or right side, lasts for 200ms. The subject was told to press specific buttons on either the left or right side of the keyboard, using the hand on the same side of the appearing image, depending on the position of the stimulus, thus keeping the subject engaged in the task. As soon as the subject sees the stimulus and presses the corresponding button on the keyboard, a time period of 2s is given prior to the presenting of the next visual stimulus. This task goes on for 60 times shown randomly on either side, forming one block of trial taking about 8 minutes. A total of three such trials are done to give 180 stimuli.

Portable EEG Acquisition System

The system requires digital (as opposed to analog) recording of EEG signals, so that the data can be digitally processed for the prediction of mental fatigue levels. Electronic components such as differential amplifiers, analog-digital converters and digital filters are essential in a digital EEG system. Many digital EEG processing solutions are readily available in the market. The BioCapture™ (a trademark of Cleveland Medical Devices Inc.) research system, which was already available in the Neurosensors Laboratory, was chosen for this project. As a programmable monitor for

recording physiological signals, it consists of 2 components, the amplifier unit and the computer unit. The electrodes are connected to the amplifier unit, which is responsible for the amplification and digitization of EEG signals. The digital data is transmitted wirelessly to the computer unit, which is connected to the computer via a standard USB connection.



Criteria	System Requirement	BioCapture Specification
Number of channels	8	8
Sampling rate	256 samples per second	128 – 960 samples per second (configurable)
Digitization resolution	12 bits or more	8, 12, 16 bits (configurable)
Common-mode rejection ratio	At least 80 dB	More than 90 dB
Noise	Less than 2 μ V peak-to-peak (0.5 – 100 Hz)	Less than 2 μ V peak-to-peak (0.5 – 100 Hz)

Figure 82: System Requirements and BioCapture Specifications

The BioCapture system was chosen because it met the specifications of the mental fatigue screening system. The electrode montage would require an amplifier with 8 input channels, and the mental fatigue level classification software would require a sampling frequency of 256Hz. The BioCapture system also fulfilled the requirements for digital EEG recording, as recommended by the American Clinical Neurophysiology Society. In addition to meeting the above requirements, the BioCapture system also offered several other

advantages. The amplifier unit was lightweight, had a compact form factor and also featured wireless data transmission, thus allowing easy handling by the user. It also came with its own data acquisition software to facilitate component testing, such as the capability testing of the dry electrodes. Furthermore, software development kits (SDK) were also provided, allowing for easy integration with MATLAB and LabView during the software development phase.

Electrode-amplifier Interface

In order to provide convenience for the user in connecting the electrodes for EEG recording, the channel connection interface on the amplifier unit was modified to a 9-pin interface. As seen in Figure 70, the 8 active electrodes and the reference electrode could be connected simultaneously via a 9-pin connector, while the ground electrode would be connected separately via standard electrode connector.

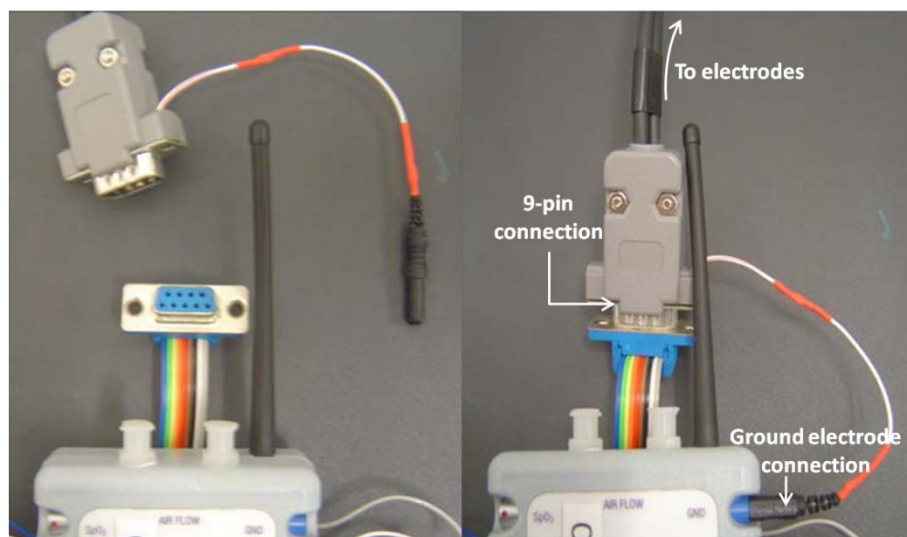


Figure 83: Modified electrode-amplifier interface

6.4 Results and Discussion

6.4.1 Basic EEG Wave Detection Capability

The average impedance over a period of 3 hours is $15\text{k}\Omega$ with a standard deviation of $1\text{k}\Omega$. From Figures 84 and 85, it can be seen that alpha waves could be picked up when the eyes are closed and when the eyes are open, beta waves dominates while alpha waves disappear. The detection of basic EEG signals, such as alpha waves, from spontaneous EEG can be used as a primary test for electrode's performance.

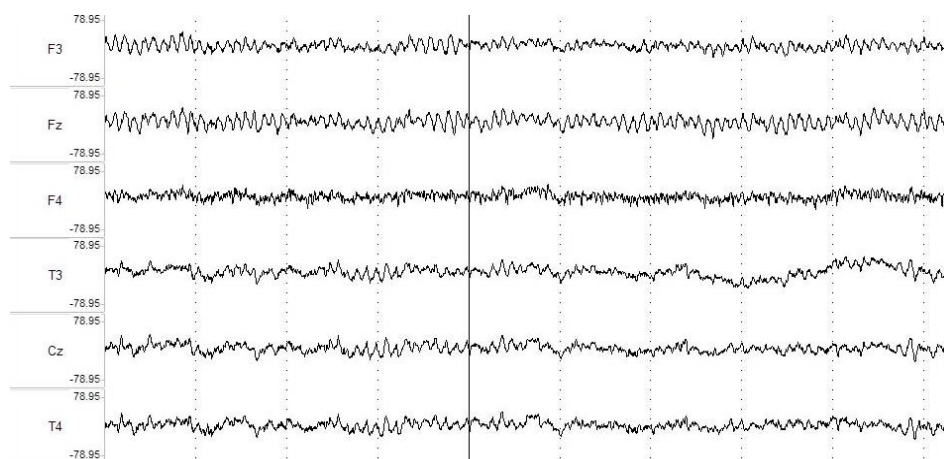


Figure 84: Recorded EEG signals with eye closed

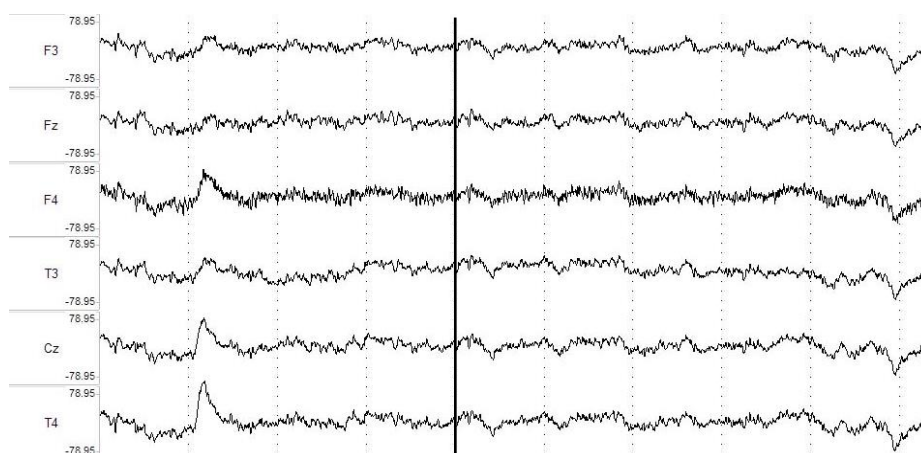
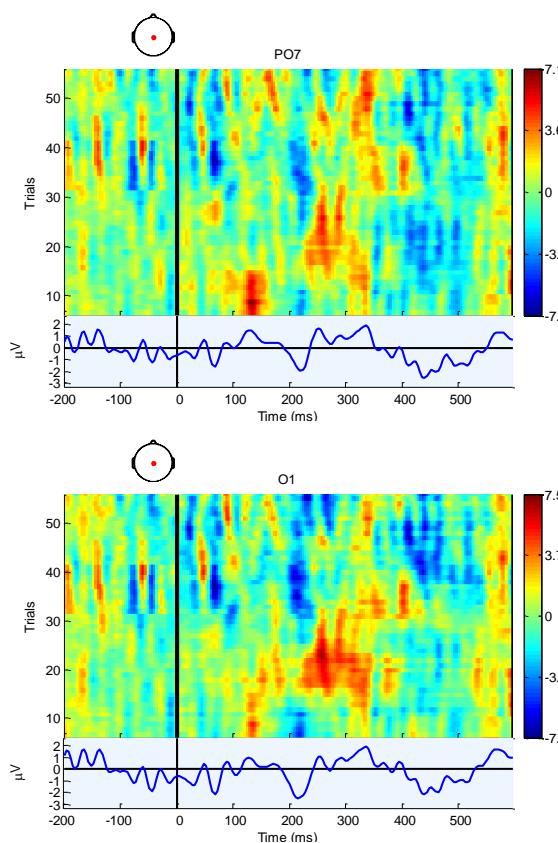


Figure 85: Recorded EEG signals with eye open

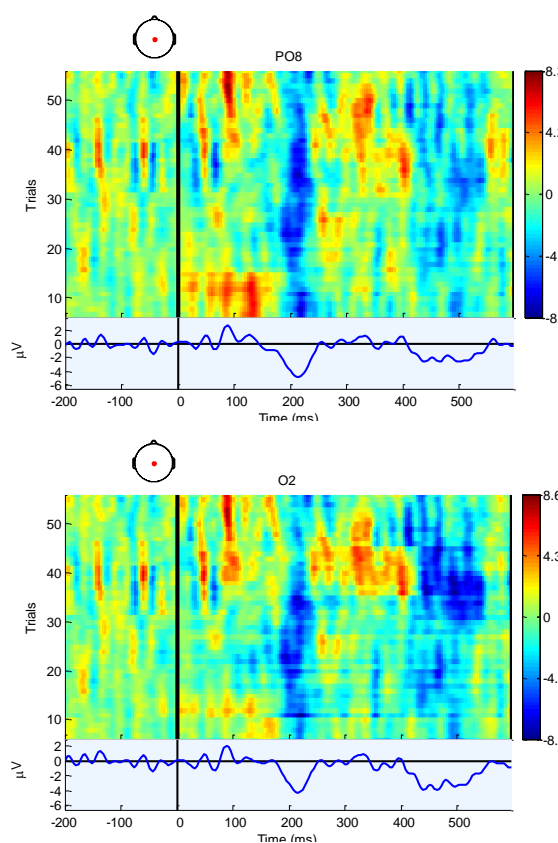
6.4.2 Signal Quality of the Gated Capillary Action Electrode

The gated capillary action electrode is used in conjunction with conventional wet electrodes by ANT in the collection of EEG according to the protocol discussed in “Materials and Methods”. Before further analysis is being done on the collected data, a band pass filter of 0.5Hz and 40Hz is used to clean up the collected EEG data from common-mode noise. Figure 86 shows the visual evoked potential (VEP) with O1 and O2 having signals collected from the gated capillary action electrode. No significant difference can be seen between the signal quality collected from the conventional wet electrode and that of the gated capillary action electrode.

Left Hemisphere



Right Hemisphere



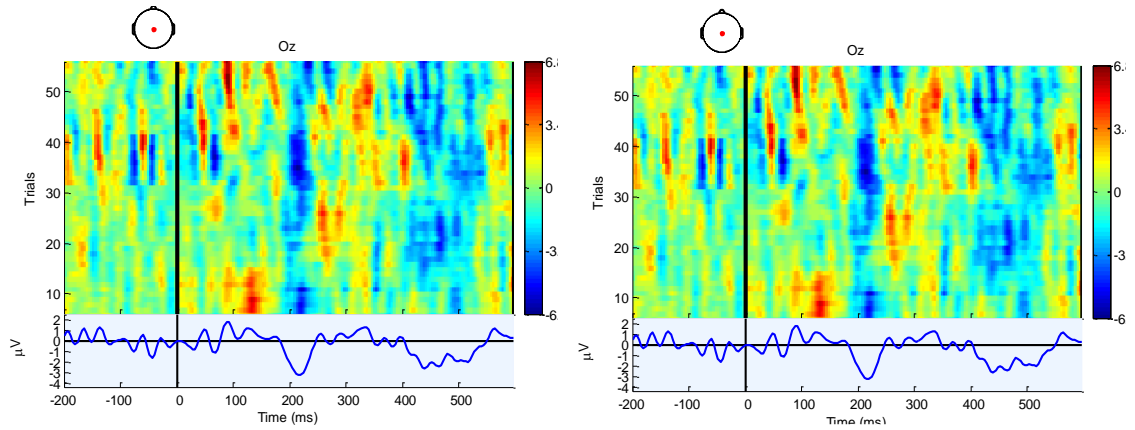


Figure 86: VEP of channels PO7, O1, OZ, O2 and PO8

After looking at the event related potentials generated with the use of EEGLAB, the signal-to-noise ratio (SNR) of the EEG data is being analyzed so as to have a better gauge of the noise level in the EEG signals collected. The widely accepted definition of SNR is:

$$\text{SNR} = 20 \log \frac{\langle V_s \rangle}{\langle V_n \rangle}, \quad \text{where } V_{s/n} = \sqrt{\frac{\sum_{i=1}^{N_{s/n}} V_{s/n,i}^2}{N_{s/n}}}$$

The SNR of the recorded EEG signals due to the visual stimulus with a mixture of electrodes is as shown in Table 9. The SNR of the dry electrodes is always higher than the wet electrodes thus the confined capillary action electrode is more sensitive than that of the conventional wet electrodes in picking up EEG signals.

Table 9: SNR to visual stimulus

Location	Type of sensor	$20 \log \left(\frac{V_s}{V_N} \right)$
PO7	Wet	6.0779
O1	Dry	7.5002
OZ	Wet	6.7687
O2	Dry	7.6077
PO8	Wet	6.8879
	Average	6.8879

Location	Type of sensor	$20 \log \left(\frac{V_s}{V_N} \right)$
PO7	Dry	9.3949
O1	Wet	8.4724
OZ	Dry	8.0630
O2	Wet	8.4959
PO8	Dry	8.4622
	Average	8.5777

CHAPTER 7

CONCLUSIONS

The objective of this thesis is to obtain the localized resistivity of the skull at different locations with differing thickness and porosity as it is an important parameter when it comes to the assumption of the human head as a volume conductor when performing source localization with EEG data. The difference in skull resistivity can contribute to great variations in the quality of measured EEG signals. It has been shown that the porosity of the skull segment plays an important role in its resultant resistivity. Even when tested with current sources of varying frequencies such as 20 Hz, 50 Hz and 100 Hz, it was found that the trend of a low porosity bone has a higher resistivity remains. It has also been verified that the sutures, which is the border of 2 pieces of skull bone, has the minimum resistivity measured.

Understanding that different locations on the scalp will have different impedance and that the difference in this impedance is critical in the reducing of EEG noise, thus the human scalp impedance distribution is studied. This impedance distribution is used to derive a loading index for different electrode locations which could then be used for the achieving of more uniform impedance across the human scalp thus reducing impedance mismatch that will cause EEG noise. This uniform impedance loading index could be used as a mechanism in the designing of dry EEG electrodes for which the headset design exploits the effect of mechanical loading on the scalp so as to

reduce the electrode-scalp impedance so as to achieve an optimum EEG recording condition with uniform impedances across various locations on the scalp.

With that, the confined capillary action electrode was designed and its capability being tested and proven to be comparable to that of the conventional wet electrodes despite not having the hassle required in the setting up of the conventional wet electrodes. The ease of use of this electrode allows it to be readily incorporated into current technologies so as to speed up the EEG measurement process.

On top of that, this electrode can also be used in ambulatory incidences that require a system that can be deployed swiftly with ease. Furthermore, the noninvasive nature of the confined capillary action electrode permits greater subject motion without much impedance variation as can be seen in the three hours study, which will definitely improve user compliance for the system eliminating the need for a more rigorous artifact removal algorithm.

References

- A. Vaskelis, A. J., R. Juskenas, E. Matulionis, E. Norkus (1996). "Structure of electroless silver coatings obtained using cobalt (II) as reducing agent" Surface and Coating Technology **82**: 165-168.
- Babiloni, F., C. Babiloni, et al. (1997). "A high resolution EEG method based on the correction of the surface Laplacian estimate for the subject's variable scalp thickness." Electroencephalogr Clin Neurophysiol **103**(4): 486-492.
- Barry, B. W. (2002). "Drug delivery routes in skin: a novel approach." Adv Drug Deliv Rev **54 Suppl 1**: S31-40.
- Barry, B. W. (2004). "Breaching the skin's barrier to drugs." Nat Biotechnol **22**(2): 165-167.
- Bentley, J. P. (1983). "Principles of measurement systems."
- Berger, H. (1929). "Uber das Elektrenkephalogramm des Menschen." Arch. Psychiatr. Nervenkr. **87**: 527-570.
- Berka, C., D. J. Levendowski, et al. (2004). "Real-Time Analysis of EEG Indexes of Alertness, Cognition, and Memory Acquired With a Wireless EEG Headset." International Journal of Human-Computer Interaction **17**(2): 151-170.
- BIOSEMI. (n.d.). *Active electrodes*. Retrieved May 5, 2011, from BIOSEMI: http://www.biosemi.com/active_electrode.htm
- Birbaumer, N. and L. G. Cohen (2007). "Brain-computer interfaces: communication and restoration of movement in paralysis." The Journal of Physiology **579**(3): 621-636.
- Boone, K. and D. S. Holder (1995). Assessment of noise and drift artefacts in electrical impedance tomography measurements using the Sheffield Mark1 system. Proc. Concerted Action on Impedance Tomography (CAIT) Workshop on The Electrode-Skin Interface in Electrical Impedance Tomography, Belfast, UK, Innov. Technol Biol. Med.

- Brown, L. and R. Langer (1988). "Transdermal delivery of drugs." Ann. Rev. Med. **39**: 221-229.
- Carim, H. M. (1983). Cohesive nonsticky electrically conductive gel composition U. S. Patent. USA. **4,406,827**.
- Carim, H. M. (1988). Bioelectrode. Encyclopedia of medical devices and instrumentation. J. G. WEBSTER. New York, John Wiley and Sons: 195-226
- Chien, Y. W. (1987). Development of transdermal drug delivery systems. Drug Devel. Ind. Pharmacy. **13**: 589-651.
- Christopher, C. and R. H. Guy (1992). "Visualization of iontophoretic pathways with confocal microscopy and the vibrating probe electrode." Solid State Ionics: 197-206.
- Cullander, C. (1992). "What are the pathways of iontophoretic current flow through mammalian skin?" Advanced Drug Delivery Reviews **9**(2-3): 119-135.
- Dankers, T. E. H. (1996). Elektrische spanningsvariaties in oppervlakte-electroden, University of Amsterdam. **Master's Thesis**.
- Darlenski, R., S. Sassning, et al. (2009). "Non-invasive in vivo methods for investigation of the skin barrier physical properties." European Journal of Pharmaceutics and Biopharmaceutics **72**(2): 295-303.
- Du, L., Z. Zhuang, et al. (2008). "Head-and-face anthropometric survey of Chinese workers." Ann Occup Hyg **52**(8): 773-782.
- Edelberg, R. (1971). Electrical properties of the skin. A treatise of the skin. H. R. Elden. New York, John Wiley & Sons.
- Egawa, M., T. Hiroa, et al. (2007). "In vivo Estimation of Stratum Corneum Thickness from Water Concentration Profiles Obtained with Raman Spectroscopy." Acta Derm Venereol **87**: 4-8.

- Eggins, B. R. (1993). "Skin contact electrodes for medical applications." Analyst **118**(4): 439-442.
- EGI. (n.d.). *HydroCel Geodesic Sensor Nets*. Retrieved May 5, 2011, from EGI: <http://egi.com/research-division-research-products/sensor-nets>
- Elias, P. M. (1983). "Epidermal lipids, barrier function, and desquamation." J Invest Dermatol **80**(1 Suppl): 44s-49s.
- Estep, J. R., J. C. Christensen, et al. (2009). Validation of a Dry Electrode System for EEG. PROCEEDINGS of the HUMAN FACTORS and ERGONOMICS SOCIETY 53rd ANNUAL MEETING, San Antonio, Texas, USA.
- Fang, M. and D. Shi (2005). "Electroless plating of thin silver films on porous Al₂O₃ substrate and the study of deposition kinetics." Tsinghua Science and Technology **10**(6): 680-689.
- Ferree, T. C., P. Luu, et al. (2001). "Scalp electrode impedance, infection risk, and EEG data quality." Clin Neurophysiol **112**(3): 536-544.
- Foley, D., J. Corish, et al. (1992). "Iontophoretic delivery of drugs through membranes including human stratum comeum." Solid State Ionics: 53-56.
- Fonseca, C., J. P. Silva Cunha, et al. (2007). "A novel dry active electrode for EEG recording." IEEE Trans Biomed Eng **54**(1): 162-165.
- G. Ruffini, S. D., L. Fuentemilla, C. Grau, E. Farrés, J. Marco-Pallarés, P. C. P. Watts, S.R.P. Silva "First human trials of a dry electrophysiology sensor using a carbon nanotube array interface."
- Gatzke, R. D. (1974). "The electrode: a measurement systems viewpoint." Biomedical electrode technology: 99-116.
- Geddes, L. A., R. Steinberg, et al. (1973). "Dry electrodes and holder for electro-oculography." Med Biol Eng **11**(1): 69-72.
- Geddes, L. A. a. B., L.E. (1989). "Principles of applied biomedical instrumentation."

- Gersing E., S., M., And Osypka, M. (1995). "The appearance of positive phase angles in impedance measurements on extended biological object." Proc. Concerted Action on Impedance Tomography (CAIT) Workshop on The Electrode-Skin Interface in Electrical Impedance Tomography, Belfast, UK, Innov. Technol. Biol. Med. **16**(2): 71-76
- Gevins, A., M. E. Smith, et al. (1998). "Monitoring working memory load during computer-based tasks with EEG pattern recognition methods." Hum Factors **40**(1): 79-91.
- Gevins, A. S., D. Duroseu, et al. (1990). Dry Electrode Brain Wave Recording System. United States Patent. **4,967,038**.
- Gondran, C., E. Siebert, et al. (1995). "Non-polarisable dry electrode based on NASICON ceramic." Med Biol Eng Comput **33**(3 Spec No): 452-457.
- Gondran, C., E. Siebert, et al. (1995). Dry electrode based on nasicon ceramic for surface biopotential measurements. Proc. Concerted Action on Impedance Tomography (CAIT) Workshop on The Electrode-Skin Interface in Electrical Impedance Tomography, , Belfast, UK, , Innov. Technol. Biol. Med.
- Greischar, L. L., C. A. Burghy, et al. (2004). "Effects of electrode density and electrolyte spreading in dense array electroencephalographic recording." Clinical Neurophysiology **115**(3): 710-720.
- Grimnes, S. (1983). "Impedance measurement of individual skin surface electrodes." Med Biol Eng Comput **21**(6): 750-755.
- Griss, P., P. Enoksson, et al. (2001). "Micromachined electrodes for biopotential measurements." Microelectromechanical Systems, Journal of **10**(1): 10-16.
- H.W.Kelly (1985). "Controlled-release transdermal drug delivery"
" Cutis **35**(204-207).
- Heingartner, D. (2009). "Mental block." Spectrum, IEEE **46**(1): 42-43.

- Hueber, F., H. Schaefer, et al. (1994). "Role of transepidermal and transfollicular routes in percutaneous absorption of steroids: in vitro studies on human skin." Skin Pharmacol **7**(5): 237-244.
- Huigen, e. a. (2002). "Investigation into the origin of the noise of surface electrodes." Med. Biol. Eng. Comput. **40**.
- Illel, B. and H. Schaefer (1988). "Transfollicular percutaneous absorption. Skin model for quantitative studies." Acta Derm Venereol **68**(5): 427-430.
- Illel, B., H. Schaefer, et al. (1991). "Follicles play an important role in percutaneous absorption." J Pharm Sci **80**(5): 424-427.
- Isaacson, D. (1986). "Distinguishability of conductivities by electric current computed tomography." IEEE Trans. **5**(2): 92-95.
- Jasper, H. (1958). "Report of committee on methods of clinical exam in EEG." Electroencephalography and Clinical Neurophysiology **10**: 370-375.
- John J. Almasi M.E., O. H. S. (1970). "Systemic and random variations of ECG electrode system impedance." Annals of the New York Academy of Sciences **170**: 509-519.
- Kalia, Y. N. and R. H. Guy (1995). "The electrical characteristics of human skin in vivo." Pharm Res **12**(11): 1605-1613.
- Kasting, G. B. (1991). "Theoretical models for iontophoretic delivery." Advanced Drug Delivery Reviews **9**(2-3): 177-199.
- Kelly, H. W. (1985). "Controlled-release transdermal drug delivery." Cutis **35**(204-207).
- Klem, G. H., H. O. Luders, et al. (1999). "The ten-twenty electrode system of the International Federation. The International Federation of Clinical Neurophysiology." Electroencephalogr Clin Neurophysiol Suppl **52**: 3-6.

- Kligman, A. M., P. Zheng, et al. (1985). "The anatomy and pathogenesis of wrinkles." Br J Dermatol **113**(1): 37-42.
- Knepp, V. M., J. Hadgraft, et al. (1987). "Transdermal drug delivery: problems and possibilities." Crit Rev Ther Drug Carrier Syst **4**(1): 13-37.
- Kohli, R., W. I. Archer, et al. (1985). "Impedance measurements for the non-invasive monitoring of skin hydration: a reassessment." International Journal of Pharmaceutics **26**(3): 275-287.
- Kontturi, K., L. Murtomaki, et al. (1993). "Electrochemical characterization of human skin by impedance spectroscopy: the effect of penetration enhancers." Pharm Res **10**(3): 381-385.
- Lademann, J., U. Jacobi, et al. (2009). "The tape stripping procedure - evaluation of some critical parameters." European Journal of Pharmaceutics and Biopharmaceutics **72**(2): 317-323.
- Lawler, J. C., M. J. Davis, et al. (1960). "Electrical characteristics of the skin. The impedance of the surface sheath and deep tissues." J Invest Dermatol **34**: 301-308.
- Lee, H. J. and S. J. Park (2008). "Comparison of Korean and Japanese head and face anthropometric characteristics." Hum Biol **80**(3): 313-330.
- Marks, J. G. M., Jeffery (2006). "Lookingbill and Marks' Principles of Dermatology."
- Martinsen, Ø. G., S. Grimnes, et al. (1999). "Measuring depth depends on frequency in electrical skin impedance measurements." Skin Research and Technology **5**: 179-181.
- Martinsen Ø. G., S. Grimnes. (2001). "Facts and Myths about Electrical Measurement of Stratum corneum Hydration State." Dermatology **202**: 87-89.
- Matteucci, M., R. Carabalona, et al. (2007). "Micropatterned dry electrodes for brain-computer interface." Microelectron. Eng. **84**(5-8): 1737-1740.

- McAdams, E. T. (1989). "Effect of surface topography on the electrode-electrolyte interface impedance (i) the high frequency, small signal, interface impedance - a review." Surface Topography **2**: 107-122.
- McAdams, E. T. (1990). "Surface biomedical electrode technology." Int. Med. Device Diagnostic Ind.: 44-48
- McAdams, E. T. and J. Jossinet (1991). "The importance of electrode-skin impedance in high resolution electrocardiography." Automedica **13**: 187-208.
- McAdams, E. T. and J. Jossinet (1992). "A physical interpretation of Schwan's limit current of linearity." Ann. Biomed. Eng **20**(3): 307-319.
- McAdams, E. T., J. Jossinet, et al. (1996). "Factors affecting electrode-gel-skin interface impedance in electrical impedance tomography." Med Biol Eng Comput **34**(6): 397-408.
- McAdams, E. T., A. Lackermeier, et al. (1994). AC impedance of the hydrogel-skin interface. 16th Ann. Int. Conf. of IEEE Engineering in Medicine and Biology Society. Baltimore. USA: 870-871.
- NeuroScan. (n.d.). *Quick_Caps*. Retrieved May 5, 2011, from Compumedics: http://www.neuroscan.com/quick_caps.cfm
- Newell, J. C. (1995). Influence of electrode size on in-vivo impedance images. Concerted Action on Impedance Tomography (CAIT). Workshop on The Reproducibility of in vivo Electrical Impedance Tomography images., Keele, UK, Innov. Technol Biol. Med.
- Ng, W. C., H. L. Seet, et al. (2009). "Micro-spike EEG electrode and the vacuum casting technology for mass production." Journal of Materials Processing Technology. **209**: 4434-4438.
- Ng, W. C., M. H. Ng, et al. (2009). "Investigation on Ethanol and Propylene Glycol as Enhancers for Skin-Electrode Conductivity in Bioelectrical Potential Measurement." Functional Materials Letters. **2**: 175-177.

- Oh, S. Y., L. Leung, et al. (1993). "Effect of current, ionic strength and temperature on the electrical properties of skin." Journal of Controlled Release **27**(2): 115-125.
- Otberg, N., H. Richter, et al. (2004). "Variations of hair follicle size and distribution in different body sites." J Invest Dermatol **122**(1): 14-19.
- Pai-Yuan, T., H. Weichih, et al. (2009). A portable device for real time drowsiness detection using novel active dry electrode system. Engineering in Medicine and Biology Society, 2009. EMBC 2009. Annual International Conference of the IEEE.
- Pecoraro, V., I. Astore, et al. (1971). "Growth rate and hair density of the human axilla. A. Comparative study of normal males and females and pregnant and post-partum females." J Invest Dermatol. **56**(5): 362-365.
- Phipps, J. B. and J. R. Gyory (1992). "Transdermal Ion Migration." Advanced Drug Delivery Reviews **9**(2-3): 137-176.
- Pikal, M. J. (2001). "The role of electroosmotic flow in transdermal iontophoresis." Advanced Drug Delivery Reviews **46**(1-3): 281-305.
- Prausnitz, M. R., V. G. Bose, et al. (1993). "Electroporation of mammalian skin: A mechanism to enhance transdermal drug delivery." Proc. Nat. Acad. Sci. **90**: 10504-10508
- Reardon, K. A., I. E. Scheffer, et al. (1999). "How long should a routine EEG be?" Journal of Clinical Neuroscience **6**(6): 492-493.
- Reilly, J. P. (1992). Electrical stimulation and electropathology, Cambridge University Press.
- Rosell, J., J. Colominas, et al. (1988). "Skin impedance from 1 Hz to 1 MHz." Biomedical Engineering, IEEE Transactions on **35**(8): 649-651.
- Rosen, M. R. (2005). Delivery system handbook for personal care and cosmetic products : technology, applications, and formulations. Norwich, NY, William Andrew Pub.

- Ruffini, G., S. Dunne, et al. (2006). "A dry electrophysiology electrode using CNT arrays." Sensors and Actuators A: Physical **132**(1): 34-41.
- Scozzafava, J., M. S. Hussain, et al. (2010). "The role of the standard 20 minute EEG recording in the comatose patient." J Clin Neurosci **17**(1): 64-68.
- Shen, K. Q., X. P. Li, et al. (2008). "EEG-based mental fatigue measurement using multi-class support vector machines with confidence estimate." Clin Neurophysiol **119**(7): 1524-1533.
- Shen, K. Q., C. J. Ong, et al. (2007). "A feature selection method for multilevel mental fatigue EEG classification." IEEE Trans Biomed Eng **54**(7): 1231-1237.
- Smith, D. C. a. W., J.R. (1995). "Surface electrodes for physiological measurement and stimulation." Eur. J. Anaesthesiol **12**: 451-469.
- Smith, R. W. M. (1990). Design of a real time impedance imaging system for medical applications, University of Sheffield. **PhD. Dissertation**: 45-49.
- Southwell, D. and B. W. Barry (1983). "Penetration enhancers for human skin: mode of action of 2-pyrrolidone and dimethylformamide on partition and diffusion of model compounds water, n-alcohols, and caffeine." J Invest Dermatol **80**(6): 507-514.
- Speckmann, E.-J. and C. E. Elger (1999). Introduction to the neurophysiological basis of the EEG and DC potentials. Electroencephalography: Basic Principles, Clinical Applications, and Related Fields. J. P. In Ernst Niedermeyer and Fernando Lopes Da Silva Cunha. Hong Kong, Lippincott Williams & Wilkins: 15-27.
- Sugibayashi, K., S. Nakayama, et al. (1992). "Mechanism of skin penetration-enhancing effect by laurocapram." J Pharm Sci **81**(1): 58-64.
- Szabo, G. (1967). "Regional Anatomy of Human Integument with Special Reference to Distribution of Hair Follicles Sweat Glands and Melanocytes." Philosophical Transactions of the Royal Society of London Series B-Biological Sciences **252**(779): 447-&.

- Taheri, B. A., R. T. Knight, et al. (1994). "A dry electrode for EEG recording." Electroencephalogr Clin Neurophysiol **90**(5): 376-383.
- Taktak, A., P. M. Record, et al. (1995). "Practical factors in neonatal lung imaging using electrical impedance tomography." Med. Biol. Eng. Comput. **33**: 202-205
- Thong, H. Y., H. Zhai, et al. (2007). "Percutaneous Penetration Enhancers: An Overview." Skin Pharmacology and Physiology **20**(6): 272-282.
- Tyagi R, S. K., Shao SY, Li XP (2009). "A novel auditory working-memory vigilance task for mental fatigue assessment." Safety Science: 967-972.
- Wang, Z., J. R. Ives, et al. (2006). "Simultaneous electroencephalogram-functional magnetic resonance imaging in neocortical epilepsies." Adv Neurol **97**: 129-139.
- Webster, J. G. (1998). Medical Instrumentation. New York, John Wiley & Sons.
- Wijk van Brievingh, R. P. V. (1988). Medische technologie. Delft, Delftse Universitaire Pers
- Wilkes GL, B. I., Wildnauer RH (1973). "The biomechanical properties of skin: a polymer composite." CRC Critical Rev Bioeng **1**: 453-495.
- Wu, K. S., W. W. van Osdol, et al. (2006). "Mechanical properties of human stratum corneum: Effects of temperature, hydration, and chemical treatment." Biomaterials **27**(5): 785-795.
- Ya-Xian, Z., T. Suetake, et al. (1999). "Number of cell layers of the stratum corneum in normal skin - relationship to the anatomical location on the body, age, sex and physical parameters." Arch Dermatol Res **291**(10): 555-559.
- Yamamoto, T. and Y. Yamamoto (1976). "Electrical properties of the epidermal stratum corneum." Med Biol Eng **14**(2): 151-158.
- Yamamoto, T. and Y. Yamamoto (1977). "Analysis for the change of skin impedance." Med Biol Eng Comput **15**(3): 219-227.

- Yamamoto, Y. and T. Yamamoto (1978). "Dispersion and correlation of the parameters for skin impedance." Med Biol Eng Comput **16**(5): 592-594.
- Yamamoto, Y., T. Yamamoto, et al. (1986). "Characteristics of skin admittance for dry electrodes and the measurement of skin moisturisation." Med Biol Eng Comput **24**(1): 71-77.
- Yamamoto, Y., Yamamoto, T., and Ozawa, T. (1986). "Characteristics of skin admittance for dry electrodes and the measurement of skin moisturisation." Med. Biol. Eng. Comput. **24**: 71-77.
- Yonghong, H., D. Erdogmus, et al. (2008). Large-scale image database triage via EEG evoked responses. Acoustics, Speech and Signal Processing, 2008. ICASSP 2008. IEEE International Conference on.
- Yoshida, N. H. and M. S. Roberts (1992). "Structure-transport relationships in transdermal iontophoresis." Advanced Drug Delivery Reviews **9**(2-3): 239-264.

APPENDIX A - DERIVATION OF MATHEMATICAL REPRESENTATIONS

The relationships between the skin impedance, appendageal and SC impedance over time can be known by deriving from the electrical model shown in Figure 4-9.

Firstly, the experimental data for the skin impedance over time can be modelled as equation A.1 using least square close fit curve method.

$$Z_T(t) = Z_0 e^{-\lambda t} + C_T \quad (\text{A.1})$$

Using Ohm's law for 2 parallel resistors, the total skin impedance is:

$$Z_T = \left(\frac{1}{Z_S} + \frac{1}{Z_A} \right)^{-1} = \frac{Z_S Z_A}{Z_S + Z_A} \quad (\text{A.2})$$

Applying Chain Rule,

$$\begin{aligned} -\frac{dZ_T}{dt} &= -\frac{(Z_S + Z_A)Z_A - Z_S Z_A}{(Z_S + Z_A)^2} \cdot \frac{dZ_S}{dt} - \frac{(Z_S + Z_A)Z_S - Z_S Z_A}{(Z_S + Z_A)^2} \cdot \frac{dZ_A}{dt} \\ -\frac{dZ_T}{dt} &= -\left(\frac{Z_A}{Z_S + Z_A} \right)^2 \cdot \frac{dZ_S}{dt} - \left(\frac{Z_S}{Z_S + Z_A} \right)^2 \cdot \frac{dZ_A}{dt} \end{aligned} \quad (\text{A.3})$$

Since the skin is modeled as having two different decay processes due to the ion diffusion of the electrolyte by the SC and appendages,

$$-\frac{dZ_T}{dt} = Z_T \lambda_S + Z_T \lambda_A = Z_T (\lambda_S + \lambda_A) \quad (\text{A.4})$$

Hence comparing A.3 and A.4,

$$-\frac{dZ_S}{dt} \left(\frac{Z_A}{Z_S + Z_A} \right)^2 = \lambda_S (Z_0 e^{-\lambda_T t} + C_T) \quad (\text{A.5})$$

and

$$-\frac{dZ_A}{dt} \left(\frac{Z_S}{Z_S + Z_A} \right)^2 = \lambda_A (Z_0 e^{-\lambda_T t} + C_T) \quad (\text{A.6})$$

Dividing the A.5 and A.6,

$$\frac{\lambda_S}{\lambda_A} = \frac{dZ_S}{Z_S^2} \cdot \frac{Z_A^2}{dZ_A} \quad (\text{A.7})$$

Applying differentiation and integration methods to remove dZ,

$$\int \frac{-d\left(\frac{1}{Z_S}\right)}{-d\left(\frac{1}{Z_A}\right)} = \int \frac{\lambda_S}{\lambda_A}$$

$$\int d\left(\frac{1}{Z_S}\right) = \int \frac{\lambda_S}{\lambda_A} d\left(\frac{1}{Z_A}\right)$$

$$\frac{\frac{1}{Z_S}}{\frac{1}{Z_A}} = \frac{\lambda_S}{\lambda_A}$$

$$\frac{\lambda_S}{\lambda_A} = \frac{Z_A}{Z_S} \quad (\text{A.8})$$

From A.2,

$$Z_T = \frac{Z_S}{\frac{Z_S}{Z_A} + 1} = \frac{Z_S}{\frac{\lambda_A}{\lambda_S} + 1} \quad (\text{A.9})$$

Finally, resolving the total impedance into the two components with time variable function,

$$Z_S = Z_T(t) \cdot \left(\frac{\lambda_A}{\lambda_S} + 1\right) = (Z_0 e^{-\lambda_T t} + C_T) \cdot \left(\frac{\lambda_A}{\lambda_S} + 1\right) = (Z_0 e^{-\lambda_T t} + C_T) \cdot \left(\frac{\lambda_T}{\lambda_S}\right) \quad (\text{A.10})$$

$$Z_A = Z_T(t) \cdot \left(\frac{\lambda_S}{\lambda_A} + 1\right) = (Z_0 e^{-\lambda_T t} + C_T) \cdot \left(\frac{\lambda_S}{\lambda_A} + 1\right) = (Z_0 e^{-\lambda_T t} + C_T) \cdot \left(\frac{\lambda_T}{\lambda_A}\right) \quad (\text{A.11})$$

APPENDIX B - SPLINE LINE CALCULATION

```
function [segLen,arcLen]=myCalculationV3 (curve)
%% Extract curve data x,y,z
x=curve(:,1); y=curve(:,2); z=curve(:,3);
data=[x,y,z];
% find the dimension of the curve, in this case 3 dimension (x,y,z)
dim=size(data,2);
%% Calculate the dL limit
% The x, y, z coordinates are function of dL
% The dL limit is stored in dl
dl=sqrt (sum(diff (data, [],1).^2,2));
if ~all (dl)
    segLen=0;
    arcLen=0;
    return
end

%% Spline interpolation
pp=cell (1,dim);
for k=1:dim
    % calculate the coefficient of the spline curve for x, y, z
    pp{k}=spline ([0;cumsum (dl)], data (:,k));
    scoeff=numel (pp{k}.coefs);
    % make sure that spline coefficient is 4 so that the
    % integration output is third order of Spline
    if scoeff<4
        pp{k}.coefs=[zeros (1,4-scoeff),pp{k}.coefs];
    end
    % derivative coefficient for 3rd order equation
    diffarray=[3 0 0;0 2 0; 0 0 1;0 0 0];
    pp{k}.coefs=pp{k}.coefs*diffarray;
    pp{k}.order=3; % third order Spline
end

%% Numerical integration along the curve
polyArray=zeros (dim,3); % initialization
segLen=zeros (pp{1}.pieces,1); % initialization
for k=1:pp{1}.pieces
    %extract polynomials for integration for x, y, z
    for m=1:dim
        polyArray (m, :)=pp{m}.coefs (k, :);
    end
    % calculate the segLen with integration
    segLen (k)=quad (@ (dL) segCalculate (dL, dim, polyArray), 0, dl (k));
end
arcLen = sum (segLen);
end
```